FAIL-SAFE SOURCE-DRIVEN FISSION AND FUSION-FISSION HYBRID REACTOR CONFIGURATIONS

BY

MONISH SINGH

THESIS

Submitted in partial fulfillment of the requirements
for the degree of Master of Science in Nuclear, Plasma, and Radiological Engineering
in the Graduate College of the
University of Illinois at Urbana-Champaign, 2013

Urbana, Illinois

Master's Committee:

Professor Magdi Ragheb, Director of Research
Professor Rizwan Uddin

ABSTRACT

A source-driven nuclear reactor configuration with a unity infinite medium multiplication factor fission core ($k_\infty = 1$), is investigated for both fission and fusion-fission hybrid systems. Such a configuration is thought to offer a desirable fail-safe reactor alternative in that the loss of the fission or the fusion neutron sources would automatically lead to a shut-down of the system into a stable subcritical state with an effective multiplication factor of less than unity ($k_{eff} < 1$). This is so since the fission core cannot sustain a chain reaction without the presence of the neutron source. A circulating liquid molten salt using the Th-^{233}U fuel cycle, where the fission products are continuously extracted, further contributes to the fail-safe characteristic by avoiding the cooling needed for the decay heat or afterheat after reactor shut-down. Through the extraction of the ^{233}Pa relatively long-lived ($T_{1/2} = 27 days$) precursor isotope, and allowing it sufficient time to decay into its ^{233}U daughter, breeding in either thermal or fast neutron spectra is a distinct possibility. The presence of trace amounts of ^{232}U and the strong gamma-emitting ^{208}Tl daughter isotope offers a desirable non-proliferation characteristic for the cycle.

As a proof of principle, a simplified analytical one-group neutronics analysis is first attempted for the pure fission core system. This is then supplemented with numerical one-group criticality calculations using an iterative finite-difference methodology. Further, a more detailed continuous energy Monte Carlo neutronics analysis of the fission core reactor driven by a ^{233}U fission neutron source, Deuterium-Tritium (DT) and Deuterium-Deuterium (DD) fusion neutron sources was conducted using the MCNP5 computer code.

The first system studied was a spherical reactor core with a unity infinite medium multiplication factor ($k_\infty = 1$) and surrounded by a reflector. A ^{232}Th and ^{233}U FLiBe molten salt was used as the fuel in the core. The reactor is made critical with the addition of a thin region of FLiBe salt with a spike of fissile material (^{233}U). With a k_∞ in the core and total system k_{eff} of unity, the flux profile for the system becomes flat, resulting in uniform fuel burnup and power profile. Such a configuration was found to have a conversion ratio of 1.4 in the core. However, ^{233}U production in the core would not be able to replace the ^{233}U consumed in the fissile source

region without exceeding a 3-5 percent concentration. This may be possibly achieved using other stockpiled fissile materials such as ^{235}U or Pu^{239} at higher enrichment levels.

Alternatively, the fissile source region can be replaced by a fusion neutron source such as from DT or DD fusion. The system studied consisted of a cylindrical core surrounded by a fusion source. It is envisioned that the source could be provided by several cylindrical electrodynamic inertial fusion generators. A small 318 MWth system can be driven by a 22.3 MW DT source or a 9 MW DD source. A DT system would be able to achieve fissile breeding at the expense of requiring an outside source of tritium. Alternatively, a DD system can use a sodium-based molten salt and breed ^{233}U with a doubling time of 9.2 years.

The results of the investigation suggest that source-driven systems associated with a molten-salt can be contemplated with substantial fail-safe benefits. Running a subcritical reactor eliminates the need for excessive reactivity control systems and provides safety in a loss of power transient situation. Furthermore, utilizing a fissile neutron source yields beneficial power and flux profiles. Lastly, such systems can breed fissile material and support a future alternative Th-^{233}U thorium fuel cycle.

ACKNOWLEDGEMENTS

I would like to acknowledge and thank my family for their unlimited love, support, and encouragement throughout my undergraduate and graduate studies. I would like to thank Prof. Magdi Ragheb as a thesis adviser, as well as Prof. Rizwan Uddin for their insight and guidance as I developed this thesis work. This work would not have been completed without their time and patience.

TABLE OF CONTENTS

LIST OF FIGURES

LIST OF TABLES

CHAPTER I

INTRODUCTION

According to the Energy Information Agency, world energy consumption is projected to increase from 505 quadrillion Btu in 2008 to 770 quadrillion Btu in 2035, representing a 35 percent increase. In light of growing global energy demand and concerns about the impact of greenhouse gas emissions on the climate, there needs to be a concerted effort from all major nations to develop and utilize clean energy technologies. As a result of these trends, renewables have become the fastest growing sources of energy with production increasing by 2.8 percent per year [1]. However, nuclear power must not be overlooked. As one of the few energy sources that can provide large base load power generation with zero carbon emissions, nuclear power can help speed the transition to a carbon-free future.

Currently, the so called "Nuclear Renaissance" has been slow to start. As of 2012, 61 new nuclear power plants are under construction with 139 reactors also having been decommissioned worldwide. This represents a net growth of only 8.767 GWe in world nuclear generating capacity when and if all projects are carried out to completion. Most of this new generating capacity is being created in China, India, Russia, and Korea. Unlike these other countries, the United States only has one nuclear power plant construction project and has far more reactors that are facing the end of their lives [2]. In the United States the slow growth of nuclear power has been primarily due to the large capital costs a utility must devote to a single project over a long construction period. However, as the political currents around the world in the wake of the Fukushima Accident have proven, the nuclear industry also needs to address the questions of economics, sustainability, safety, nonproliferation and how to best to manage nuclear waste.

While the nuclear industry is seeking to address current hurdles by developing cheap small modular reactors in the short term and safer, more efficient, advanced Generation IV reactors in the long term, there are other nuclear technologies worth considering. Source-driven systems offer many practical advantages to existing technologies. They remove the necessity to achieve criticality, reduce enrichment requirements, alleviate the need for moderation, simplify reactivity control, and offer the ability to transmute waste and breed fissile material.

This work aims to compare several different fail-safe source-driven systems. The emphasis is to design a reactor that will solve some of the pressing challenges for the nuclear industry such as waste and safety while offering promising new ideas in an area some have labeled as stagnant. This thesis will focus on a thorium molten salt reactor due to its inherent safety characteristics and small waste footprint. A fissile source and an IEC based DT and DD fusion source will be compared for their performance in driving a thorium reactor.

In order to understand the design considerations presented in this thesis, an overview of source driven systems is given as well as the different neutron sources. Additionally, the theory which will be used to evaluate the efficiency of the proposed hybrid fusion-fission coupled system is detailed.

1.1 Source Driven Reactors

Source driven systems are not a new concept and have existed particularly as subcritical assemblies for experimentation and education for a while. These systems are reactors that are subcritical $(k_{eff} < 1)$ and can sustain a reaction only when an external neutron source is present. Source-driven systems are sometimes encountered in laboratories where low-flux neutron irradiations can be conducted and students can study reactor systems. The advantage is that these systems are extremely stable, and difficult to initiate criticality accidents. Unfortunately, these subcritical systems are small due to the low neutron flux that can be provided by fixed isotopic neutron sources such as ^{252}Cf. However, it is possible to use large neutron sources such as from a spallation source or a fusion reaction to drive power producing reactors that exhibit characteristics such as the ability to breed fissile fuel or to transmute nuclear waste.

1.2 Fusion-Fission Hybrids

Fusion–fission hybrid reactors have been proposed since the 1950's. At the onset of fusion studies it was realized that fusion reactors would produce a plethora of high energy neutrons. These neutrons were of some use, though, as it was soon devised that heavy-element-multiplying blankets could be used to regenerate sufficient tritium to be consumed in fusion reactors.

As early as 1953, the California Research and Development Company proposed the use of a fusion device surrounded by a blanket of depleted uranium. The neutrons from the fusion reactor would induce fast fission in the blanket and could be used to form ^{239}Pu as well as breed tritium with the addition of a ^{6}Li blanket. This study was followed by a similar one proposed by D. Imhoff et al. in 1954 and J.D. Lawson in 1955. The main advantages proposed by these studies were increased production of tritium and fissile material, producing a near-economical fusion reactor, and lowering the requirements for satisfying the Lawson criteria. Since these early studies, there have been many types of fusion-fission systems proposed.

L. M. Lidsky classified fission-fusion systems into three distinct categories, hybrid, symbiotic, and augean. In a hybrid system, a fusion core is surrounded by fissile or fissionable material which is utilized to primarily produce power within the blanket. Symbiotic systems contain fissionable material which is used to breed fissile material for pure fission reactors. Augean systems contain spent nuclear fuel in the blanket, which is subsequently disposed of by transmutation and fission reactions [14]. Each of these systems has their strengths and weaknesses. However, the focus of this thesis will be a power producing system that is capable of breeding if achievable.

1.3 Accelerator Driven Systems

Accelerator-driven systems are much like fusion-fission hybrids, with the exception that instead of a fusion reactor, a particle accelerator such as a linac or cyclotron produces high energy spallation neutrons which are used to drive subcritical assemblies. Like the fusion systems, accelerator driven systems produce fast neutrons (with kinetic energies greater than 1 MeV) which can be utilized for a variety of purposes such as driving a breeder reactor or burning nuclear waste. It is argued that accelerator technology is more developed than fusion systems and thus more viable in the short term. However, fusion systems offer the potential of a greater energy gain as an accelerator by itself will never be able to produce more energy than is invested into it. Thus, it is the fusion-fission coupling that will be explored in detail in this work.

1.4 Inertial Electrostatic Confinement IEC Fusion

While magnetic and inertial confinement fusion represent the two most popular methods of confinement under study, there are other confinement types. Inertial electrostatic confinement (IEC) retains a plasma using an electrostatic field. The most well-known, IEC device is the Farnsworth-Hirsch Fusor. It consists of two concentric spherical electrical grids inside a vacuum. A small amount of fusion fuel is introduced and a voltage is created across the grids to ionize the fuel. These ions are then accelerated toward the center of the chamber where they will eventually collide with another ion and fuse. IEC devices are easy to construct and do not cost anywhere near the billions of dollars that are required to make Inertial Confinement Fusion (ICF) and magnetic fusion Tokamaks.

Unfortunately, this type of confinement is not very efficient as ion collisions with the grids lead to unavoidable energy losses. However, newer approaches have developed unique ways of preventing ions from colliding with the grids, such as using magnetic fields to confine the plasma. Various magnetic cusped configurations have been proposed, including the modified Penning Trap and the Polywell concepts which have produced notable improvements. Due to recent advances that have suggested the prospect of net generation of electricity and to their relatively small development costs, an IEC type fusion device will be the type of fusion device at the heart of the reactor design considered in this work.

1.5 Theory

Before exploring the details of the reactor imparted in this work, it is important to present the basic analytical equations used to evaluate the efficiency of the design. There are several figures of merit that can be used for the assessment of a fusion-fission reactor, the total power produced, the energy multiplication, fissile conversion ratio, and the tritium conversion ratio. In order to derive these figures, it is important to first understand several other terms.

1.5.1 Energy Balance

An important measure of any power system is the net power produced, which can be deduced from an energy balance of the system. A good place to start the derivation of the fusion energy balance is with the plasma power amplification factor, Q_p. The plasma power amplification factor can be defined as the ratio of the thermonuclear power produced and the power input to generate and heat the plasma to thermonuclear fusion temperatures. Figure 1-1 maps the energy and material balances and flows in the hybrid system.

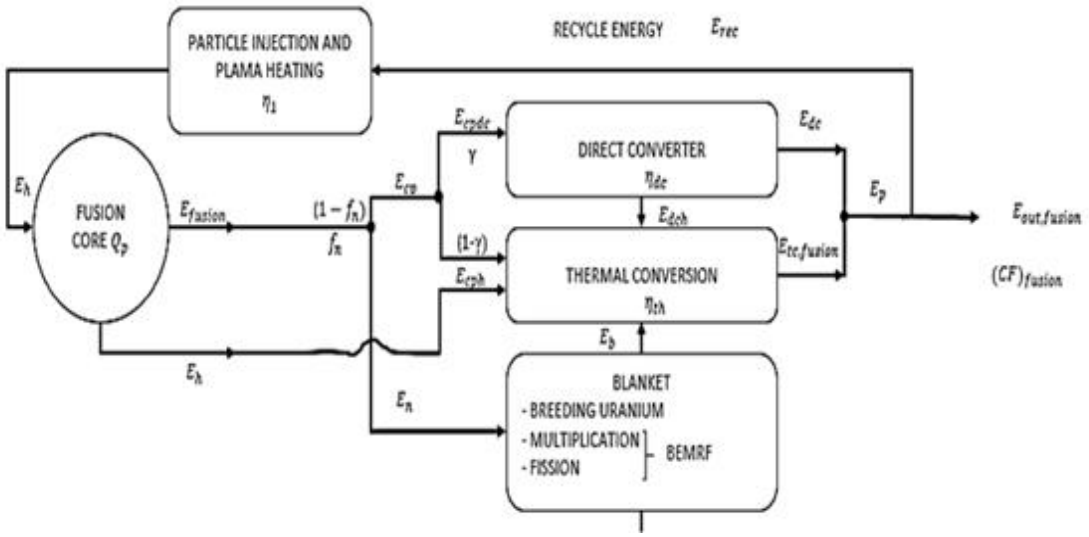

Figure 1-1 Energy and material flows in a fusion-fission hybrid [77].

$$Q_p = \frac{P_{thermonuclear}}{P_{input}} = \frac{E_{fusion}}{E_h} = \frac{fusion\ energy\ generated\ in\ the\ plasma}{energy\ required\ to\ heat\ the\ plasma} \quad (1\text{-}1)$$

Q_p is typically large for closed systems, such a Tokamak or Stellarator device. After energy from the fusion reaction in the plasma exceeds losses, plasma ignition should occur, $Q_p > 1$. Thusly, the plasma burn becomes self-sustaining as long as it remains confined and fuel is continuously supplied. However, for open systems such as mirror or cusped confinement systems, Q_p is low due to end losses of high energy ions and electrons.

The term E_h used in Equation 1-1 is also related to the recycle energy for particle injection and heating energy, E_{rec} by:

$$E_h = \eta_I E_{rec} \tag{1-2}$$

where

η_I = the beam injection and plasma heating efficiency

Additionally, the E_{fusion} term in Equation 1-1 is used to derive expressions for charged particle energy, E_{cp}, and neutron energy, E_n. Since, fusion events produce both charged particles and/or neutrons, the total energy produced from a fusion event is the sum of E_{cp} and E_n. Thus, the relations for E_n and E_{cp} can be written as:

$$E_n = f_n E_{fusion} \tag{1-3}$$

$$E_{cp} = (1 - f_n) E_{fusion} \tag{1-4}$$

where f_n is the fraction of fusion energy carried away by the neutrons in a fusion reaction, which varies by type of fusion event.

Additionally, the neutron energy E_n gets multiplied in the fusion blanket through fission of ^{233}U. The energy produced in the blanket will be designated E_b, with *BEMR* representing the blanket energy multiplication ratio:

$$E_b = BEMR.E_n = BEMR.f_n.E_{fusion} \tag{1-5}$$

$$BEMR = \frac{energy\ deposited\ in\ the\ blanket\ (MeV)}{source\ neutron\ energy\ (MeV)} \tag{1-6}$$

As shown in Equation 1-5, E_n is multiplied by the BEMR which is the sum of the energy deposited in the blanket divided by the source neutron energy. For Equation 1-6, the number 190.0 (MeV/fission) represents the effective energy released following fission of ^{233}U [15]. The BEMR

represents the potential multiplication for the hybrid system. At first order approximation for a DT system, each 14.06 MeV neutron can yield 13.5 times more energy by being utilized to drive a fission system, thus proving the motivation for pursuing such a hybrid system.

Additionally, since there are charged particles produced in the fusion process, a factor γ is defined as the fraction of charged particle energy that flows to the direct energy converter and that is not converted into radiation or conveyed to the thermal conversion cycle. Using this factor, the charged particle energy reaching the direct energy converter can be written as

$$E_{cpdc} = \gamma E_{cp} = \gamma(1 - f_n)E_{fusion} \tag{1-7}$$

Likewise, the energy reaching the thermal conversion cycle can be defined as

$$E_{cph} = (1 - \gamma)E_{cp} = (1 - \gamma)(1 - f_n)E_{fusion} \tag{1-8}$$

Equation 1-7 can be developed further by considering the charged particle conversion efficiency, η_{dc}.

$$E_{dc} = \eta_{dc}E_{cpdc} = \eta_{dc}\gamma(1 - f_n)E_{fusion} \tag{1-9}$$

Similarly, δ can represent the fraction of energy rejected by the direct energy converter that is recoverable through the thermal cycle.

$$E_{dch} = (1 - \eta_{dc})\delta E_{cpdc} = (1 - \eta_{dc})\delta\gamma(1 - f_n)E_{fusion} \tag{1-10}$$

Thus, the overall thermal cycle energy production can be written as

$$\begin{aligned} E_{tc} &= \eta_{th}\left(E_{dch} + E_{cph} + E_b + E_h\right) \\ &= \eta_{th}E_{fusion}\left[(1 - \eta_{dc})\delta\gamma(1 - f_n) + (1 - \gamma)(1 - f_n) + BEMR.f_n + \frac{1}{Q_p}\right] \end{aligned} \tag{1-11}$$

Adding the overall energy produced from the thermal cycle and direct conversion yields the combined electrical output from the hybrid system.

$$E_p = E_{tc} + E_{dc} \tag{1-12}$$

However, E_{rec} must be subtracted as that energy is recycled for particle injection and plasma heating.

$$E_{out} = \mathrm{E_p} - \mathrm{E_{rec}} = \mathrm{E_{tc}} + \mathrm{E_{dc}} - \mathrm{E_{rec}} \tag{1-13}$$

The net output from the hybrid system can be represented by E_{out} multiplied by a capacity factor [77].

$$E'_{out} = E_{out}.\,\mathrm{CF_{fusion}} \tag{1-14}$$

1.5.2 Fissile and Fusile Production

The hybrid system is not just capable of producing energy by breeding fissile material such as ^{233}U and fusile material such as tritium. The production of these isotopes can be calculated by performing the following calculations. The rate of fissile material production/consumption in the blanket can be written as:

$$\frac{dm_f}{dt} = U.S_n.\frac{M_f}{N_0}C_1 \ \ (\frac{kg}{year}) \tag{1-15}$$

where:

U = number of Th(n,γ)/U(n,f) reactions per source neutron

S_n = neutron source strength

M_f = atomic weight of the bred fissile nuclide

N_0 = Avogadro's number

C_1 = conversion factor = $3.15\text{x}10^4$ $(\frac{kg.s}{year})$

The neutron source strength, S_n can be written as

$$S_n = P_{fusion} \cdot \frac{1}{E_{fusion}} . C_2 . CF_{fusion} \ (\frac{n}{s}) \quad (1\text{-}16)$$

where:

P_{fusion} = fusion power

E_{fusion} = energy release per fusion event

C_2 = conversion factor = $6.24 \text{x} 10^{18}$ $(\frac{W.MeV}{MW.J})$

Thus the ratio of the production and consumption rate is the conversion ratio for the system. The tritium production rate is:

$$\frac{dm_t}{dt} = U_T . S_n . \frac{M_f}{N_0} . C_1 (\frac{kg}{year}) \quad (1\text{-}17)$$

where

U_T = the tritium nuclei yield per source neutron

Likewise the tritium consumption rate is proportional to fusion source rate, as one tritium is consumed to produce one neutron.

CHAPTER 2

LITERATURE SURVEY

There have been many previous studies conducted on fusion-fission reactors systems. Since the design considerations in this thesis depend on the separate systems, an investigation will be conducted on the fusion as well as the fission systems. The literature review begins with a survey of the physical, chemical and nuclear properties of thorium. Additionally, the non-proliferation characteristics of thorium are also described. IEC devices and implementations of cusped magnetic fields for confinement are then examined. Having described the constituent parts of the reactor, a review of previous fusion-fission designs and studies are presented. Lastly, information on studies with similar concepts such as accelerator driven systems is given.

2.1 Physical, Chemical and Nuclear Properties

Thorium is a naturally occurring radioactive element that was discovered in 1828 by Swedish chemist Jons Jakob Berzelius. It gets its name from Thor, the Norse god of war. The primary isotope found in nature is ^{232}Th, which has a half-life of about 14 billion years. When pure, it is soft, ductile, and silvery white. In oxide form, thorium has a black or gray color. It is often found in rare earth deposits and can be commercially extracted from monazite mineral which contains around 3 to 22 percent ThO_2. Thorium oxide (ThO_2) has one of the highest melting points of all oxides at 3,300 degrees Celsius. In powdered form, thorium can ignite and burn with a bright white light when heated. Because of this property, thorium is often used in light bulb elements and lantern mantles. In addition, lenses are often doped with thorium to give them a high refractive index and low dispersion. Thorium is also used as a catalyst in the conversion of ammonia to nitric acid and in the production of sulfuric acid [16].

Thorium is four times as abundant as uranium in the Earth's crust. It can be found in granite rocks, phosphate rocks, rare earths, tin ores, and coal and uranium mine tailings. Estimates of the available thorium resources vary widely. The NEA has published 4.4 million tonnes of total

known and estimated reserves of thorium. Table 2-1 shows the estimated world thorium resources by country. These numbers represent data for reasonably assured and inferred resources recoverable at $80/kg or less [17]. It is estimated that India has the largest reserves of thorium at 846,000 tonnes, followed by Turkey, Brazil, Australia, and the U.S.

Table 2-1 Estimated thorium reserves [17].

Country	Thousand Tonnes
India	846
Turkey	744
Brazil	606
Australia	521
USA	434
Egypt	380
Norway	320
Venezuela	300
Canada	172
Russia	155
South Africa	148
China	100
Greenland	86
Finland	60
Sweden	50
Kazakhstan	50
Other Countries	413
World Total	5,385

Thorium is a fertile nuclide, meaning that it is not fissionable by thermal neutrons. However, thorium can be converted to a fissile material, ^{233}U, as demonstrated by the following nuclear reactions [18]:

$$
\begin{aligned}
&{}^{1}_{0}n + {}^{232}_{90}Th \rightarrow {}^{233}_{90}Th + \gamma \\
&{}^{233}_{90}Th \rightarrow {}^{0}_{-1}e + {}^{233}_{91}Pa \\
&{}^{233}_{91}Pa \rightarrow {}^{0}_{-1}e + {}^{233}_{92}U
\end{aligned}
\qquad (2\text{-}1)
$$

The thorium fuel cycle has many benefits over the uranium-plutonium cycle. For example, thorium is a better fertile material than ^{238}U due to its higher thermal neutron absorption cross-section, 7.4 versus 2.7 barns. This means that the conversion of ^{232}Th to ^{233}U is more efficient than that of ^{238}U to ^{239}Pu in a thermal neutron spectrum. Additionally, the neutron regeneration factor (η), or the number of neutrons released per neutron absorbed, is greater than two for a large spectrum of neutron energies. In other words, breeding is easier to achieve with either thermal or fast neutrons.

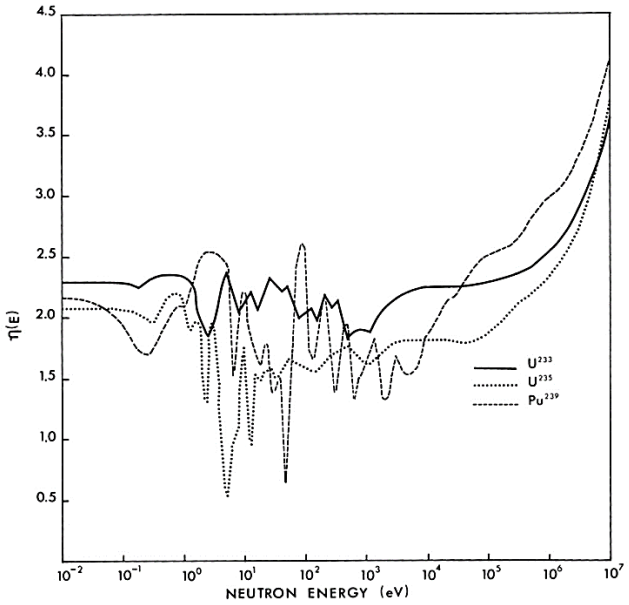

Figure 2-1 Neutron regeneration factor as a function of neutron energy [16].

Furthermore, the capture-cross section of ^{233}U is much smaller than ^{235}U and ^{239}Pu for thermal neutrons, while the fission cross-section is of the same order. This means that non-fissile absorption is less probable in ^{233}U, leading to easier recycling. Most importantly, the thorium cycle produces fewer long-lived Minor Actinides and plutonium, thereby minimizing toxicity and decay heat problems as well as the lifetime of spent fuel [19].

In general the thorium fuel cycle has many benefits to the uranium cycle. Thorium is more abundant than uranium and easier to mine and extract. Radon impact in mining is far smaller than that for uranium mining. This results in simpler tailings management and less occupational dose. Thorium dioxide is relatively inert and is less prone to oxidation like UO_2. This characteristic is favorable for long term storage of solid fuel. ThO_2 also has a higher thermal conductivity and a

lower coefficient of thermal expansion [18]. Because of these characteristics and its favorable nuclear properties, thorium can be viewed as a more advantageous fuel compared to uranium.

2.2 Non-Proliferation Characteristics

One of the biggest concerns with nuclear power is the proliferation of weapons material. Fissile material such as ^{235}U, ^{239}Pu, and even ^{233}U can be used to make a nuclear warhead. As such, it is necessary to assess how resistant the thorium fuel cycle can be to the proliferation of weapons material. At first glance, ^{233}U has advantages as a weapons material over ^{239}Pu. ^{233}U has a fast critical mass that is nearly identical to that of ^{239}Pu and its spontaneous fission rate is much lower, making it easier to assemble a stable weapon.

Table 2-2 Comparison of some nuclear characteristics of ^{233}U, ^{235}U, ^{239}Pu [20].

Property	^{233}U	^{235}U	^{239}Pu
Neutrons released per neutron absorbed (energy of neutron causing fission)	2.5 (1 MeV) 2.28 (0.025 eV)	2.3 2.07	2.9 2.11
Critical mass (kg) (reflector)	8.4 (98.3% ^{233}U) (3.7 cm Be)	21 (93.5% ^{235}U) (5.1 cm Be)	7.5 (4.9% ^{240}Pu) (4.2 cm Be)
Spontaneous fission rate (sec-kg)$^{-1}$	0.5	0.6 (for 1% ^{234}U and 5.5% ^{238}U)	2.5×10^{4} (for 6% ^{240}Pu)
Decay heat (W/kg)	0.3	10^{-4}	2.4 (6% ^{240}Pu)
Delayed neutron fraction	0.00266	0.0065	0.00212

However, the reason why ^{233}U is not suitable for weapons production is in part due to the presence of ^{232}U in irradiated thorium fuel. There are four routes to producing ^{232}U as shown by the following two and three-step reactions:

$$n + {}^{232}_{90}Th \rightarrow {}^{233}_{90}Th \rightarrow {}^{233}_{91}Pa + e^{-}$$

$$n + {}^{233}_{91}Pa \rightarrow 2n + {}^{232}_{91}Pa \rightarrow {}^{232}_{92}U + e^{-} \quad (2\text{-}2)$$

$$n + {}^{232}_{90}Th \rightarrow {}^{233}_{90}Th \rightarrow {}^{233}_{91}Pa + e^{-} \rightarrow {}^{233}_{92}U + e^{-}$$
$$n + {}^{233}_{92}U \rightarrow 2n + {}^{232}_{92}U \quad (2\text{-}3)$$

$$n + {}^{232}_{90}Th \rightarrow 2n + {}^{231}_{90}Th \rightarrow {}^{231}_{91}Pa + e^{-}$$
$$n + {}^{231}_{91}Pa \rightarrow {}^{232}_{91}Pa \rightarrow {}^{232}_{92}U + e^{-} \quad (2\text{-}4)$$

$$n + {}^{232}_{90}Th \rightarrow 3n + {}^{230}_{90}Th$$
$$n + {}^{230}_{90}Th \rightarrow {}^{231}_{90}Th \rightarrow {}^{231}_{91}Pa + e^{-}$$
$$n + {}^{231}_{91}Pa \rightarrow {}^{232}_{91}Pa \rightarrow {}^{232}_{92}U + e^{-} \quad (2\text{-}5)$$

The reactions listed above cannot take place with neutrons below 6 MeV. This means that the production of ^{232}U can be much greater from fusion rather than fission neutrons [21]. Additionally, the isotope ^{232}U is also formed from a reversible (n, 2n) and (n, γ) path as seen from the following reactions:

$$n + {}^{233}_{92}U \rightarrow 2n + {}^{232}_{92}U$$
$$n + {}^{232}_{92}U \rightarrow \gamma + {}^{233}_{92}U \quad (2\text{-}6)$$

Furthermore, ^{232}U can be produced from two successive neutron captures in ^{230}Th, a trace isotope found in thorium ores that contains mixtures of uranium and thorium.

$$n + {}^{230}_{90}Th \rightarrow \gamma + {}^{231}_{90}Th$$
$${}^{231}_{90}Th \rightarrow e^{-} + {}^{231}_{90}Pa$$
$$n + {}^{231}_{90}Pa \rightarrow \gamma + {}^{232}_{90}Pa$$
$${}^{232}_{90}Pa \rightarrow e^{-} + {}^{232}_{92}U \quad (2\text{-}7)$$

^{232}U poses a problem as a weapons material due to the high energy gamma rays that result from its decay:

$$
\begin{aligned}
&{}_{92}U^{232} \xrightarrow{72a} {}_{90}Th^{228} + {}_{2}He^{4} \\
&{}_{90}Th^{228} \xrightarrow{1.913a} {}_{88}Ra^{224} + {}_{2}He^{4} \\
&{}_{88}Ra^{224} \xrightarrow{3.66d} {}_{86}Rn^{220} + {}_{2}He^{4} \\
&{}_{86}Rn^{220} \xrightarrow{55.6s} {}_{82}Po^{216} + {}_{2}He^{4} \\
&{}_{84}Po^{216} \xrightarrow{0.15s} {}_{82}Pb^{212} + {}_{2}He^{4} \\
&{}_{82}Pb^{212} \xrightarrow{10.64h} {}_{83}Bi^{212} + {}_{-1}e^{0} \\
&{}_{83}Bi^{212} \xrightarrow[64\%]{60.6m} {}_{84}Po^{212} + {}_{-1}e^{0} \\
&{}_{83}Bi^{212} \xrightarrow[36\%]{60.6m} {}_{81}Tl^{208} + {}_{2}He^{4} \\
&{}_{84}Po^{212} \xrightarrow{0.298\mu s} {}_{82}Pb^{208}(stable) + {}_{2}He^{4} \\
&{}_{81}Tl^{208} \xrightarrow{3.053m} {}_{82}Pb^{208}(stable) + {}_{-1}e^{0} + \gamma(2.6146MeV)
\end{aligned}
\qquad (2\text{-}8)
$$

As seen in the above decay chain, a 2.6146 MeV gamma is produced from the decay of ^{208}Tl. This represents a significant barrier to weapons because of the occupational dose and the shielding requirements. In comparison, the U-^{239}Pu fuel cycle with a significant admixture of ^{241}Pu produces most of its gamma rays from the decay of ^{241}Am. The gamma rays produced from ^{241}Am are only 0.1 MeV and do not represent a significant occupational hazard for weapon-grade plutonium (0.36% ^{241}Pu). However, their dose becomes a barrier for reactor-grade plutonium which contains around 10 percent ^{241}Pu [18].

According to a study conducted by Kang and von Hippel a worker who is 0.5 meters from an unshielded 5-kg sphere of one year separated ^{233}U containing 1 ppm of ^{232}U would be exposed to 8.2 mrem/hr. If one considers that the occupational limit for a radiation worker in the U.S. is 5 rem/year, said worker would be limited to 610 contact hours per year. For one year separated ^{233}U with 5 ppm of ^{232}U, a worker would be limited to about 80 contact hours. The figure below compares the dose rate buildup for ^{233}U and ^{239}Pu fuel [20].

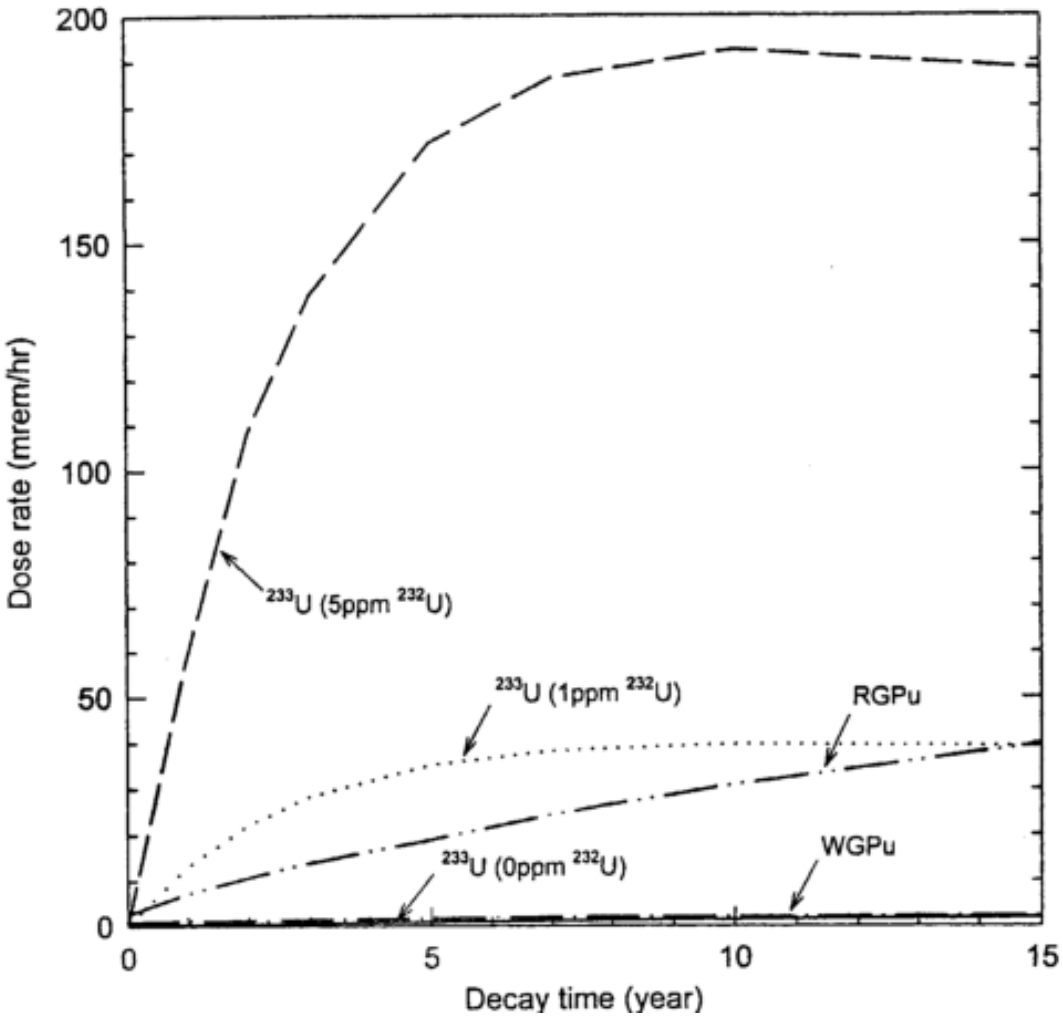

Figure 2-2. Radiation-dose-rate buildup at 0.5 m from 5 kg spheres of ^{233}U and ^{239}Pu with admixtures of ^{232}U and higher plutonium isotopes, respectively [20].

As one can conclude, maximizing the contamination of ^{232}U can improve the non-proliferation aspects of the thorium fuel cycle. This type of barrier is known as a material barrier. Such barriers are considered by the Nuclear Energy Research Advisory Committee (NERAC) to be deterrents to threats posed by covert efforts undertaken by unsophisticated states or subnational groups. The presence of high energy gamma poses a significant barrier and requires adequate shielding. Below is a table showing the lead shielding thickness in centimeters that is necessary to reduce the gamma dose rate at 1 meter distance to 2.5 μSv/h from 1 kg of ^{233}U with various concentrations of ^{232}U [6].

Table 2-3 Shielding thickness necessary to reduce the gamma dose at 1 m to 2.5 μSv/h from 1 kg of ^{233}U with various concentrations of ^{232}U [6].

$^{232}U/^{233}U$	10 days	30 days	100 days	400 days	4,000 days
100 ppm	6.72 cm	10.4 cm	13.3 cm	16.4 cm	18.4 cm
1,000 ppm	12.1 cm	15.5 cm	18.4 cm	21.5 cm	23.5 cm
10,000 ppm	17.2 cm	20.8 cm	23.5 cm	26.0 cm	28.1 cm

The important question is how much is enough to deter weapons production. The IAEA defines materials that expose a person to a dose rate of 100 rem/hour at 1 meter away as self-protecting. Self-protecting materials are those that, due to their inherent radiation emissions, can prevent recipients from completing a set of actions to facilitate malevolent use [22]. According to Kang and von Hippel, a level of 2.4 percent ^{232}U would be required to meet the IAEA's self-protection requirements [20]. The concentration of ^{232}U in spent thorium fuel depends on the type of reactor used, the level of burnup, and how the fuel is utilized. Nonetheless, Kang and von Hippel's calculations should be taken in consideration when developing reactors that utilize the thorium cycle.

In situations where it is desired to separate the bred ^{233}U from spent fuel to be recycled, such as reprocessing of ceramic fuels or on-line separation in molten salt reactors, ^{238}U can be used as a denaturant. The resulting mixture of ^{233}U and ^{238}U is difficult to separate making it harder to create a usable weapon from the material. In contrast, there is no natural denaturant for plutonium isotopes.

Even if ^{233}U contaminated with ^{232}U were to be assembled into a weapon, the high explosives would be degraded due to radiation exposure. According to a study by R.W. Moir, high explosives used in nuclear weapons can withstand up to $1.0x10^8$ R. If the concentration of ^{232}U is 2.4%, with a dose rate of 100 rem/hr, and the explosives occupy a distance of 0.04 m, the shelf life of the weapon would be around 1600 hours after 1 year separation [21]. Because of the potential high gamma radiation exposure to personnel, the ability to damage high explosives in nuclear weapons, and the capability to denature using natural uranium, the thorium cycle can be considered more proliferation resistant over the U-^{239}Pu fuel cycle.

2.3 IEC Fusion Devices

Perhaps the most credited researchers for the advent of IEC fusion are P.T. Farnsworth and R.T. Hirsch and their work in the ‘60s. Inspired by earlier work done by Langmuir and Blodgette [23] on concentric spheres as a vacuum tube configuration, Farnsworth and Hirsch [24-25, 26-27] developed a type of device that would accelerate and spherically converge ions. Known as the Hirsch-Farnsworth fusor, this type of device consists of two charged concentric spheres; an outer vacuum sphere (anode) and an inner grid (cathode). Gas is introduced into the system and is ionized, with the fuel ions formed at the outer grid being accelerated toward the inner grid. They pass through the inner grid, which is designed to be as open as possible, to the center of chamber. At the center, the ion density rises increasing the probability of fusion. Elmore, Tuck, and Watson [28] introduced a variation of this design by deciding to accelerate electrons instead of ions. The inner grid is positively charged and the outer is negatively charged. Electrons are injected into the system and pass thru the inner grid and converge on the center resulting in a virtual cathode. Ions are generated in the inner grid by collisions between the electrons and the gas atoms. These ions are then accelerated toward the virtual cathode and, possibly, fuse with one another. Ions that don’t fuse oscillate back through again until they do.

Unfortunately, researchers have found that ion or electron collisions with the inner grid wire cause them to lose energy and limit the efficiency of the system. This is one of the main impediments to a break-even IEC system. More recently work done by Miley et al. [29-31] have tried to improve upon previous designs by delivering a more compact device to be used as a neutron source. Instead of using ion guns such as Hirsch and Farnsworth, they used a grid-discharge design to produce ions in the system. This method avoids the high cost of the ion guns and reduces the complexity of the system. Miley and his colleagues identify four discharge modes that are used in their studies; central spot, star, halo mode, and jet. Of the discharge modes, the star mode has been the primary focus. In the star mode, the cathode grid is made such that the grid opening diameter is a significant fraction of the major circumference of the grid. The openings create a local depression of the potential surface and in turn cause the ion flow to become focused, forming radial ion “spokes”. The large effective grid transparency of the cathode allows for numerous passes of ions through the center before being intercepted by the grid. Experimental

results have reliably produced 10^7 DD neutrons per second when operated with a steady-state deuterium discharge of 70 kV.

In addition, Miley et al. have also done work with ion injection for IEC devices [32-34]. The ILLIBS (Illinois Ion Beam Source) is an RF-generated plasma that provides high ion current and extraction efficiency. A D-D fusion neutron rate of 2×10^7 n/sec with an IEC grid voltage and current at 75 kV and 15 mA. The ILLIBS was operated at 100 Watt R power and 20 Watt DC magnetic field. Recent developments suggest that at full gun operation a D-D neutron yield of $1x10^8$ n/sec is achievable at 50 mA with cathode voltage 75 kV. Furthermore, additional gains can be achieved by introducing more RF guns to create ion beams within all grid holes. This type of configuration would emulate star mode operation but with higher ion currents.

In an effort to eliminate the ion grid collision problem, several researchers have proposed replacing grids with magnetic fields. One concept proposed by Barnes and Turner [35] utilizes a modified Penning Trap to confine the fusion plasma. A penning trap is formed by a strong homogeneous axial magnetic field to confine the particles radially and a quadruple electric field to confine the particles axially. The electric field is produced by the hyperbolic end cathode caps and the center plane hyperboloid anode. Low energy electrons are introduced through an aperture in one of cathode caps. The electrons are subsequently accelerated toward the center point of the system forming a virtual cathode. This negative charge space is used to ionize and confine the fusion gas introduced in the system. For a DT system with a dense plasma radius of 0.3 mm and ion temperature of 7.8 KeV, the power output is 50 mW and the energy gain $Q = 10^{-3}$. While such a penning trap would not be useful for producing power it could produce useful fusion reactions in a laboratory scale device. Furthermore, it is suggested that higher order multipole traps could generate larger power outputs.

Another concept is the Polywell proposed by Robert Bussard [36-37]. The Polywell, shown in Figure 2-3, consists of a polyhedral array of magnetic point cusps, formed by a grid of magnetic coils called the Magrid, to confine the plasma. Magnetic field lines in cusped systems are designed to curve away from the diamagnetic plasma everywhere, thus creating a system that is highly stable. Electrons are injected at 10-100 kV along point cusp axes to provide a virtual cathode at the center. Ions are then injected at low energies (<100 eV) along cusp axes. The ions are then accelerated to the core region to fuse. Electrons are not static in the system, they recirculate along the cusp axes. The high electron populations in the system have the effect of

pushing the magnetic field outward within the Magrid. This creates a "Wiffle Ball" shaped magnetic field, with the holes of the ball corresponding to the point cusps. The "Wiffle Ball" phenomenon is high advantageous as it squeezes the cusp holes to a very small diameter, leading to better electron confinement and thus lower losses. Bussard was able to achieve a fusion rate of 10^9 DD fusions per second at 12.5 kV drive energy and 10 kV well depth. This is 100,000 times greater than what Farnsworth was able to achieve at similar well depth and drive conditions. Bussard is confident that a 100 MW p-B^{11} is feasible with a $200 million budget and five years development time. This represents a promising milestone for a small, low cost path toward net power producing fusion.

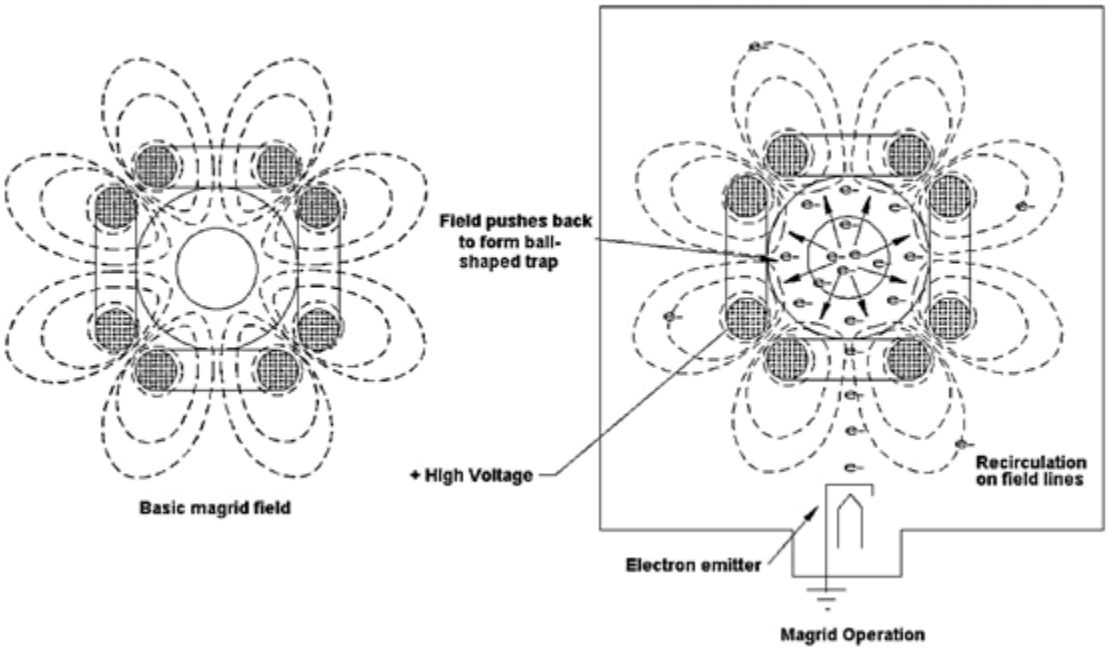

Figure 2-3 Diagram of Polywell operation [38].

2.4 Fusion-Fission Hybrid Reactors

Despite early interest in the idea, support for fusion-fission systems waned from the 70's onward. However, the idea has seen a revival of interest since the 90's. With the Yucca Mountain waste disposal plan facing political roadblocks and continual delays, some started looking for other

ways to tackle the waste issue. Fusion-fission system's, with their ability to transmute and burn waste, was seen as a possible solution. Most notable among fusion-fission advocates is Georgia Institute of Technology Professor, Weston Stacey. Stacey has led a number of design projects on such systems which have resulted in the Subcritical Advanced Burner Reactor (SABR) [39-40]. The SABR reactor is envisioned as a 3,000 MWth sodium cooled, TRU fueled, slightly subcritical (k=0.95) fission system with a tokamak as the fusion driver. The SABR fission system is adapted from previous ANL fast reactor designs and consists of four concentric rings made up of hexagonal fuel assemblies. The TRU fuel consists of 40Zr-10Am-10Np-40Pu. Tritium self-sufficiency is achieved with a Li_4SiO_4 tritium breeding blanket surrounding the outside of the fission blanket. The strength of the neutron source is varied to achieve deep TRU burnup. Also, the fusion neutron source is designed to produce 500 MW_{th}. According to Stacey et al., the SABR reactor operating at 80% availability could burn the TRU produced from the annual discharge of up to four 1,000 MWe light water reactors.

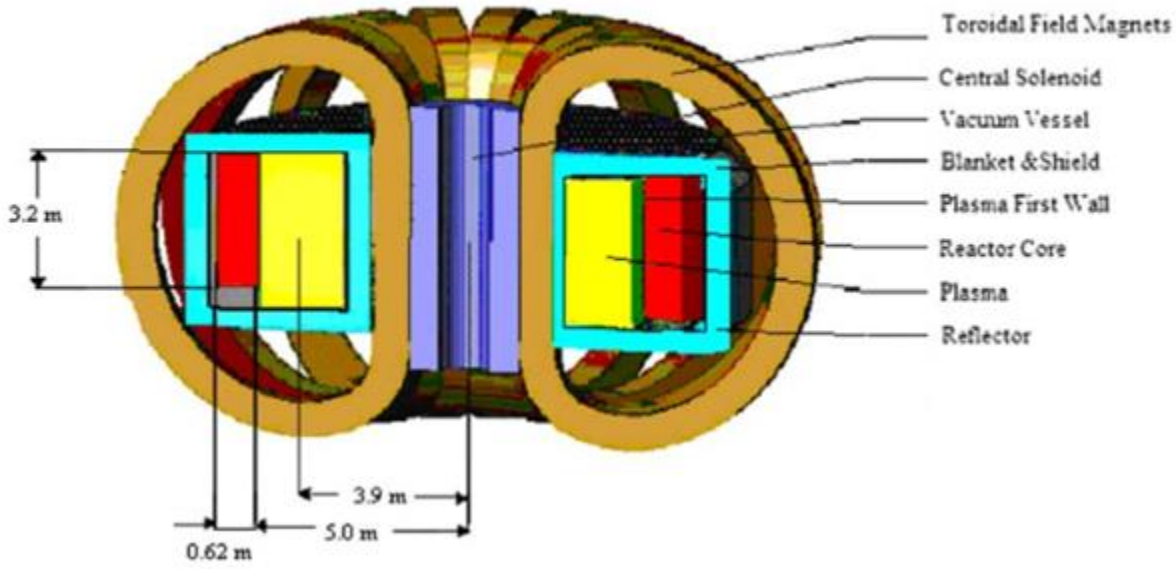

Figure 2-4 Configuration of the SABR [39].

Another Tokamak based Augean system is one being developed at the University of Texas [41]. The design involves a Tokamak that is compact enough to fit inside a subcritical fast-fission

assembly as a remotely handled, replaceable module. It is capable of generating 100 MW_{th} of fusion power and a strong source of 3.6 x 10^{19} [n/s]. The key to the Tokamak's compact design and high power density is the development of the SuperX-Divertor (SXD). Developed by the University of Texas, the diverter utilizes a new magnetic configuration that allows the fusion system to safely exhaust large heat and particle fluxes. The fission blanket is liquid sodium cooled with HT-9 –clad metallic TRU/Zr cylindrical fuel elements. Driven by the fusion neutrons, the subcritical blanket is capable of generating 3,000 MW_{th}. Additionally, a tritium breeding blanket of Lithium Titanate with a breeding ratio 1.1 allows for tritium production for the fusion plant.

Other than tokamak based systems, many have proposed ICF based hybrids. Lawrence Livermore National Laboratory is currently developing a hybrid reactor named LIFE (Laser Inertial Confinement Fusion Fission Energy Reactor) [42-43]. The blanket is a subcritical blanket cooled by molten salt FLiBe (2LiF-BeF2). The fuel is TRISO based and consists of depleted uranium. The first wall coolant is LiPb, which also provides neutron multiplication. There is also a beryllium pebble layer for additional neutron multiplication before the fission blanket. The fusion system is composed of a 2.5 m fusion chamber which produces 500 MW_{th} of fusion power. The power multiplication of the blanket is 4 to 8 and it can operate at a total power of 2 GW for 50 years and burn 99% of all actinides.

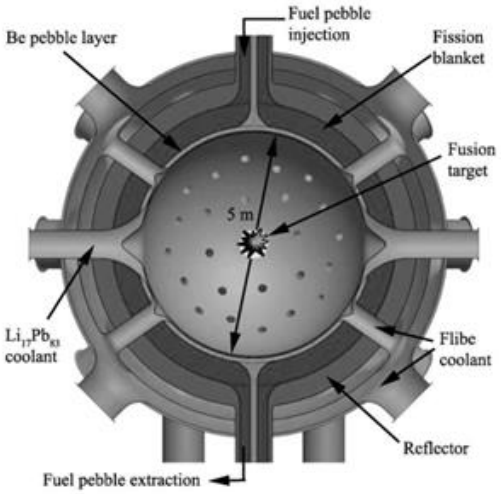

Figure 2-5. Configuration of the LIFE Reactor [43].

R.W. Moir [44] and M. Ragheb [45-46] have both advocated thorium based blankets for fissile breeding. Moir proposes a tokamak based fusion reactor with molten salt thorium blanket. The tokamak would run at 3000MW and would be surrounded by a cylindrical shell blanket 127 meters long. The neutron wall load is 2 MW/m^2 and the blanket energy multiplication at the beginning of life is 1.6. The first wall is made of 1 cm thick iron followed by a 50 cm region consisting of 10mm beryllium spheres with molten salt circulating in steel tubes. The molten salt is 70%LiF + 12%BeF_2 + 18%ThF_4. This is followed by a 30 cm graphite reflector. A fuel production rate of $2660\ \frac{kg}{1000MW_{fusion} \times year}$ is generated from the hybrid system.

While the concept of fusion-fission hybrids is hardly new, the recent revival of the idea over the past 20 years has seen a resurgence of proposals. Thus the reactor designs presented are not the only ones, however, they represent the most developed. The multitude of hybrid designs underscores just what can be achieved with this sort of coupling.

2.5 Accelerator Driven Systems

A fusion reactor is not the only external neutron source that can be used to drive fission systems. Accelerator driven systems (ADS) have also been proposed as a means to transmute waste, produce energy, or breed fuel as early as 50 years ago [47-56]. Much like the fusion-fission hybrids discussed in the previous section, accelerator driven systems involve a sub-critical core which is irradiated by a neutron source that is independent of the fission system. In the case of ADS, a particle accelerator such as a linear accelerator (linac) or a circular accelerator (cyclotron) are used to drive the system instead of a fusion reactor. Neutrons can be generated with an accelerator system by colliding high energy protons with a spallation target made up of a high-atomic numbered element such as tungsten, tantalum, depleted uranium, thorium, zirconium, lead, lead-bismuth, or mercury. For each 1 GeV proton, around 20-30 spallation neutrons can be produced.

Current advances in accelerator technology and the growing desire for a solution to nuclear waste has prompted resurgence in the idea in the past 20 years. Carlo Rubbia is among those that restarted the conversation on accelerator driven systems. The system proposed by Rubbia dubbed an ‘Energy Amplifier’ is a cyclotron driven reactor, based on thorium fuel and a fast neutron

spectrum [57-59]. The cyclotron has a proton current of approximately 12.5 mA and a spallation target made of liquid lead. In addition, the fuel is a mixed oxide fuel that contains actinide waste and thorium in the approximate ratio of 0.16 to 0.84 by weight. The entire system will be subcritical with a k value between 0.96-0.98. Furthermore, the system has a long burn up of up to 200 GW d/t corresponding to 5-10 years of operation without external intervention. Afterwards the actinides are reprocessed and burnt with newly added thorium. Lead is the primary coolant driven by convection, eliminating the need for pumps in the primary loop. The main vessel is 6.0 m in diameter and 30 m tall. Four 375 MWt heat exchangers are located above the core to transfer the heat from primary lead to the intermediate heat transport system. The entire system is rated to a capacity 1500 MWt or about 675 MWe, with a thermal amplification of 120 (the thermal energy from the system divided by the energy deposited by the accelerator).

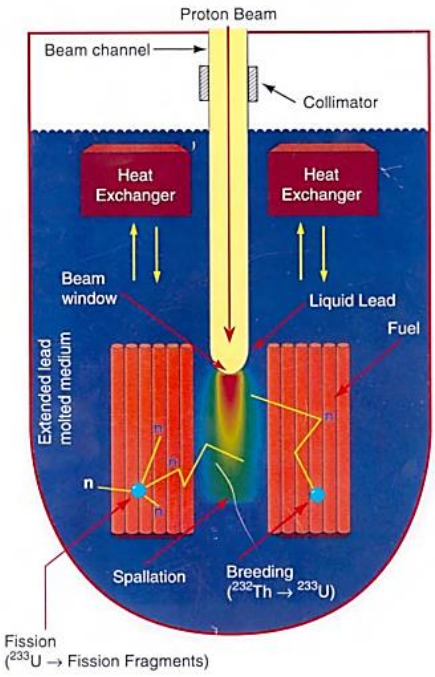

Figure 2-6 Rubbia Energy Amplifier [60].

The first detailed conceptual design of an ADS system for transmutation with thermal neutron was published by a group at Los Alamos led by C.D.Bowman [61-62]. Dubbed The Accelerator Transmutation of Waste (ATW), the system is composed of a linear accelerator with an actinide fuel dissolved in molten salt. Unlike the Rubbia design with its dual purpose of burning

transuranics and utilizing a thorium cycle, Bowman et al. posits two blanket designs one focused on a U-Pu cycle and another on a Th-U cycle. A linac accelerates 1.6 GeV protons at a liquid lead target. However, the neutrons produced from spallation are moderated by heavy water, resulting in a thermal spectrum. The system involving a Th-U cycle has three regions to the blanket; outer, middle, and inner. The outer region consists of D_2O with thorium dissolved as a salt. The fertile thorium is converted to ^{233}Pa which is filtered out and added to the middle region as ^{233}U consisting of a molten salt ($LiF\text{-}BeF_2$). Fission products are continually removed from the salt in the middle region and those that need to be transmuted are returned as dissolved salts to the D_2O in the inner region.

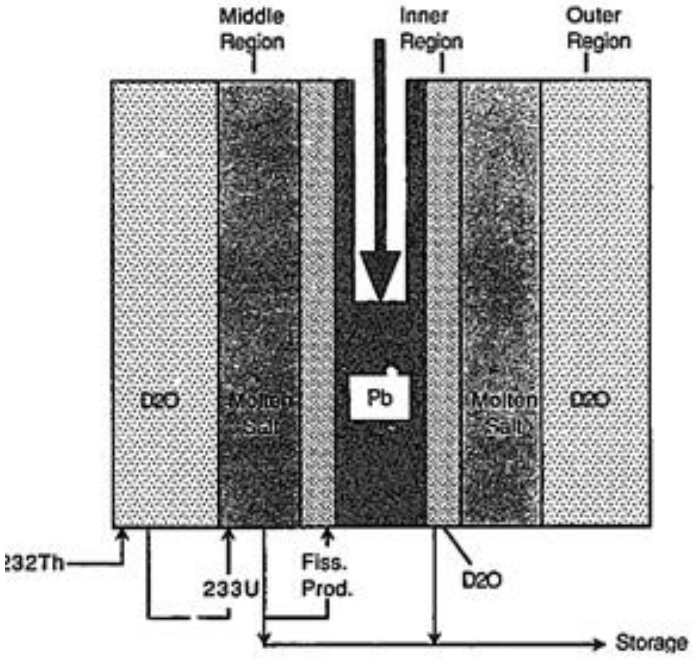

Figure 2-7 Accelerator Transmutation of Waste (ATW) Th-U cycle [61].

In a U-Pu cycle focused on transmutation of commercial nuclear reactor waste, a similar three region setup is proposed as well. The fission products with small capture cross sections are dissolved as salts in the inner region; those with larger cross sections in the outer region. The higher actinides along with some of the Pu mixture are dissolved in the molten salt region. Ultimately, Bowman's goal is to deliver a reactor that would utilize a closed fuel cycle (Th-U or

U-Pu) with minimal end waste through the aid of a linac. High thermal fluxes (10^{16} n/cm^2 s^{-1}), which the inner regions of the blanket are subjected to, reduce the lifetime of actinides such as Pu^{239}. Furthermore, due to the high thermal flux, only a small inventory of plutonium is needed (8kg with a daily burn of 3.5 kg) to produce 3 GW.

Another major conceptual design for ADS is advocated by Kazuo Furukawa [63-65]. For the past 20 years, Furukawa has advocated his Accelerator Molten-Salt Breeder reactor. Much like Rubbia, Furukawa envisions his reactor as a way to start the thorium cycle by breeding fissile material. The design calls for a 1 GeV proton beam with a target/coolant that is composed of a LiF-BeF_2-ThF_4 salt, though more recent designs call for small amounts of Pu^{239} to increase power and U^{233} production. The blanket would function much like any MSR. Continual in situ chemical processing is utilized to remove ^{233}Pa and other fission products. According to the most recent designs a 1400 MWth plant with 700 kg/y U^{233} production rate is achievable with a 1GeV, 300 mA accelerator and a salt composition of LiF–BeF_2– ThF_4–^{233}UF4–$^{239}PuF_3$ (64–18–17.15–0.3–0.55 mol%).

While Rubbia, Bowman, and Furukawa's ADS designs are not the only ones, they represent the most developed and are worth mentioning. ADS are still in their infancy and there are countless proposals being worked on all over the world. However, many countries have already begun plans to develop and build demonstration plants in this area. The Belgian Nuclear Research Centre has been working on the design of its Multipurpose Hybrid Research Reactor for High-tech Applications (MYRRHA) since 1998 [66]. It consists of a 600 MeV, 2.5 mA proton accelerator with a liquid lead-bismuth eutectic (LBE) spallation target. The blanket consists of a sub-critical MOX fueled core cooled with LBE. The reactor is set to see full operation by 2023. Additionally, experimental work has been conducted on the feasibility of accelerator driven systems at Kyoto University utilizing the Kyoto University Critical Assembly (KUCA) [67-68]. Using a fixed field alternating gradient (FFAG) accelerator to deliver 100 MeV protons at a tungsten target, a neutron intensity of 10^6 n/s was achieved. Various fuels have been irradiated including highly enriched uranium fuel (93%) with a polyethylene moderator/reflector and thorium/thorium-graphite fuel. Numerous projects are being developed in other countries as well; CIRCE in Italy, CIEMAT in Spain, and XADS in France [69]. Because ADS concepts are still in their infancy, there are still many challenges that need to be overcome before it becomes a commercial technology. Some problems include increased complexity of the reactor compared to

a traditional system, the introduction of new types of reactivity and source, and the fact that the beam window and targets are subjected to high stresses, corrosion, and irradiation conditions. As technology and experience is developed in this area, ADS may become a promising method for transmuting waste and breeding fuel.

Chapter 3

FAIL-SAFE REACTOR DESIGN

In designing a source driven system, the goal was to produce a design which would be safer than current reactors. The chosen configuration of the core of the reactor allows for uniform flux distribution and prevents the core from maintaining criticality without the aid of an external neutron source or region of fissile material. In the following sections, the design of the reactor is established, followed by investigations of reactors that use either an additional fissile region, a DT fusion source, or a DD fusion source. These reactor designs are subsequently evaluated using the MCNP5 code.

3.1 Introduction

Consider a spherical reactor core with radius R and surrounded by an infinite reflector. If the infinite medium multiplication factor of the core is unity ($k_\infty = 1$), the system would be essentially subcritical due to leakage from the core to the reflector ($k_{eff} < 1$). Such a system could be made critical ($k_{eff} = 1$) by adding a layer of fissile material or be driven by an external source of neutrons, such as from a fusion reactor.

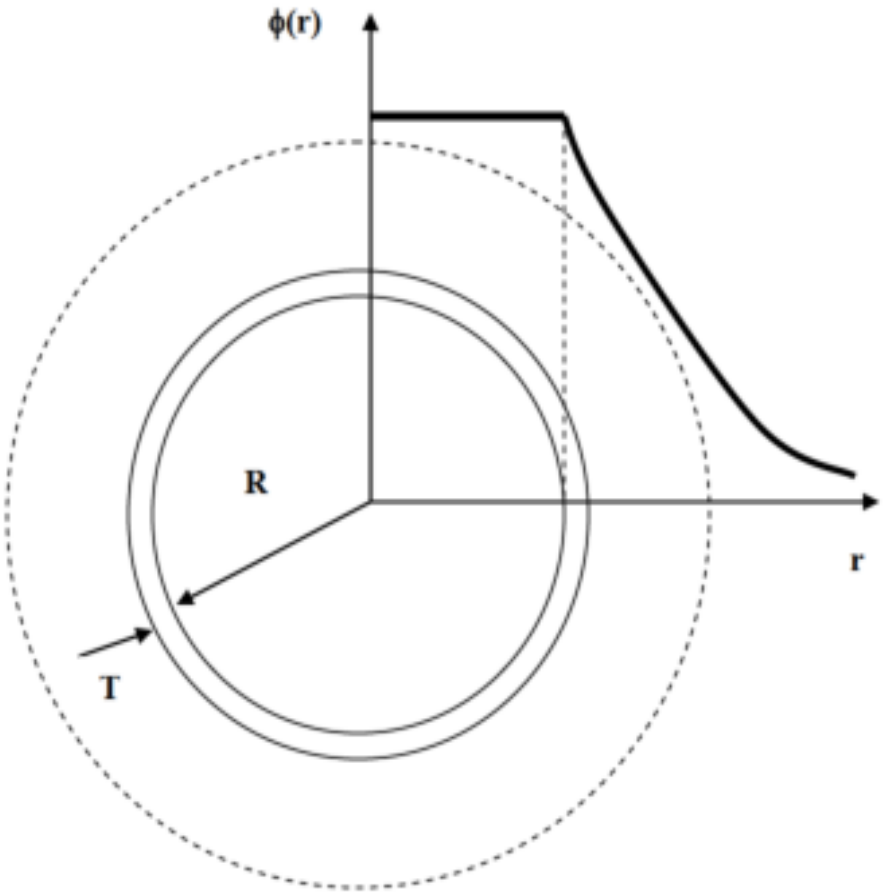

Figure 3-1. Geometry of a spherical core with an infinite reflector and a fissile spiked core-reflector interface.

The neutron flux for such a system can be modeled by the one-group diffusion equations:

Core: $$D_c \nabla^2 \phi_c - \Sigma_a^c \phi_c + \eta_c \Sigma_a^{Fc} \phi_c = 0 \quad (3\text{-}1)$$

Reflector: $$D_r \nabla^2 \phi_r - \Sigma_a^r \phi_r = 0 \quad (3\text{-}2)$$

For a fast unmoderated reactor material in the core with unity resonance escape probability and fast fission factor:

$$\eta_c \Sigma_a^{Fc} = \eta_c \frac{\Sigma_a^{Fc}}{\Sigma_a^c} \Sigma_a^c = \eta_c f \Sigma_a^c = k_\infty \Sigma_a^c \quad (3\text{-}3)$$

Substituting the result into the core and reflector equations yields:

$$\nabla^2 \phi_c + \frac{k_\infty - 1}{L_c^2} \phi_c = 0 \quad (3\text{-}4)$$

$$\nabla^2 \phi_r - \frac{1}{L_r^2} \phi_r = 0 \quad (3\text{-}5)$$

where

$$L^2 = \frac{D}{\Sigma_a}$$

Because the core is chosen with an infinite medium multiplication factor of unity, the material buckling of the core is zero.

$$B_c^2 = \frac{k_\infty - 1}{L_c^2} = \frac{1-1}{L_c^2} = 0 \quad (3\text{-}6)$$

Solving for the flux in a spherical core yields:

$$\nabla^2 \phi_c(r) = 0$$
$$\frac{1}{r^2} \frac{d}{dr} \left(r^2 \frac{d\phi_c(r)}{dr} \right) = 0$$
$$d\left(r^2 \frac{d\phi_c(r)}{dr} \right) = C$$
$$\frac{d\phi_c(r)}{dr} = \frac{C}{r^2}$$
$$d\phi_c(r) = \int \frac{C}{r^2} dr$$
$$\phi_c(r) = -\frac{C}{r} + A$$

For a finite flux in the core, C = 0 and the flux in the core is therefore equal to a constant. This means that the flux and the power distribution in the core are constant, a desirable characteristic for uniform fuel burnup.

$$\phi_c(r) = A \tag{3-7}$$

The flux in the reflector region is:

$$\phi_r(r) = E\frac{e^{\frac{-r}{L_r}}}{r} + F\frac{e^{\frac{r}{L_r}}}{r} \tag{3-8}$$

For a finite flux, F = 0.

$$\phi_r(r) = E\frac{e^{\frac{-r}{L_r}}}{r} \tag{3-9}$$

Before applying the interface boundary condition, the net current at the interface is needed.

$$\begin{aligned} J_{source\ region} &= \nu\Sigma_f\phi_c(R).T - \Sigma_a^F\phi_c(R).T \\ &= \nu\frac{\Sigma_f}{\Sigma_a^F}\Sigma_a^F\phi_c(R).T - \Sigma_a^F\phi_c(R).T \\ &= (\eta_{source\ region} - 1)\Sigma_a^F\phi_c(R).T \end{aligned} \tag{3-10}$$

where

T = the thickness of the source region and $\eta_{source\ region}$ is the regeneration factor

Because the extra fissile layer (source region) is considered thin, the thin interface boundary conditions can be applied.

$$\phi_c(R) = \phi_r(R) \tag{3-11}$$

$$J_c(R) = J_r(R) - J_{source\ region}(R) \tag{3-12}$$

Applying the boundary conditions:

$$A = E\frac{e^{\frac{-R}{L_r}}}{R} \tag{3-13}$$

$$D_c\nabla\phi_c(R) = D_r\nabla\phi_r(R) + J_{source\ region}(R) \tag{3-14}$$

Therefore, the current boundary condition becomes:

$$0 = -E\frac{D_r}{R}\left[\frac{e^{\frac{-R}{L_r}}}{L_r R} + \frac{e^{\frac{-R}{L_r}}}{R^2}\right] + \left(\eta_{source\ region} - 1\right)\Sigma_a^F E\frac{e^{\frac{-R}{L_r}}}{R}T \tag{3-15}$$

The critical condition for the system becomes:

$$D_r[\frac{1}{R} + \frac{1}{L_r}] = \left(\eta_{source\ region} - 1\right)\Sigma_a^F T \tag{3-16}$$

3.2 One-Group Finite-Difference Model

With the foundations of the reactor laid out, the next step is to verify the theory numerically. A multi-region one-group diffusion theory code written by Magdi Ragheb was utilized (Appendix A.2) to model a two region spherical reactor with a reflector (Figure 3-2). The core region contains a FLiBe molten salt of the following composition $^{7}LiF - BeF_2 - ThF_4 - {}^{233}UF_4$. The molar concentrations of the salt components are modeled after the FLiBe salt suggested for the single fluid FUJI-II MSR [70]. It is made up of (72-x) – 16 – 12 – x [mol%] where the ^{233}U concentration is varied to achieve an infinite medium multiplication factor of unity. The lithium in the salt is enriched so that a negligible amount of ^{6}Li is present. This is to reduce the tritium production in the salt. The fissile source region is composed of a similar FLiBe molten salt, but with the thorium removed from the salt and replaced with beryllium. Additionally, the reflector is made of graphite.

Furthermore, the salt is contained in an 85 mm thick Hastelloy N vessel of the following composition: 77.6% Ni – 12% Mo – 7% Cr – 2.36% Ti – 1% Nb – 0.02% Mn – 0.01% Fe – 0.01% Si.

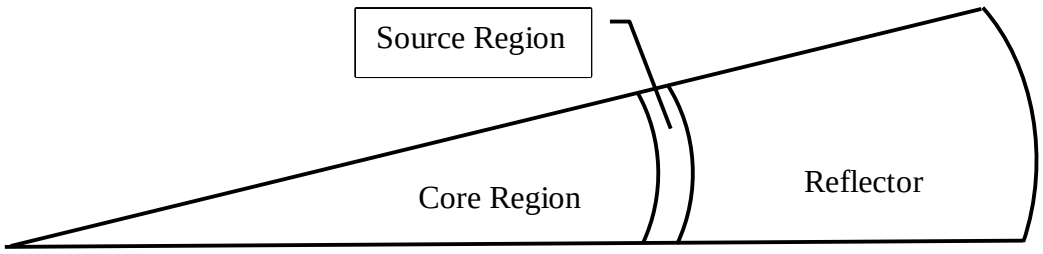

Figure 3-2 Reactor geometry.

The input for the code requires the diffusion coefficient of the material, the macroscopic absorption cross section, and the product of the number of neutrons per fission and macroscopic fission cross section. A sample input file is provided in Appendix A.3. Compiled input data for the core salt, the source region salt, and the graphite reflector are listed in Appendix A.1. Using fission spectrum averaged cross sections from the JENDL3.2 data files, the core salt composition was selected to be 16% BeF_2 – 69% ^{7}LiF – 12% ThF_4 – 3% $^{233}UF_4$ in order to achieve a k_∞ that was equal to unity. The graphs below shows the normalized flux for different criticality conditions. The core region has a radius of 40 cm, while the source region and the reflector are 4.4 and 40 centimeters thick respectively. In order to achieve different criticality conditions, the concentration of fissile material in the source region was varied. As shown in Figure 3-3, when the effective and infinite multiplication factors are both equal to unity in the system, the normalized flux is constant throughout the core region. This is very beneficial for uniform fuel burn up.

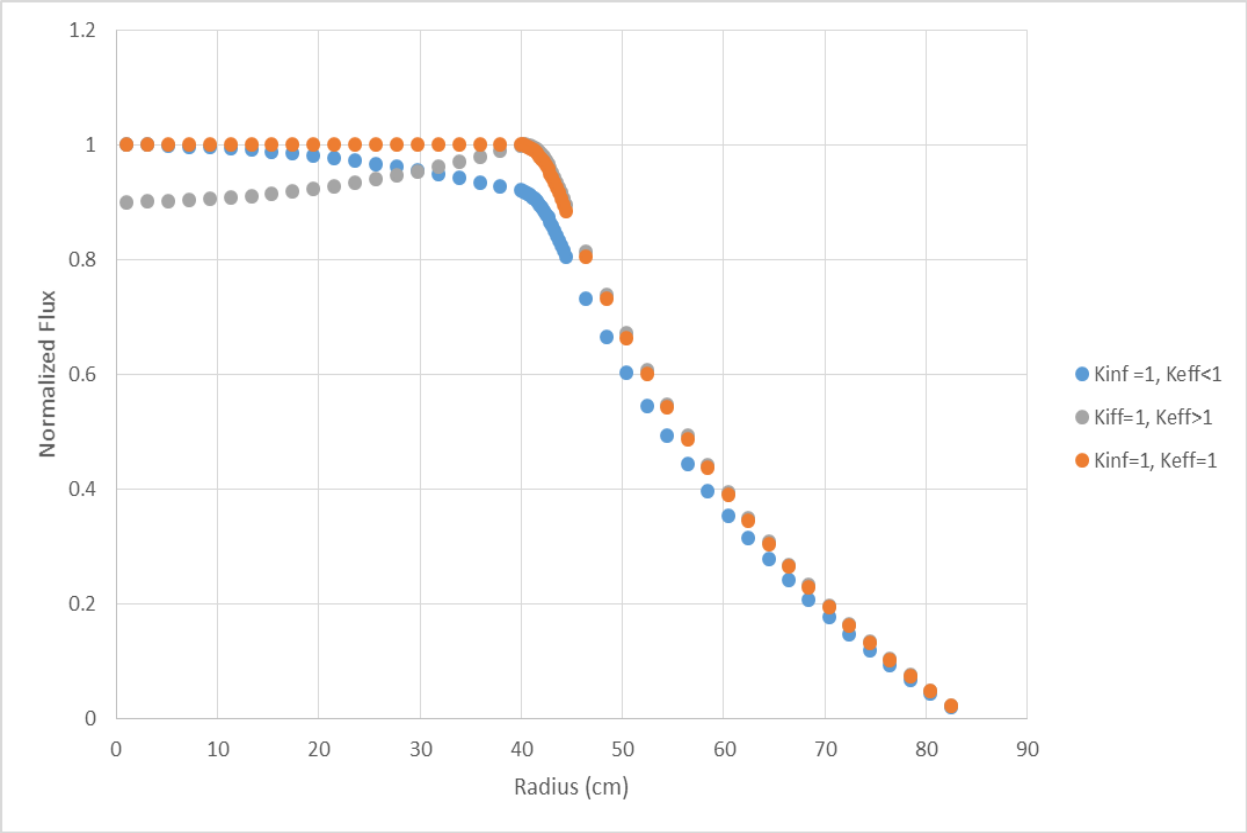

Figure 3-3. Normalized flux vs radius for various criticality conditions (k_∞ =1).

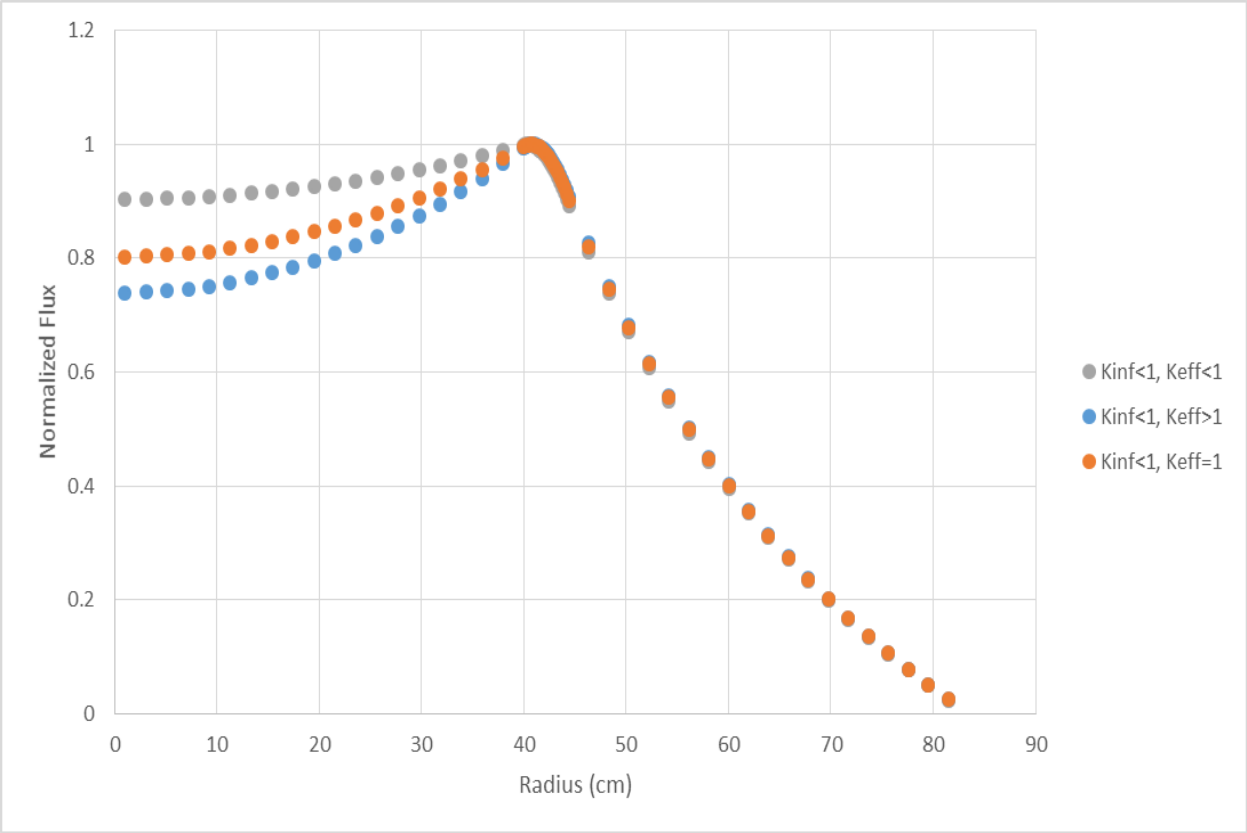

Figure 3-4 Normalized flux vs radius for various criticality conditions ($k_\infty<1$).

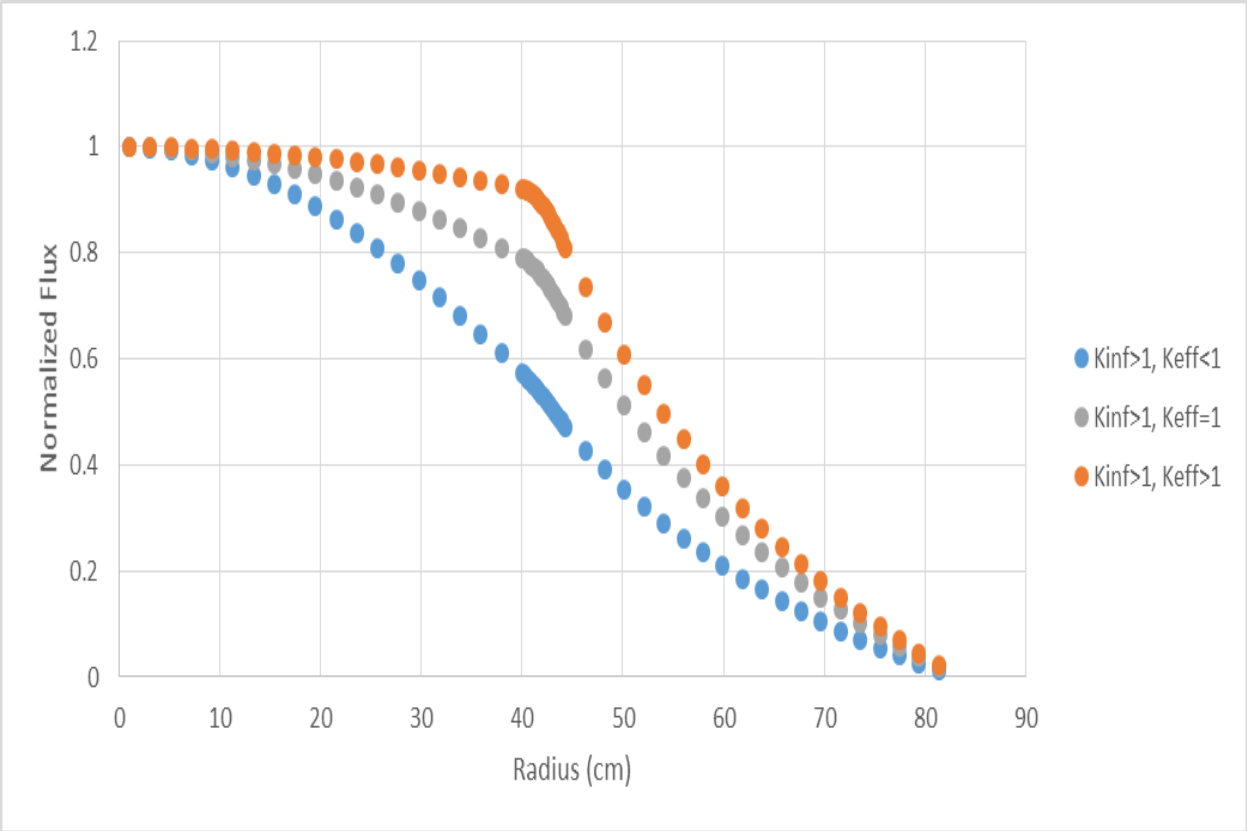

Figure 3-5 Normalized flux vs radius for various criticality conditions (k_∞>1).

CHAPTER 4

METHODOLOGY

Because the bulk of this work utilizes the computer code MCNP, it is prudent to give a brief introduction about the code and the adopted simulation parameters. MCNP5 is a general purpose Monte Carlo particle transport code developed and maintained by Los Alamos National Laboratory. It is capable of calculating the k_{eff} values and reaction rates averaged over a user defined system by statistically sampling the integral of the Boltzmann Transport Equation. For the simulations done in this study, the F4, F5, F6, and FM tallies were utilized.

4.1 MCNP5 Tallies

Perhaps the most useful tally in MCNP5, the F4 tally, measures the particle flux per source neutron in units of particles/cm^2. The F4 tally is governed by the following equation:

$$\overline{\phi}_V = \frac{1}{V}\int dE \int dt \int dV \int d\Omega \Psi(\vec{r},\Omega,E,t) = \frac{1}{V}\int dE \int dV \int ds N(\vec{r},E,t) \qquad (4\text{-}1)$$

where

$\Psi(\vec{r},\Omega,E,t)$ = angular flux

$N(\vec{r},E,t)$ = density of particles, regardless of their trajectories at a point

The quantity $N(\vec{r},E,t)$ds can be thought of as the track length density and therefore the average flux can be solved by summing the track lengths. MCNP calculates the average flux by summing the particle weight multiplied by the track-length per unit volume in the cell.

The F5 tally measures the flux at a point in units of particles/cm^2 and can be considered a limiting case of a surface flux tally. Take a point detector to be sphere whose radius is shrinking to zero as illustrated in the figure below.

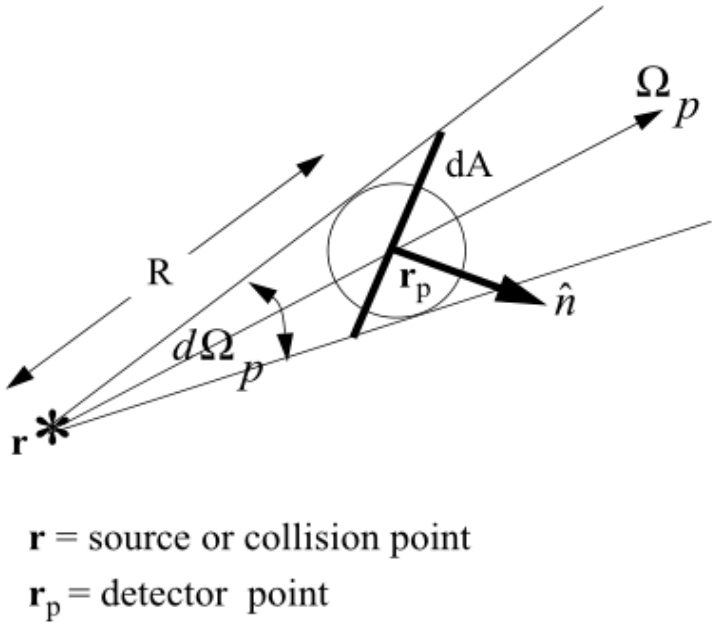

Figure 4-1 Point detector illustration [72].

Ω_p is the direction to the center of the sphere and $d\Omega_p$ is the solid angle subtended by the sphere from r. Let dA be defined by the intersection of an arbitrary plane passing through the detector and the collapsing cone. The probability that a particle scatters into the solid angle $d\Omega_p$ is defined by:

$$p(\Omega_p)\mathrm{d}\Omega\mathrm{p} \tag{4-2}$$

Furthermore, the particle must not only scatter toward dA but it also must have collisionless free-flight for the distance R. This is governed by:

$$e^{-\int_0^R -\Sigma_t(s)ds} \tag{4-3}$$

where

$\Sigma_t(s)$ = the total macroscopic cross section at a distance *s* from the collision point

The probability that the particle satisfies the previous two events, is governed by product of the two probabilities. Another term, the cosine of the angle between the particle direction and the unit normal to the area dA ($\hat{n}$) is defined by:

$$\eta = \Omega_p * \hat{n} \tag{4-4}$$

If a particle of statistical weight *w* reaches dA, it will contribute $\frac{w}{|\eta| dA}$ to the flux. As the sphere shrinks to a point, the solid angle subtended by dA becomes $\frac{|\eta| dA}{R^2}$. Therefore the F5 tally becomes:

$$F5 = w \frac{p(\Omega_p)}{R^2} e^{-\int_0^R -\Sigma_t(s) ds} \tag{4-5}$$

This can be further simplified, as MCNP assumes azimuthal symmetry. The angle Ω_p can be expressed in polar coordinates where the cosine of the polar angle is μ and φ is the azimuthal angle. The probability density of scattering into $d\Omega_p$ can be written as:

$$p(\Omega_p) d\Omega_p = p(\mu, \varphi)\ d\ \mu\ d\ \varphi \tag{4-6}$$

$$p(\mu) = \int_0^{2\pi} p(\mu, \varphi)\ d\ \varphi \tag{4-7}$$

$$p(\mu, \varphi) = \frac{p(\mu)}{2\pi} \tag{4-8}$$

Substituting this last expression for Equation 4-5 yields:

$$F5 = w \frac{p(\mu)}{2\pi R^2} e^{-\int_0^R -\Sigma_t(s) ds} \tag{4-9}$$

The F6 tally measures the average energy deposition in the cell in units of MeV/g. Heating due to neutron and photon interactions are done separately. In order to get the true

heating, one must sum the neutron and photon F6 tallies in a coupled neutron/photon calculation. The F6 tally is governed by the following equation:

$$H_t = \frac{\rho_a}{m} \int dE \int dt \int dV \int d\Omega \, \sigma_t(\mathrm{E})\mathrm{H}(\mathrm{E})\Psi(\vec{r}, \Omega, E, t) \tag{4-10}$$

where

ρ_a = the atom density (atoms/barn-cm)

m = the cell mass

σ_t = the microscopic total cross section (barns)

H = the heating number (MeV/collision)

As is evident from the above equation, the F6 tally is merely the F4 tally multiplied by an energy dependent multiplier. The heating function listed in the above equation is given by the following expressions for neutrons and for photons:

$$H_{neutrons}(E) = E - \sum_i p_i(E)[\overline{E}_{i,out}(E) - Q_i + [\overline{E}_{i,\gamma}(E)] \tag{4-11}$$

where

p_i = the probability of reaction *i* at neutron incident energy *E* ($\sigma_i(E)/\sigma_t(E)$)

$\overline{E}_{i,out}$ = the average exiting neutron energy for reaction *i* at neutron incident energy *E*

Q_i = the Q-value for reaction *i*

$\overline{E}_{i,\gamma}$ = the average exiting gamma energy for reaction *i* at neutron incident energy *E*

$$H_{photons}(E) = E - \sum_i^3 p_i(E)[\overline{E}_{i,out}(E)] \tag{4-12}$$

where

i = 1 is incoherent (Compton) scattering with form factors

i = 2 is pair production

i = 3 is photoelectric absorption ($\overline{E}_{i,out}$= 0)

$\overline{E}_{i,out}$ = the average exiting gamma energy for reaction *i* at neutron incident energy *E*

The FM card multiplies the F1, F2, F4, and F5 tallies by any continuous-energy quantity available in the MCNP data libraries. This takes the following form:

$$C \int R(E)\varphi(E)dE \tag{4-13}$$

where $\varphi(E)$is the energy-dependent fluence

C = a designated constant

R(E) = any combination of sums and products of energy-dependent quantities

In the simulations conducted, fission energy deposition in a cell (MeV/cm^3), (n,γ) reactions per unit volume, fission reactions per unit volume, and (n,t) reactions per unit volume are all computed utilizing the FM card.

In order to simulate problems effectively, MCNP contains continuous-energy nuclear and atomic data libraries. Throughout this work, unless otherwise specified, the ENDF/B-VI libraries were used. Furthermore, MCNP accompanies all results with an associated relative error. The relative error is obtained from standard deviations or sigma values commonly used in statistics. *Sigma one*, *two*, and *three* values correspond to confidence intervals of 68.3%, 95.4%, and 99.7%, respectively. In this work, unless otherwise specified, all error values are reported as those corresponding to a *sigma one* value.

4.2 Scaling Tallies

All tallies in MCNP are given per source neutron. To scale a tally calculation to a desired steady-state power level, one can use the following equation:

$$N\left[\frac{n}{s}\right] = \frac{P_{fission}[W]*\bar{\upsilon}[\frac{neutron}{fission}]}{E_{fission}[\frac{MeV}{fission}]*\left(1.602\ x\ 10^{-13}[\frac{J}{MeV}]\right)} \tag{4-14}$$

where

$P_{fission}$ = the thermal power of the reactor

$\bar{\upsilon}$ = the number of neutrons released per fission reaction

$E_{fission}$ = the amount of energy released per fission reaction

It must be noted however, that Equation 4-14 is applicable only to critical (k_{eff} = 1) systems. For subcritical systems, the scaling factor is given by dividing Equation 4-14 by the k_{eff} of the system.

$$N[\frac{n}{s}] = \frac{P_{fission}[W]*\bar{\upsilon}[\frac{neutron}{fission}]}{E_{fission}[\frac{MeV}{fission}]*\left(1.602\ x\ 10^{-13}[\frac{J}{MeV}]\right)} * \frac{1}{k_{eff}} \quad (4\text{-}15)$$

For a source driven system, the required source strength can be calculated by using the subcritical multiplication factor (M):

$$M = \frac{Total\ neutron\ strength\ due\ to\ source\ and\ fissions}{Neutron\ strength\ due\ to\ source\ alone} = \frac{N}{S} \quad (4\text{-}16)$$

The number of neutrons after (m-1) generations is:

$$N = S(1 + k_{eff} + k_{eff}^2 + \cdots + k_{eff}^{m-1}) \quad (4\text{-}17)$$

$$= S\frac{1-k_{eff}^m}{1-k_{eff}}, \text{ m} > 0 \quad (4\text{-}18)$$

as $m \rightarrow \infty$

$$M = \frac{N}{S} = \frac{1}{1-k_{eff}} \quad (4\text{-}19)$$

Plugging this into Equation 4-16 and solving for S:

$$S \times M = N \quad (4\text{-}20)$$

$$S = \frac{P_{fission}[W] * \bar{\upsilon}[\frac{neutron}{fission}]}{E_{fission}[\frac{MeV}{fission}] * \left(1.602\ x\ 10^{-13}[\frac{J}{MeV}]\right) * k_{eff}} * \frac{1}{M}$$

$$= \frac{P_{fission}[W]*\bar{\upsilon}[\frac{neutron}{fission}]}{E_{fission}[\frac{MeV}{fission}]*\left(1.602\ x\ 10^{-13}[\frac{J}{MeV}]\right)} * \frac{1-k_{eff}}{k_{eff}} \quad (4\text{-}21)$$

One caveat, the source strength can be approximated by Equation 4-21 only if the fixed source distribution is nearly the same as the eigenmode source generated in the eigenvalue problem. This will not be the case for the fusion source driven systems investigated later in this thesis. Thus, to solve this problem, MCNP provides a value called the net multiplication (M_{net}) in a given problem output file.

$$M_{net} = 1 + G_f + G_x = W_e + W_c \quad (4\text{-}22)$$

where

G_f = the gain in neutrons from fission

G_x = the gain from nonfission multiplicative reactions

W_e = the weight of neutrons escaped per source neutron

W_c = the weight of neutrons captured per source neutron

In terms of M_{net} and $\bar{\upsilon}$, the effective multiplication factor for a fixed source, k_{eff}^{FS}, can be defined as:

$$k_{eff}^{FS} = \frac{M_{net}-1}{1-\frac{1}{\bar{\upsilon}}} \quad (4\text{-}23)$$

This factor can then replace k_{eff} in Equation 4-21 to produce S_{fusion}, the fusion neutron source strength.

$$S_{fusion} = \frac{P_{fission}[W]*\bar{\upsilon}[\frac{neutron}{fission}]}{E_{fission}[\frac{MeV}{fission}]*\left(1.602\ x\ 10^{-13}[\frac{J}{MeV}]\right)} * \frac{1-k_{eff}^{FS}}{k_{eff}^{FS}} \quad (4\text{-}24)$$

CHAPTER 5

FISSILE SOURCE DRIVEN FAIL-SAFE REACTOR

Expanding on the one-group diffusion model, a more detailed analysis of the fissile fail-safe reactor was performed using MCNP5. A similar two region spherical reactor, shown in Figure 3-2 was modeled. The fuel salt is of the same composition (72-x)% ^{7}LiF – 16% BeF_2 – 12% ThF4 – x% $^{233}UF_4$. To determine the concentration of ^{233}U that would yield an infinite medium multiplication factor of unity, the core geometry was initially modeled so that all neutrons would reflect from the boundary back into the fuel (Appendix B.1). A FLiBe composition of 16% BeF_2 – 71.02% ^{7}LiF – 12% ThF_4 – 0.98% UF_4 yielded a satisfactory k_∞ equal to 1.00073 +/- 0.00057. Similarly, the source region contains a FLiBe salt as well, however thorium is removed and replaced by beryllium. The concentration of ^{233}U in this salt was chosen to make the reactor's effective multiplication factor equal to one. A source region salt composition of 31% BeF_2 – 67.9% ^{7}LiF –1.1% UF_4 yielded a k_{eff} of 1.00883 +/- 0.00188. The salt in the core and source regions are contained in an 85mm Hastelloy N vessel (77.6% Ni – 12% Mo – 7% Cr – 2.36% Ti – 1% Nb – 0.02% Mn – 0.01% Fe – 0.01% Si). Lastly, the 40 cm radial core and 10 cm thick source region is surrounded by a 40 cm thick graphite reflector.

A sample MCNP input file for the reactor is listed in Appendix B.2. The code was run to calculate a number of tallies, such as the F4 tally, F5 Tally, F6 tally, and an FM tally for the fission rate. Figure 5-1 shows the neutron flux as a function of distance in the system. The flux profile matches well with what was expected based on the analytical and numerical results in Chapter 3. Figure 5-2 shows the average flux over core and source regions and Figure 5-4 shows the average flux over incremental sections of the core region. The flux is epithermal with 81.46% of the neutrons that cause fission in the 0.625 eV – 100 keV range and neutron flux peaks at 25 keV and 1 MeV. In comparison, the source region has a harder spectrum, due to the fact that there is a higher fission rate in the region. This is evidenced by the larger 1 MeV peak from prompt fission neutrons. The spectrum for the core can be compared to Figure 5-3 which shows the Th(n,γ) cross sections as a function of neutron energy.

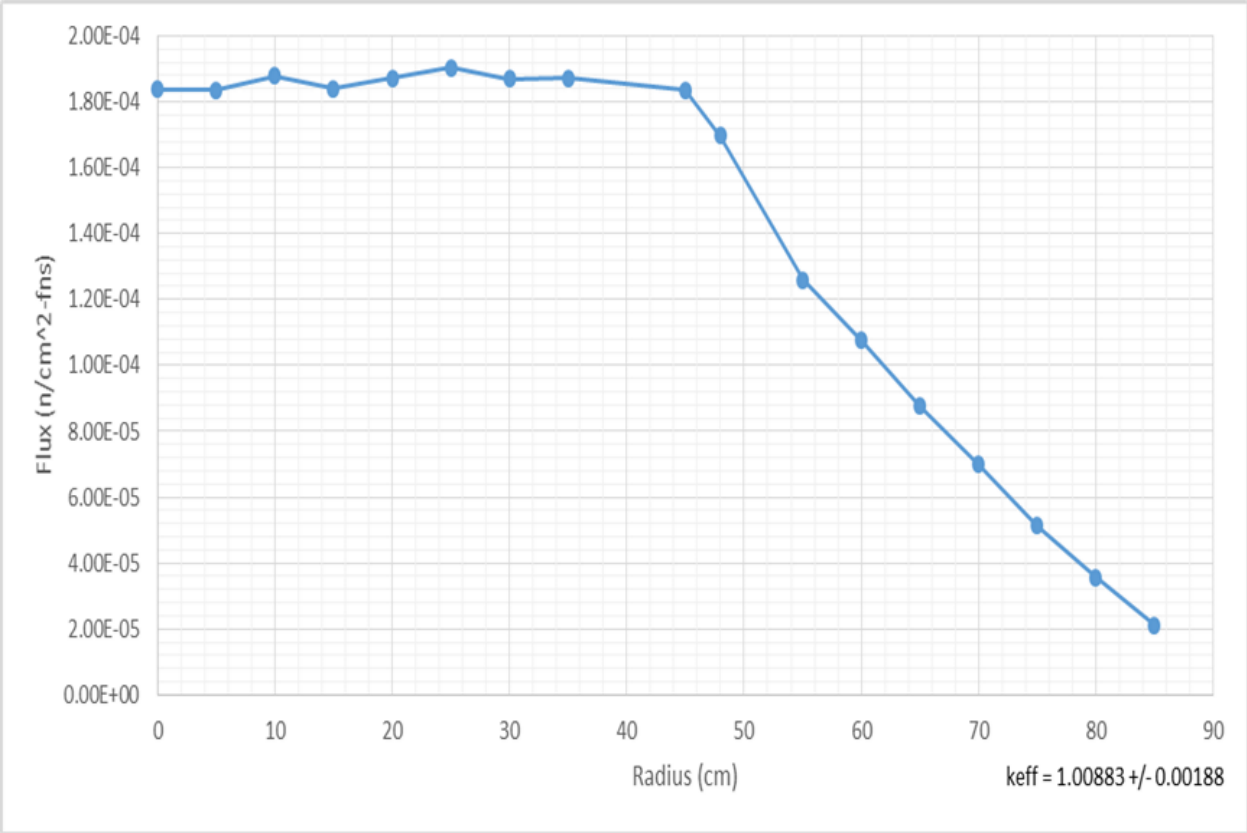

Figure 5-1 Flux vs radius for core surrounded by fissile source region.

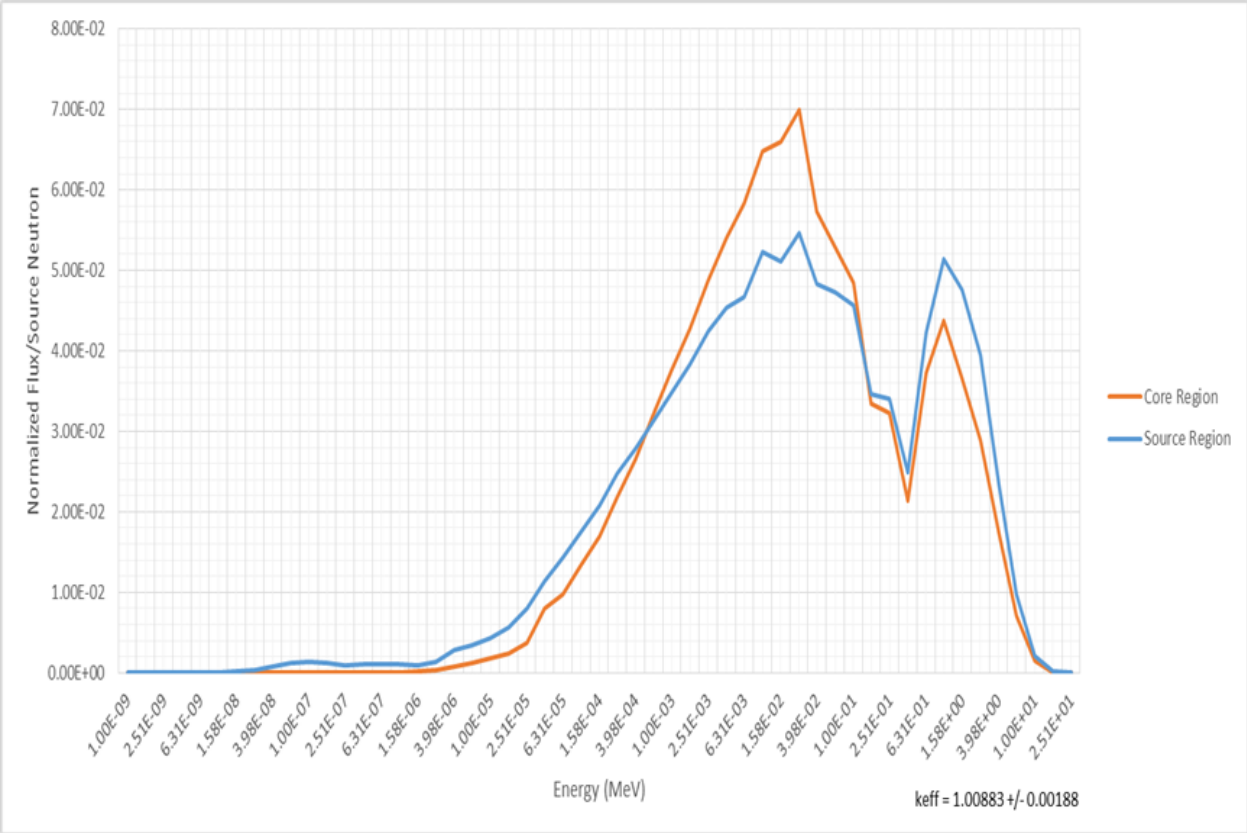

Figure 5-2 Averaged flux spectrum over the core and source regions.

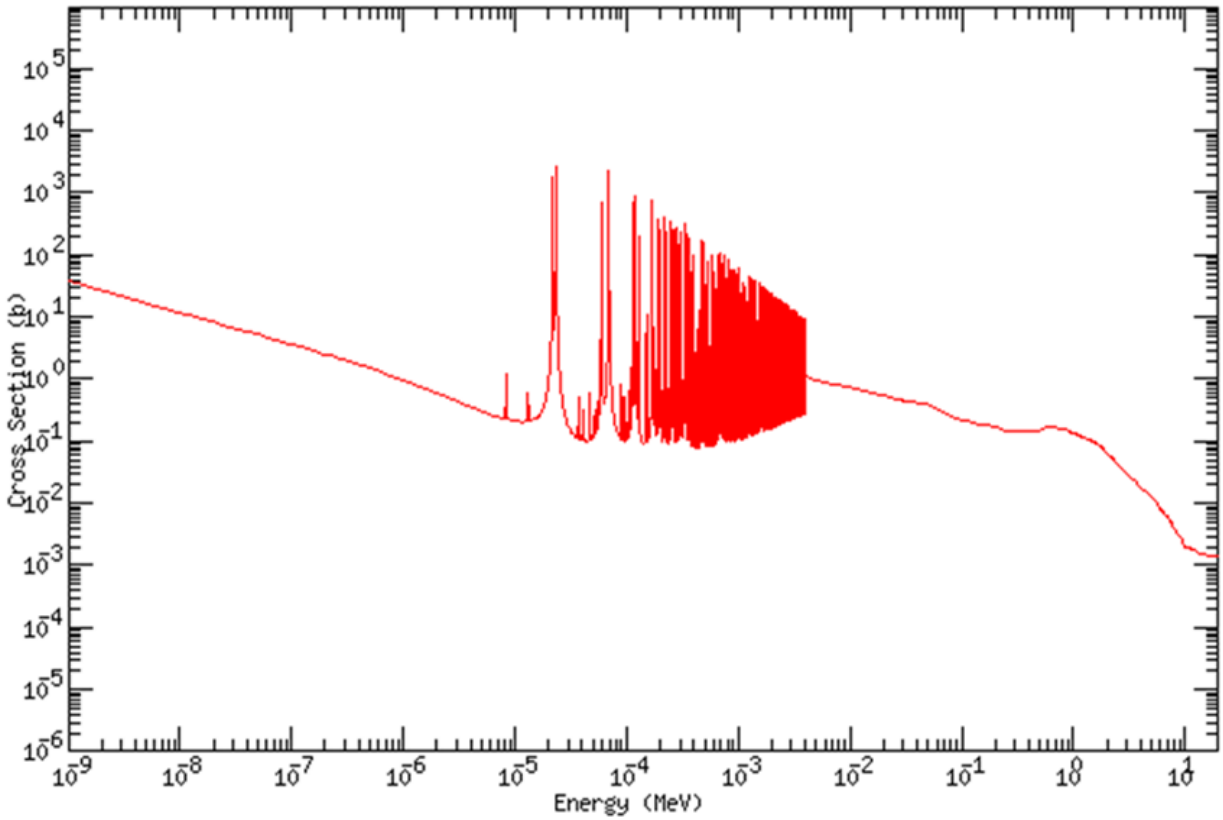

Figure 5-3 Thorium radiative capture cross section vs energy [76].

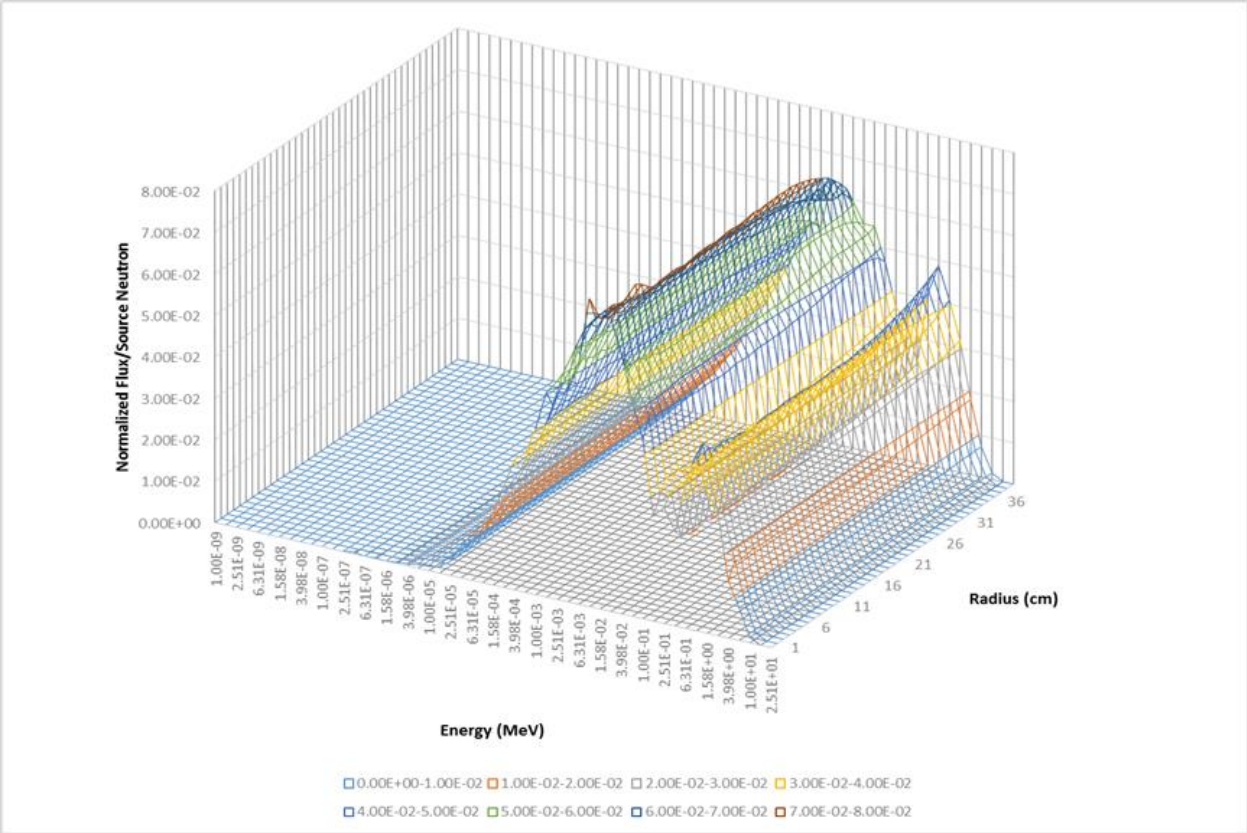

Figure 5-4 Average flux spectrum over incremental radial sections in the core region.

The comparison shows that the spectrum for the reactor is adequate for breeding ^{233}U. Table C.1 in Appendix C lists the results from the MCNP5 model. From the F6 tally, the total energy per fission source is 25.4 MeV in the core and 47.8 MeV in the source region. Limiting the power density to 120 kW/L, each region can produce up to 32 MW. Since the source region has a higher heating rate, this means that the core region will have a lower power. From Equation 4-14:

$$N = \frac{32\ [MW]}{47.8\left[\frac{MeV}{n}\right] * 1.602\ x\ 10^{-13}[\frac{J}{MeV}]} = 4.2E18\ n/s$$

$$4.2E18\ n/s = \frac{P_{core}[MW]}{25.4\left[\frac{MeV}{n}\right] * 1.602\ x\ 10^{-13}[\frac{J}{MeV}]}$$

$$P_{core} = 17\ MW$$

$$4.2E18\ n/s = \frac{P_{source\ region}[MW]}{47.8\left[\frac{MeV}{n}\right] * 1.602\ x\ 10^{-13}[\frac{J}{MeV}]}$$

$$P_{source\ region} = 32\ MW$$

The neutron rate calculated from Equation 4-14 is 4.2E18 n/s, thus, given a fixed neutron rate in both regions, the total power for the system would be 49 MW_{th}. The fission rate in the core is 0.134 per neutron source. Conversely, the Th(n,γ) reaction rate is 0.197 per neutron source. Taking the ratio of fissile production to consumption, yields 1.4 for the breeding ratio in the core. However, the fission rate in the source region is 0.272 per source neutron. Thus, the entire system is not breeding, but has a conversion ratio of 0.49. This poses a problem as ^{233}U is only produced in nuclear reactors, so being able to supply itself with the isotope is an important aspect of thorium reactors. An option to alleviate this problem would be to use another fissile isotope in the source region such as ^{239}Pu or ^{235}U. Alternatively, one could also drive the system in a subcritical state with a fusion neutron source.

CHAPTER 6

DT DRIVEN FAIL-SAFE REACTOR

Instead of a spherical core as in the fissile fail-safe reactor, the fusion source driven system is modeled in a cylindrical geometry. The radius of the core is 75 cm and the height of the cylinder is 150 cm. Surrounding the core is a 40 cm reflector. Between the reflector and the core is a fusion source, of which could be any number of IEC type devices of which will be explored in a following section.

The system is kept subcritical with a $k_\infty = 1$ and keff ≤ 0.90. This k_{eff} value places an important condition on the fusion device, the lower the k_{eff} for the system, the greater the fusion rate required to keep the fission system at the desired power level.

Since the system is driven by a DT source, it is imperative to make sure that the fuel salt can breed enough tritium to replace what is consumed to power the system. Two isotopes of interest can be used to produce tritium in the fuel salt, ^{7}Li and ^{6}Li. The two (n,T) reactions can be described by the following equations:

$$^{6}_{3}Li + n \rightarrow {}^{4}_{2}He + {}^{3}_{1}T \quad (6\text{-}1)$$

$$^{7}_{3}Li + n \rightarrow {}^{4}_{2}He + {}^{3}_{1}T + n \quad (6\text{-}2)$$

The ^{6}Li reaction is possible for a wide range of neutron energies as shown in Figure 6-1, while the ^{7}Li reaction only occurs with high energy neutrons. It is important not to have too much ^{6}Li in the fuel salt, which is why it is excluded from all other salt compositions in this thesis. If too many ^{6}Li(n,t) reactions occur, then neutrons will be diverted from fissile breeding.

Thus, a parametric study of the fissile and fusile breeding with increasing concentration of ^{6}Li in the salt was performed. The fuel salt is kept at the same composition as with the fissile fail-safe reactor, however ^{6}Li concentrations have been adjusted along with ^{233}U concentrations in order to keep the core at the same k values without altering the dimensions. As shown in Figure 6-2, the system cannot have breeding ratios of one or above for both tritium and ^{233}U at the same

time. Because, ^{233}U breeding is considered more important for the reactor, a concentration of ^{6}Li that yields a maximal amount of tritium breeding (0.89) while maintaining a fissile breeding of one was selected. Thus, an external source of tritium will need to be supplied to the fusion reactor. This concentration is lower than the 7.2% abundance of ^{6}Li in natural lithium and can be attributed to the fact that lithium composes such a large fraction of the salt and that the DT source can breed some of the tritium from the ^{7}Li. The tabulated results of the tallies for each of the trial salts in Figure 6-2 are listed in Appendix C Table C.2.

With the fuel salt selected, the reactor design can be analyzed. The system has an initial inventory of 4.3 metric tonnes of thorium and 578.7 kg of ^{233}U. Using the same salt power density as the fissile fail-safe reactor, the reactor power is calculated to be 318 MW_{th}. Figure 6-3 shows the average flux spectrum for the core. Much like the fissile driven system, the spectrum is more epithermal than fast. There are three clear peaks this time, one at 25.1 keV, 1 MeV, and one at 14.6 MeV. The 14.6 MeV peak is due to the fusion source and shows up as a small peak in the core averaged flux spectrum. From Figure 6-4 one can see the average flux spectrum at 3 cm radial increments. The fusion neutron energy is shown prominently at the edge of the reactor core and dissipates radially in the core.

From the MCNP output, the net multiplication for the system is 3.09 and the average neutron emitted per fission is 2.5. Using Equation 4-23, k_{eff}^{FS} is 0.776 compared to the KCODE k_{eff} which is 0.883. Using the average heating rate, 231.47 MeV/source neutron; the fission rate, 1.28 per source neutron; and the k_{eff}^{FS}, the source strength can be calculated with Equation 4-24.

$$S_{fusion} = \frac{318{,}000{,}000[W]*2.5\left[\frac{neutron}{fission}\right]*1.28\left[\frac{fissions}{source\ neutron}\right]}{231.47\left[\frac{MeV}{source\ neutron}\right]*\left(1.602\ x\ 10^{-13}\left[\frac{J}{MeV}\right]\right)} * \frac{1-0.776}{0.776} = 7.92E18\ n/s \qquad (6\text{-}3)$$

The source strength can be converted to total fusion power by utilizing the amount of energy released per DT fusion event, 17.57 MeV.

$$P_{source} = S\left[\frac{n}{s}\right] * E\left[\frac{MeV}{n}\right] * 1.602\ x\ 10^{-13}\left[\frac{J}{MeV}\right] \qquad (6\text{-}4)$$

$$= 7.92E18\ *17.57*1.602\ x\ 10^{-13} = 22.3\ \text{MW}$$

Furthermore the annual fissile production/consumption is given by:

$$S * U * \frac{M}{N_A} * 3.15E4 \left[\frac{kg.s}{g.yr}\right] \quad (6\text{-}5)$$

where

S = the source strength

U = the number of Th(n,γ)/U(n,f) reactions per source neutron/

Using the above equation, the total annual production for the reactor is 123.6 kg/year. This is just enough to replace the amount of fissile material annually consumed by the system. Lastly, Figures 6-5 and 6-6 show the radial and axial flux profiles for the core. The radial flux is fairly stable across the core and rises on the edges due to the fusion source. This follows the expected profile for a core with k_∞ and k_{eff} less than one with an external source shown in Figure 3-4.

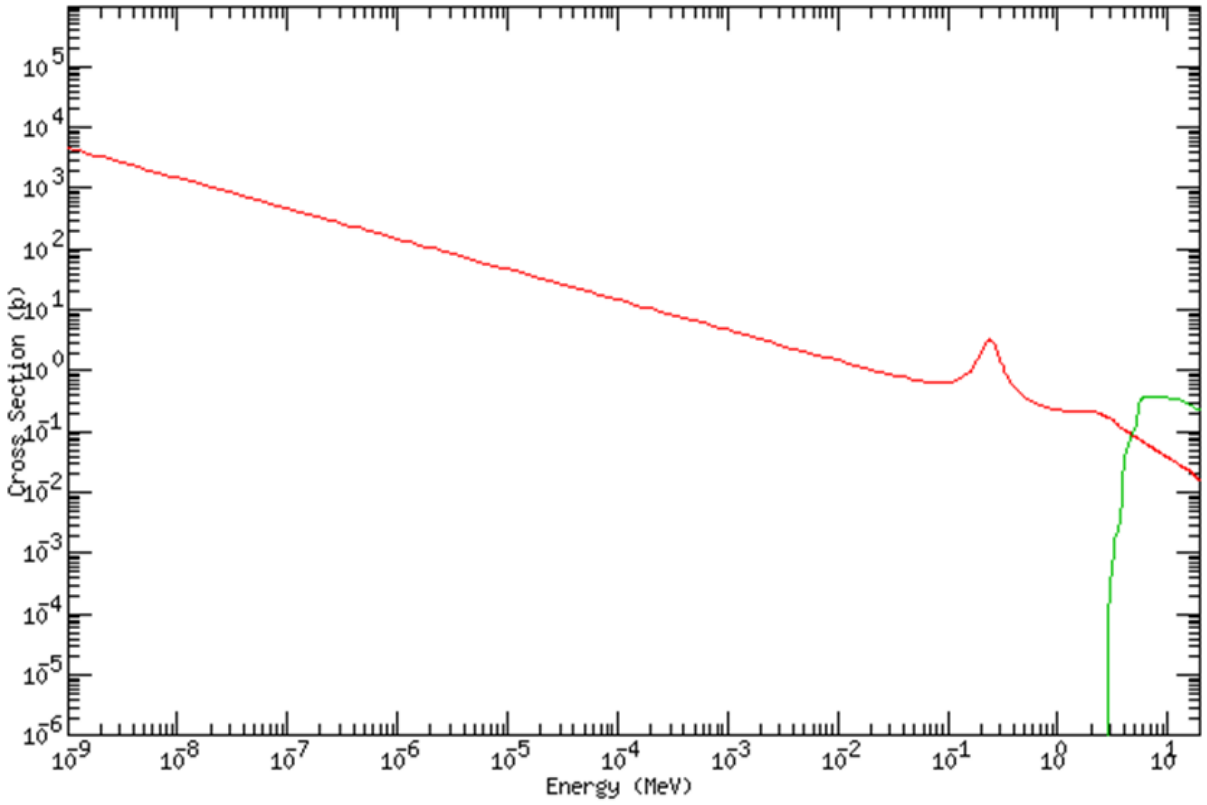

Figure 6-1 Tritium breeding cross sections for ^{6}Li (red) and ^{7}Li (green) [76].

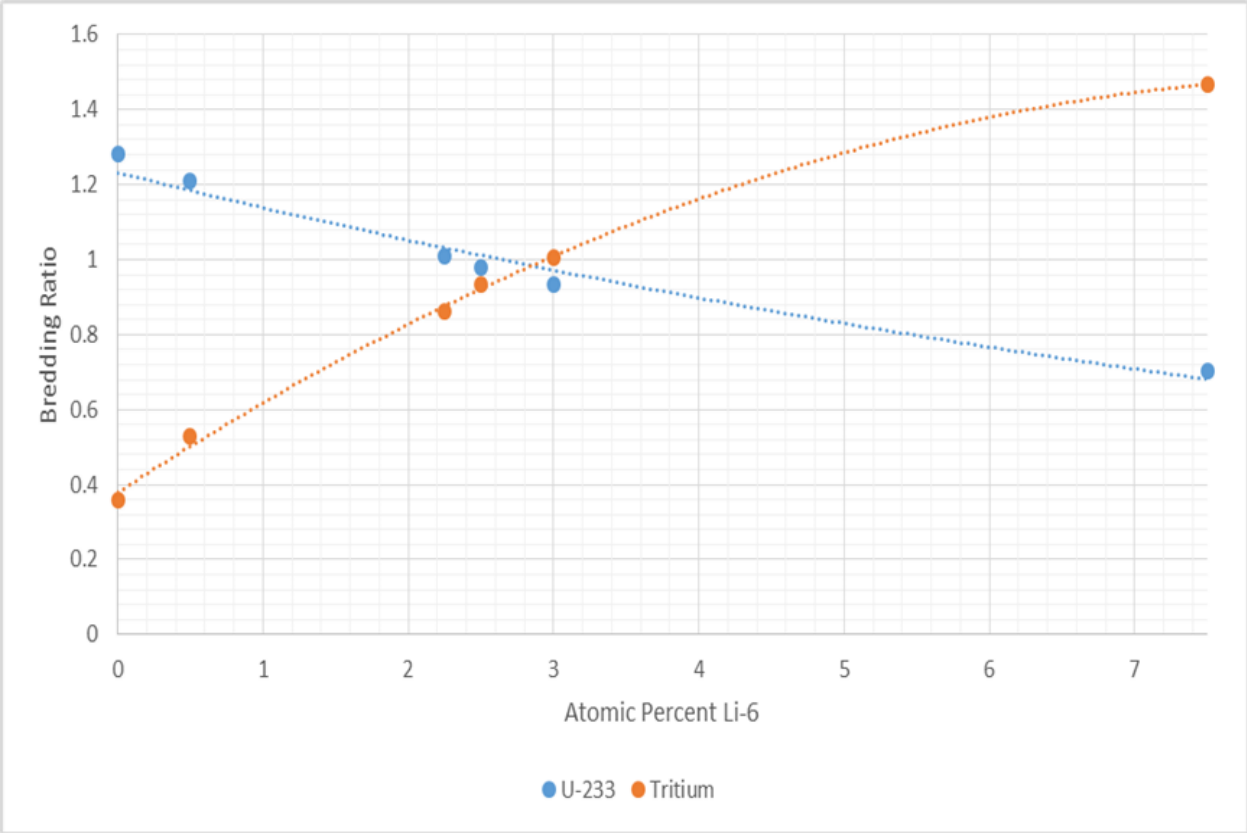

Figure 6-2 Fissile and fusile breeding vs ^{6}Li concentration.

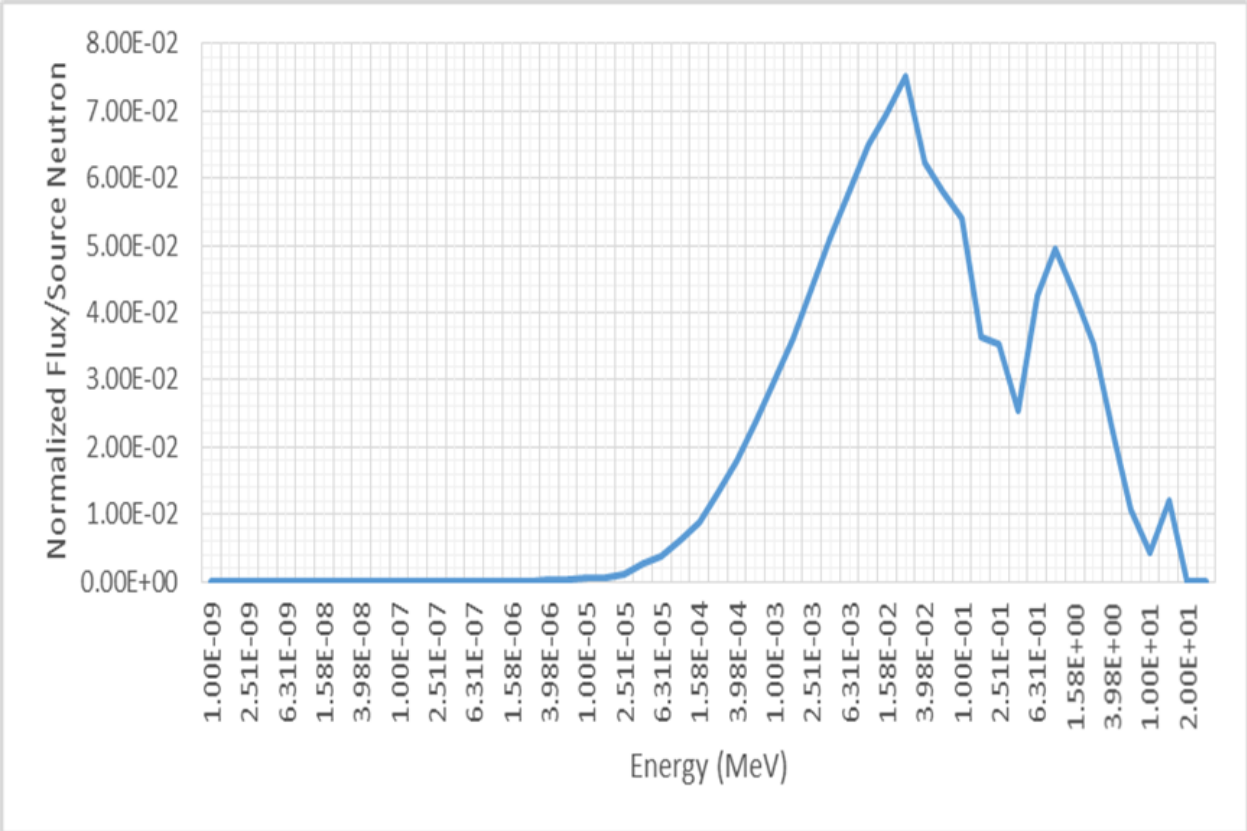

Figure 6-3 Flux averaged over the core for DT system.

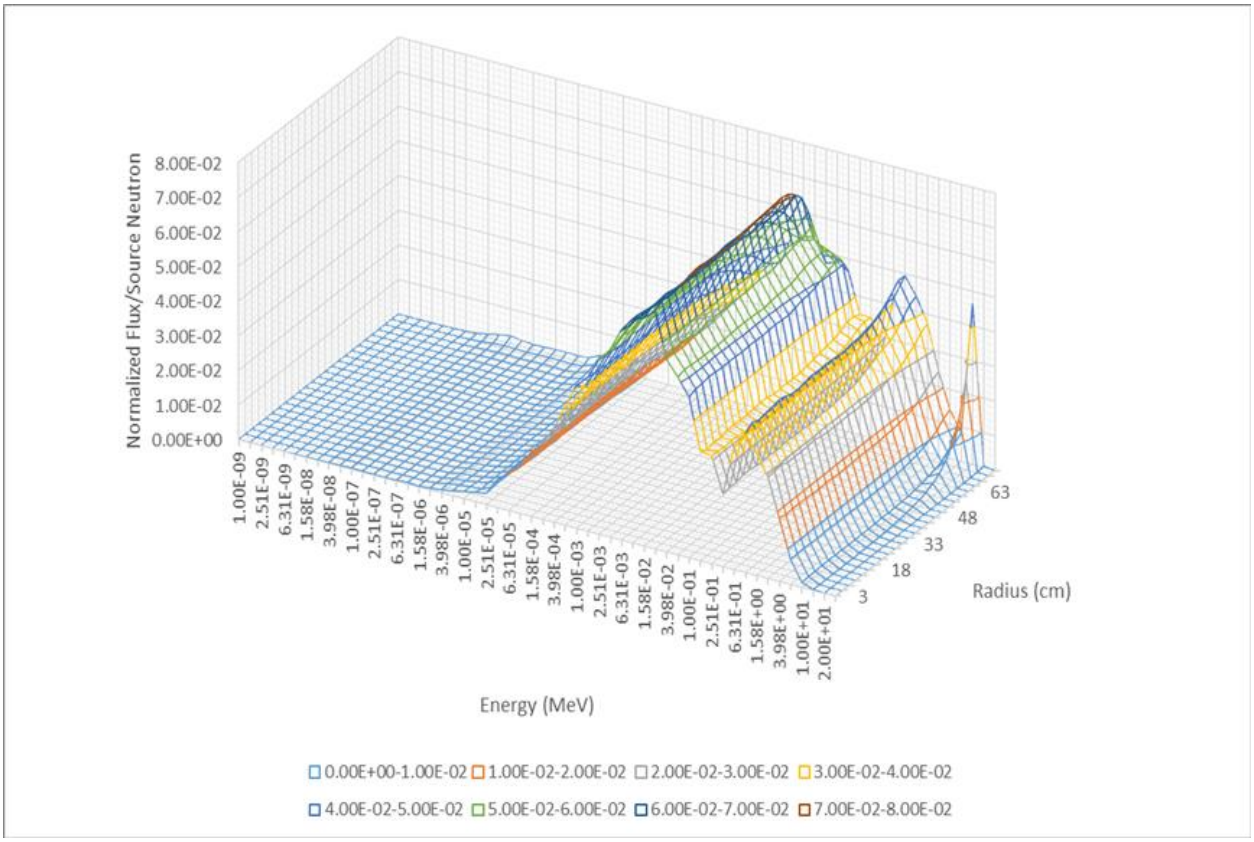

Figure 6-4 Average flux spectrum over incremental radial sections for DT system.

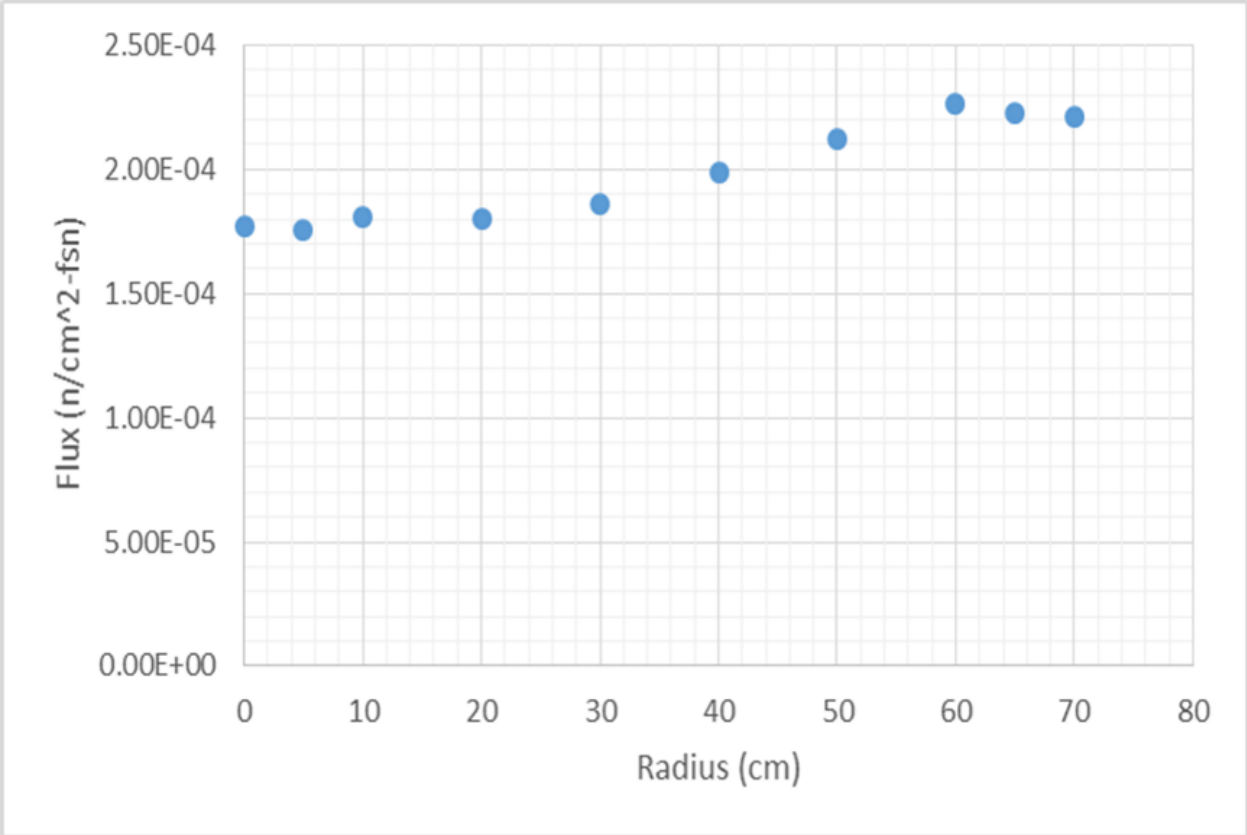

Figure 6-5 Radial flux profile for DT system.

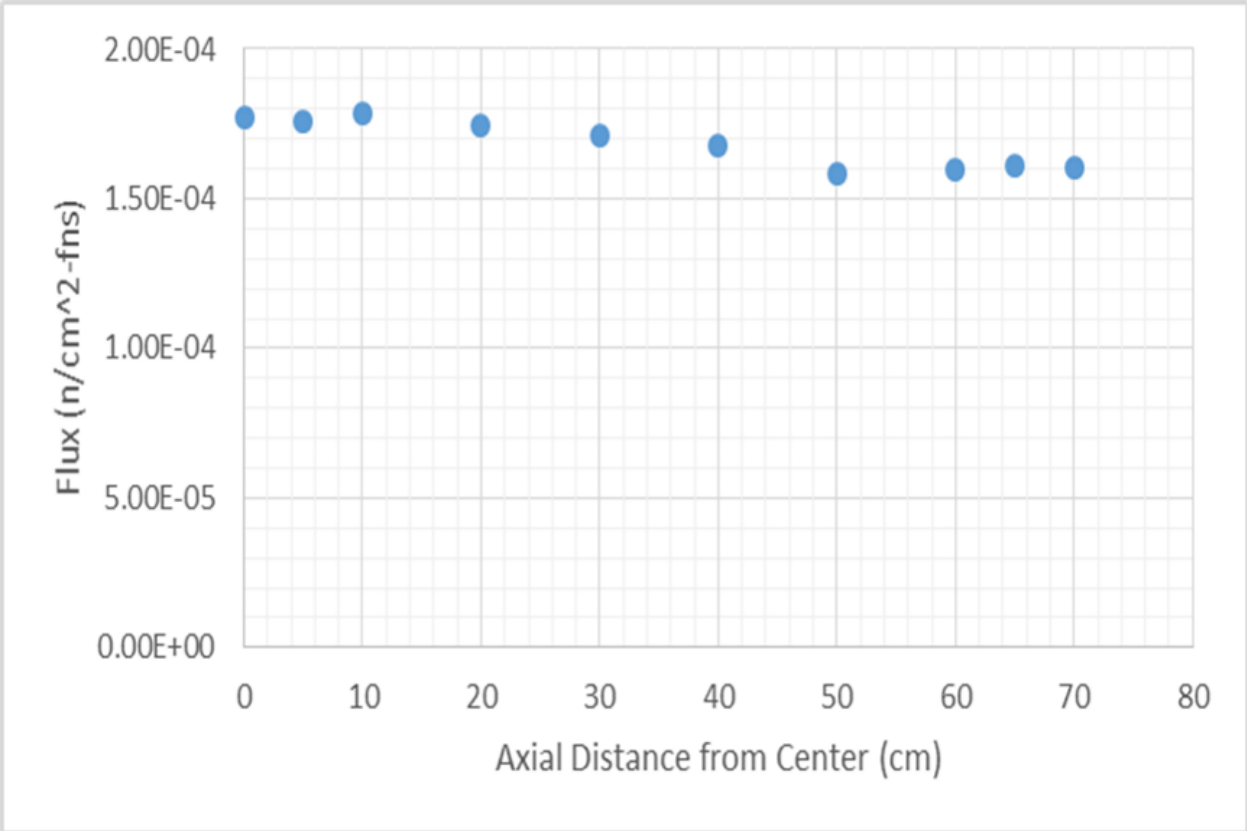

Figure 6-6 Axial flux profile for DT system.

CHAPTER 7

DD DRIVEN FAIL-SAFE REACTOR

The DD driven system utilizes the same geometry as the DT driven system. Because the DD driven system does not require tritium, lithium in the salt can be replaced by sodium. A comparison will be made between these two salt systems.

The DD system with a lithium salt is composed of 16% BeF_2 – 71.02% ^7LiF – 12% ThF_4 – 0.98% UF_4, while the sodium salt is composed of 16% BeF_2 – 70.94% NaF– 12% ThF_4 – 1.06% UF_4. Compositions for the different salts were chosen such that the $k_\infty = 1$ and the $k_{eff} \leq 0.90$. The results of the two salt compositions are compared in Appendix C, Table C.3. Figure 7-1 compares the flux spectrum for the two fuel salts. Notice that both have peaks at 25 keV and 1 MeV, while the sodium salt appears to have an additional peak at 1.58 keV. However, this additional peak is actually caused by sodium's large absorption cross section at around 3 keV (Figure 7-2). Aside from sodium's preferential absorption at around 3 keV, the two salts produce a remarkably similar flux spectrum.

From the MCNP output, the net multiplication in the sodium salt is 3.0642 versus 3.3706 for lithium. Using Equation 4-23, the k_{eff}^{FS} for the sodium system is 0.775 and 0.798 for the lithium system. The sodium system has a lower heat rate at 251.28 MeV per source neutron versus 292.67 MeV per source neutron. This is attributable to the higher fission rate in the lithium system, as the ratio of the heat rate to fission rate for both systems is the same. Keeping the power of the DD system the same as the DT system, 318 MW_{th}, and using Equation 4-24, the required fusion source strength is 6.72E18 n/s for the Li salt and 7.20E18 n/s for the Na salt.

DD fusion can be described by the following two reactions:

$$_1D^2 + {}_1D^2 \rightarrow {}_1T^2\,(1.01\text{ MeV}) + {}_1H^1\,(3.03\text{ MeV}) \qquad (7\text{-}1)$$

$$_1D^2 + {}_1D^2 \rightarrow {}_2He^4\,(0.82\text{ MeV}) + {}_0n^1\,(2.45\text{ MeV}) \qquad (7\text{-}2)$$

Each of these reactions occur with approximately equal rates. This means that a neutron is emitted only half of the time, and thus to achieve the required neutron source strength twice as many fusion

events will need to occur. Thus, the DD source power can be calculated from Equation 6-4 with the average fusion energy from DD fusion, 3.66 MeV, multiplied by two. The required fusion power for the lithium system is 7.9 MW and 9.0 MW for the sodium system.

The initial fissile inventory for the sodium system is slightly lower at 300.8 kg versus 359 kg in the lithium system. Additionally the initial thorium inventory is lower at 3.39 tonnes versus 4.3 tonnes. With a breeding ratio of 1.26 and a core power of 318 MW, the net fissile production rate is 32.9 kg/year in the sodium system. Likewise, for a similar power lithium system with 1.27 breeding ratio, the net fissile production is 35.2 kg/year. This translates to a shorter doubling time of 9.2 years for the sodium system versus 10.2 years in the lithium salt system. Figures 7-3 to 7-6 show the radial and axial flux profiles for each of the salt system. Both have a fairly flat profile in the radial direction that increases toward the edge of the core. This is consistent with a core with k_∞ and k_{eff} below unity with an external source as show in Figure 3-4. Overall the sodium system is quite similar to the lithium system. The advantage lies in the fact that the for the lithium system, all the ^6Li has to be removed and this can be quite costly. However, the sodium system can achieve favorable results while being much cheaper.

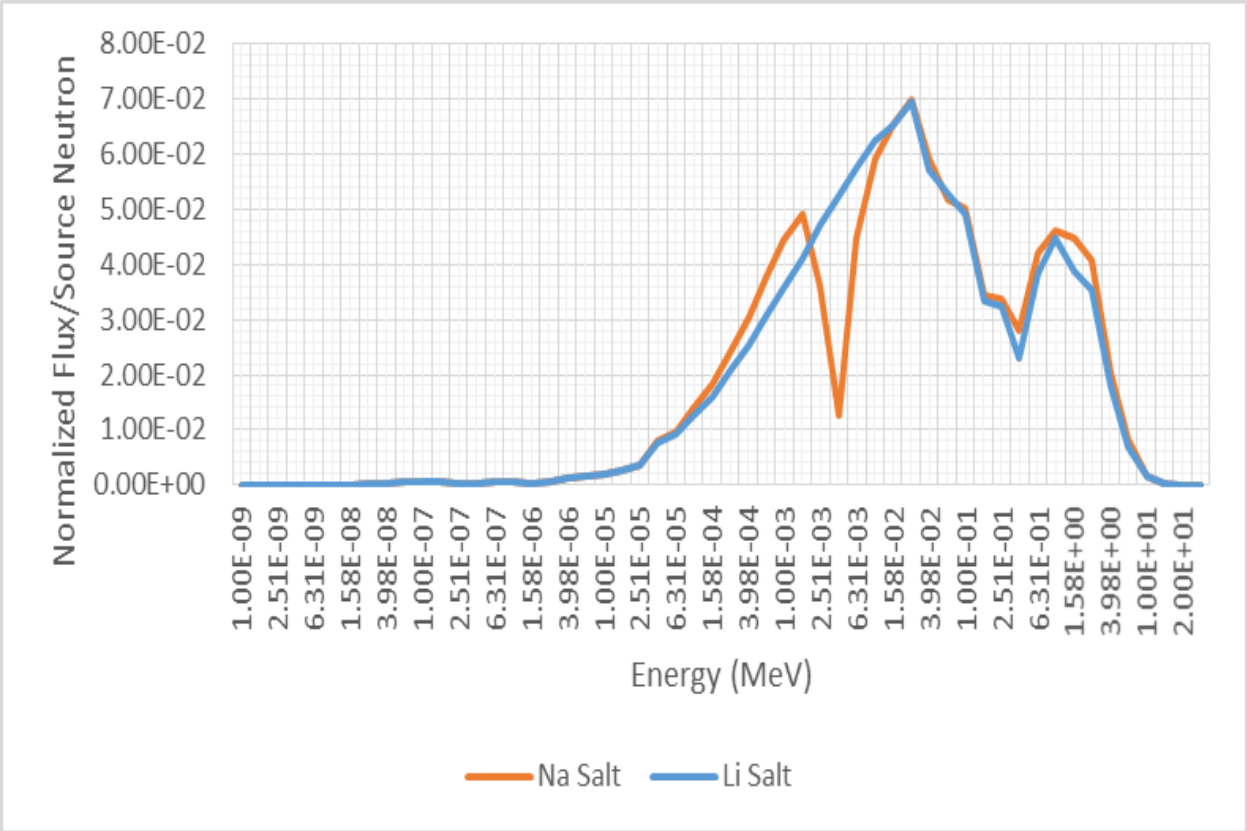

Figure 7-1 Flux averaged over the core region of the Li and Na salt systems.

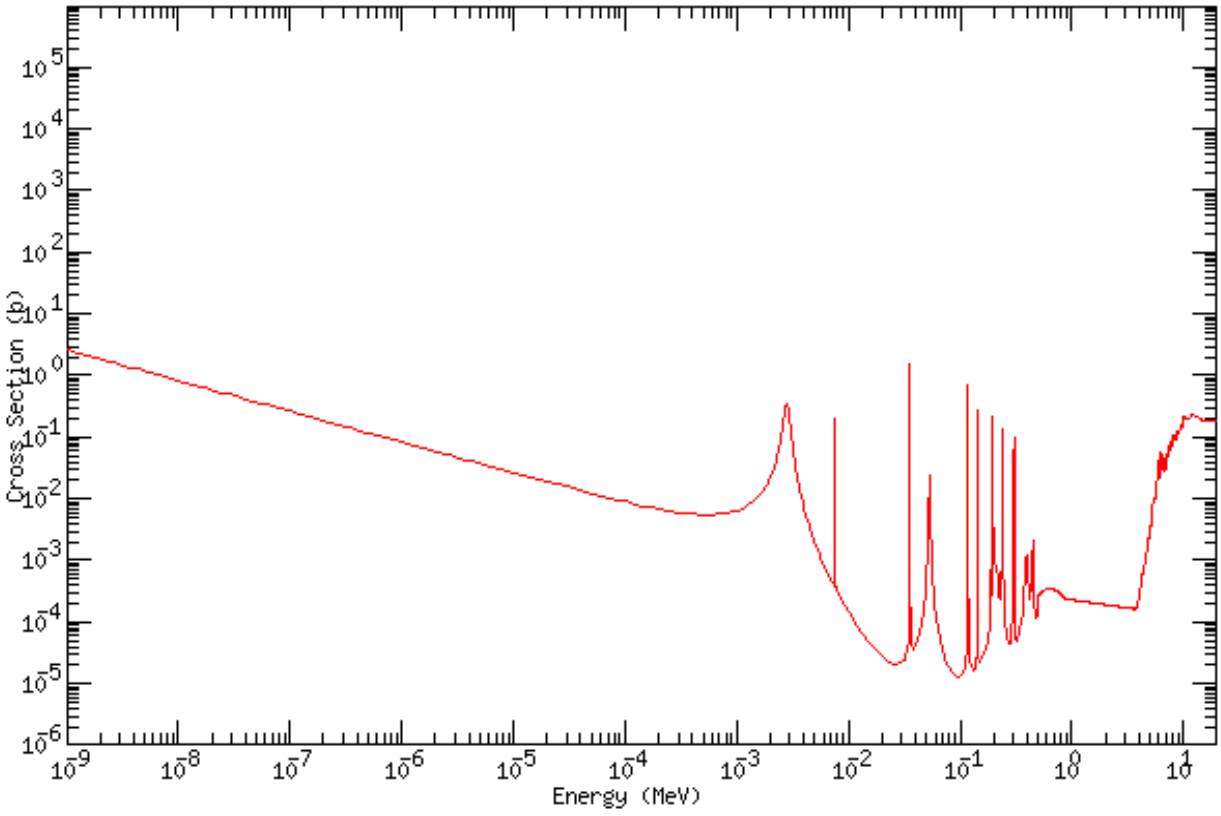

Figure 7-2 Na Absorption cross sections as a function of energy [76].

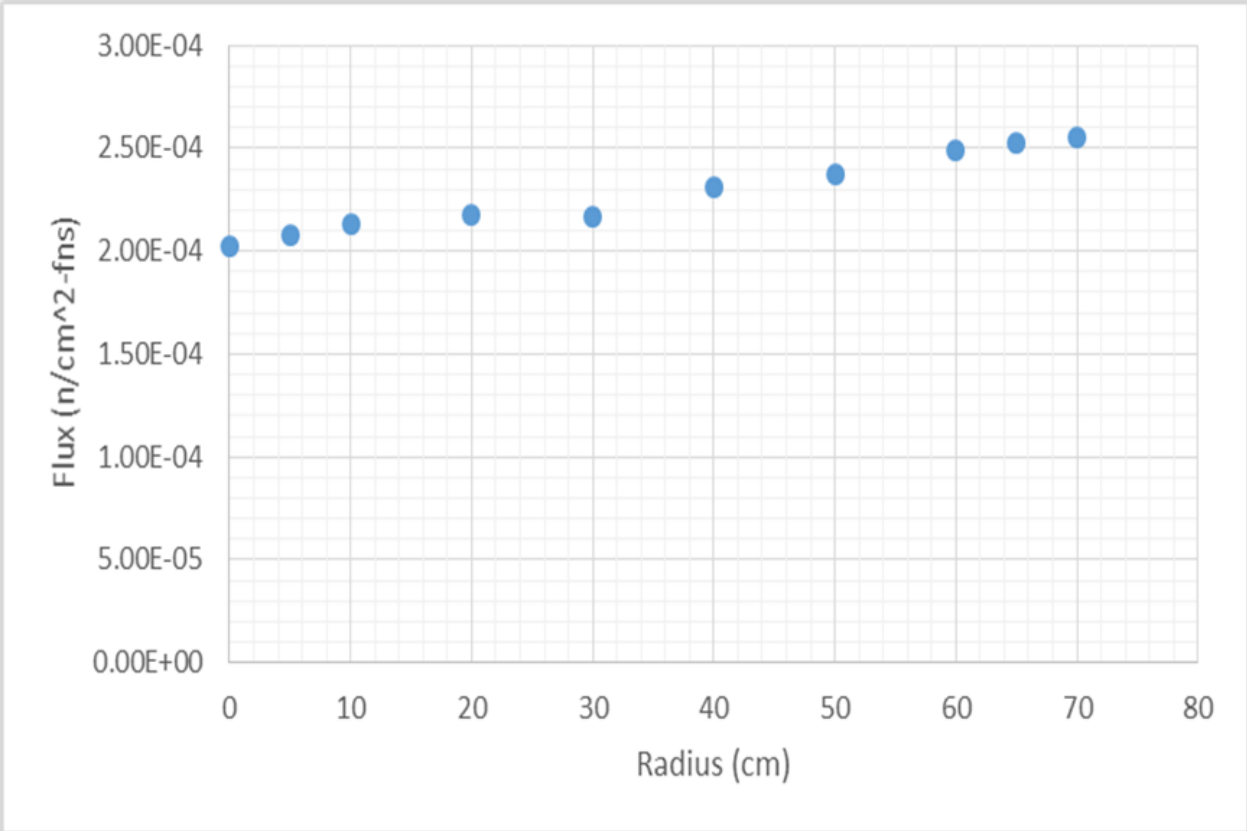

Figure 7-3 Radial flux profile for Na system.

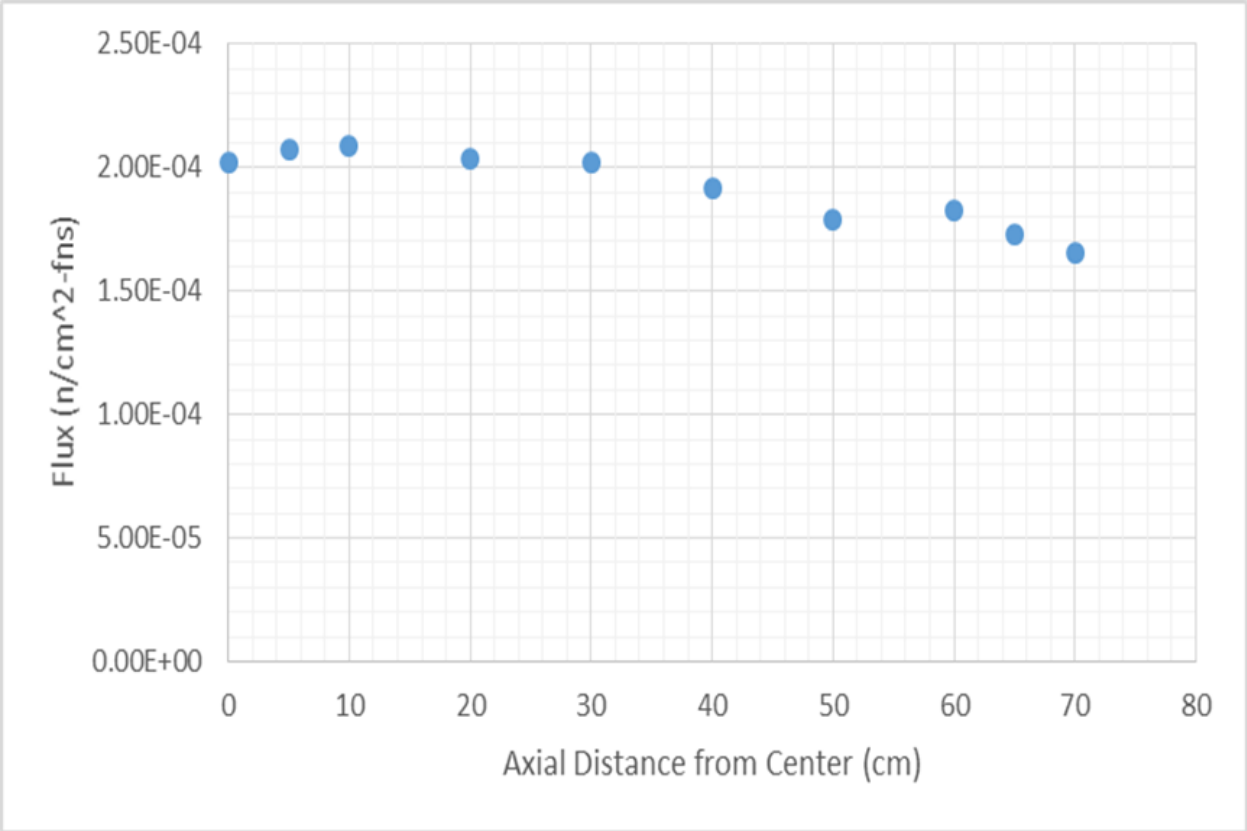

Figure 7-4 Axial flux profile for Na system.

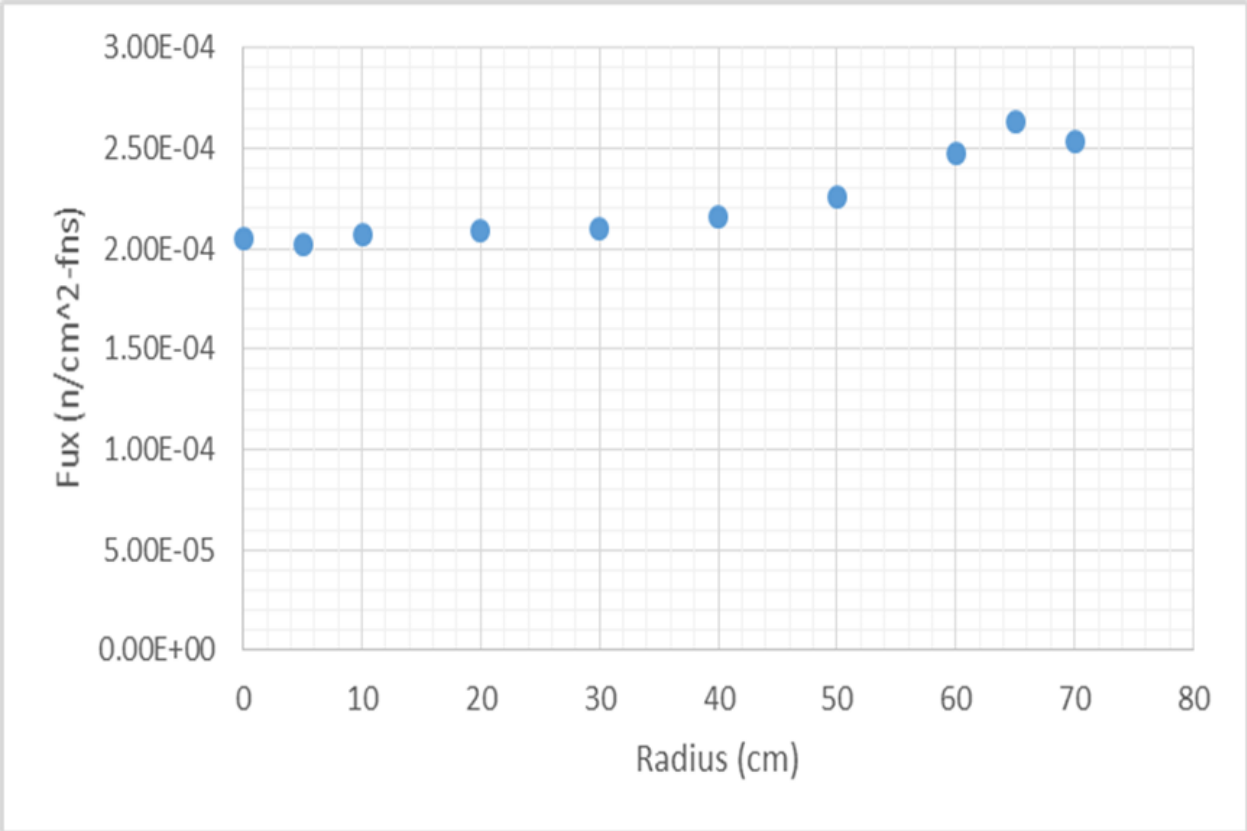

Figure 7-5 Radial flux profile for Li system.

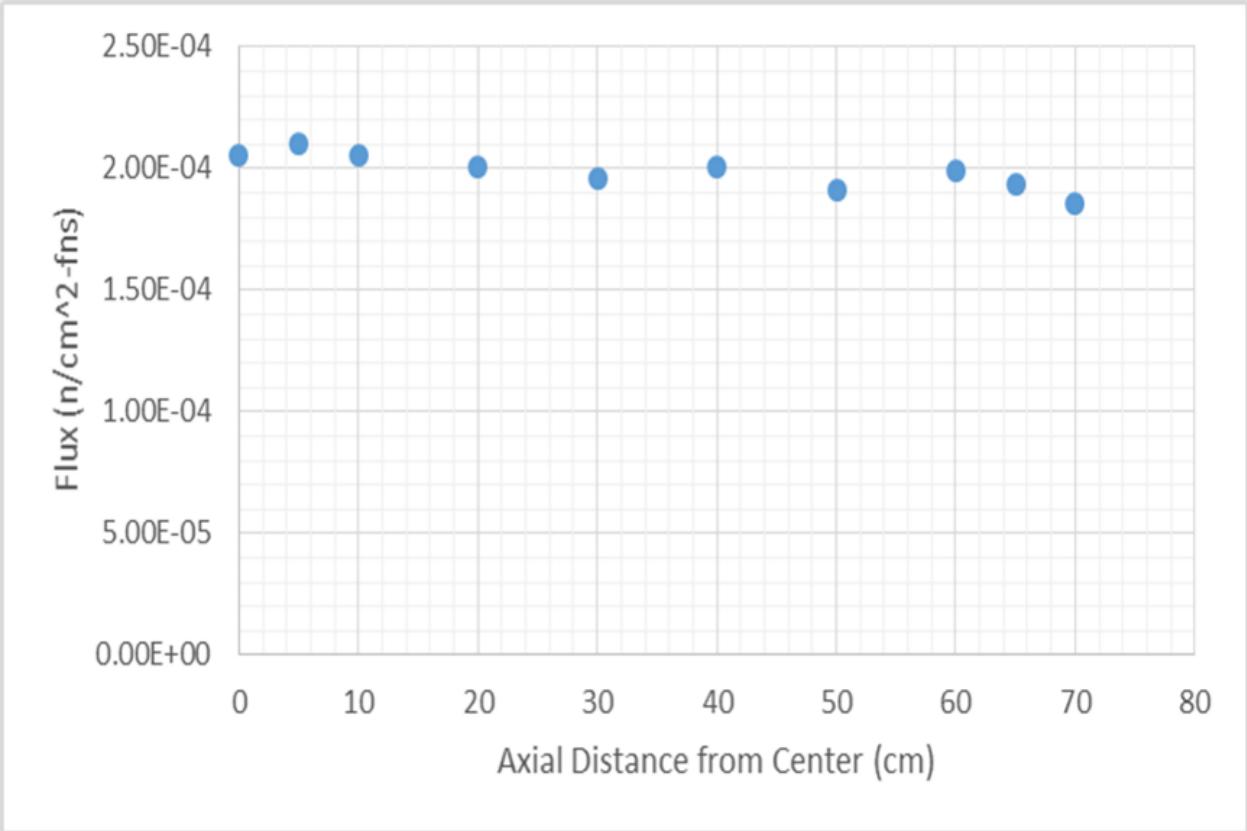

Figure 7-6 Axial flux profile for Li system.

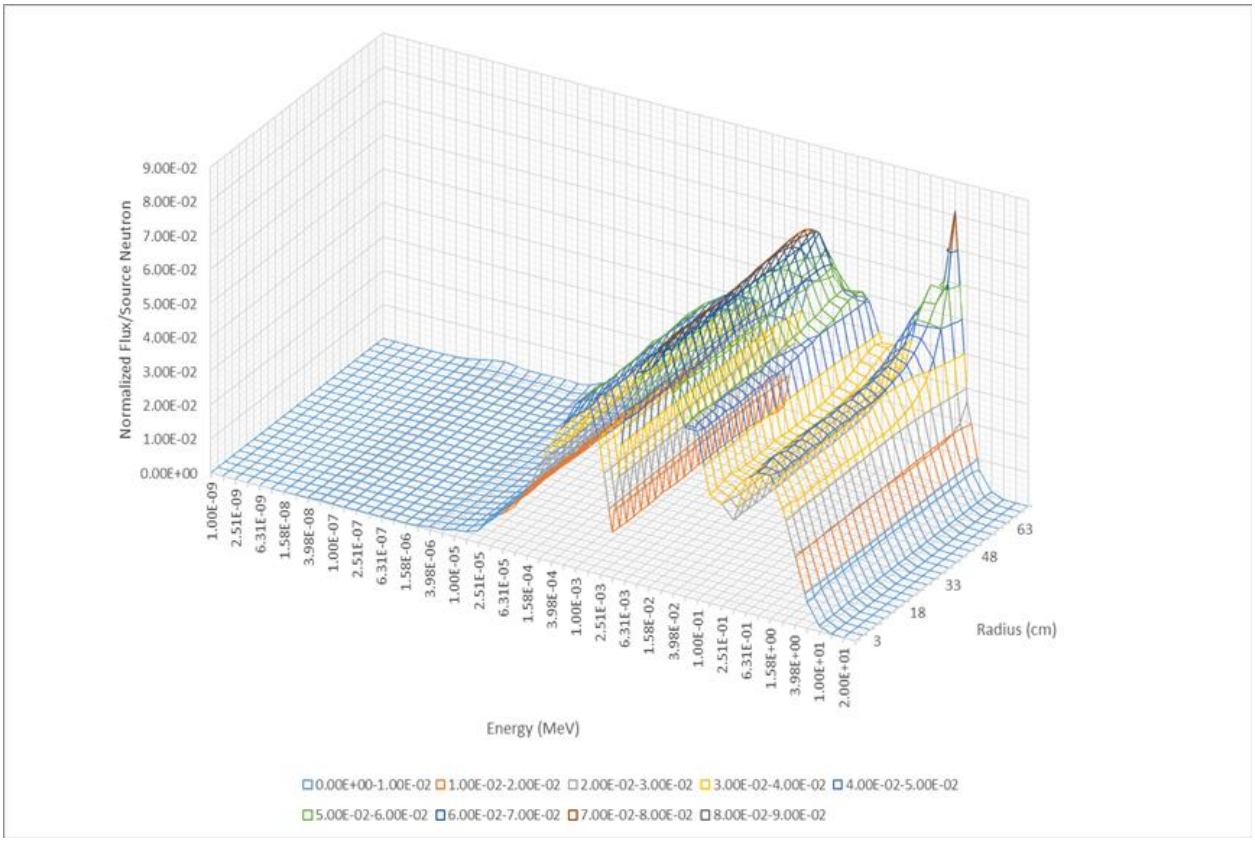

Figure 7-7 Average flux spectrum over incremental radial sections in Na system.

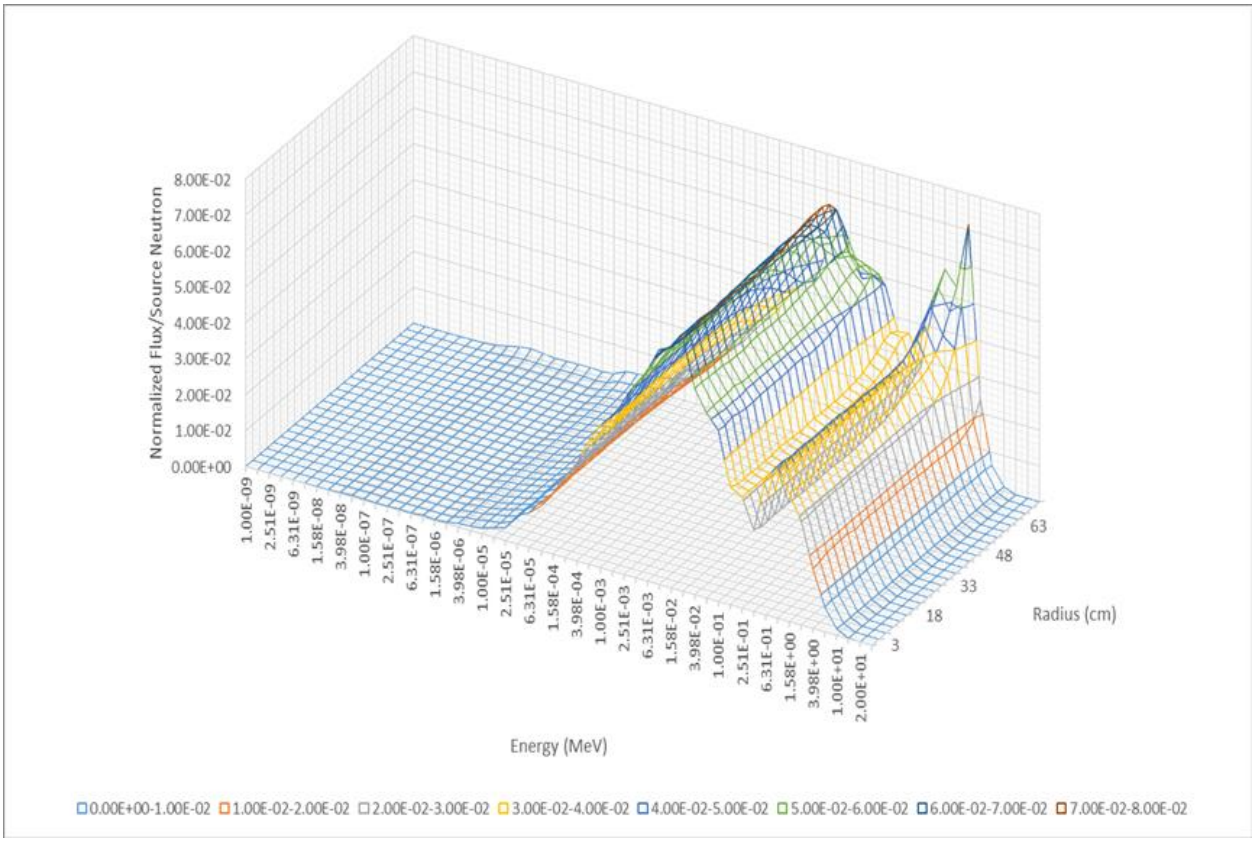

Figure 7-8 Average flux spectrum over incremental radial sections in Li system.

CHAPTER 8

OTHER DESIGN CONSIDERATIONS

8.1 Reactivity Control and Safety

First and foremost molten salt reactors offer a great deal of stability compared to their solid fuel counterparts. MSR's are designed with a salt plug drain below the reactor vessel. The plug must be actively cooled and in the case of a loss of power accident or if the fluid becomes too hot, the salt plug will melt and the molten salt will drain into a passively cooled containment vessel capable of removing the decay heat from the system. Furthermore, molten salts have a very strong negative temperature and void coefficients.

Another advantage of molten salt systems is the ability to process the fuel during plant operation to remove fission products. To remove the uranium from the salt, the fluoride volatility process can be utilized. Hydrogen fluoride and then F_2 gas is bubbled through the salt. The uranium is converted from UF_4 to UF_6 and is released from the salt as a gas. The UF_6 is then converted back to UF_4 as needed. This method is also applicable to higher actinides such as plutonium. Fission products can also be removed by several methods such as vacuum distillation or liquid bismuth reductive extraction [73]. Gaseous fission products, such as xenon and krypton are continuously removed by sparging the salt with helium gas [74]. This ability to remove fission products and adjust the fissile concentrations in the salt during operation allows one to maintain stable reactivity and removes the need for burnable poisons. A single control rod can be included for start-up and shutdown but is not necessary due to the ability to drain fuel out of the core and into criticality safe storage tanks.

The reactors detailed in this thesis offer even greater safety features than traditional molten salt reactors. In the fissile fail-safe reactor, the extra fissile material surrounding the core offers greater flexibility in reactivity control, as the core and source salt fissile concentrations can be varied during operations to maintain optimal conditions. Furthermore, the core cannot achieve criticality without the source region material present. This is because the core is at $k_\infty = 1$ and therefore $k_{eff} < 1$ due to neutron losses. Without the source region, the fissile source driven fail-

safe reactor modeled in Chapter 5 would have a $k_{eff} = 0.61365 \pm 0.00045$. The neutrons produced in a given neutron generation can be modeled by:

$$N_n = k_{eff}^n \tag{8-1}$$

where

n = the neutron generation

Thus the number of neutrons produced by fission in the reactor can be modeled by Figure 8-1. This can be extended to show the evolution of the neutron flux with each generation in Figure 8-2.

Similarly, the fusion source driven systems are subcritical. This makes criticality accidents near impossible, since k_{eff} is not near 1. Additionally, reactivity can be easily controlled by varying the source strength. Again, without the source present, the system cannot maintain criticality, making the system very stable.

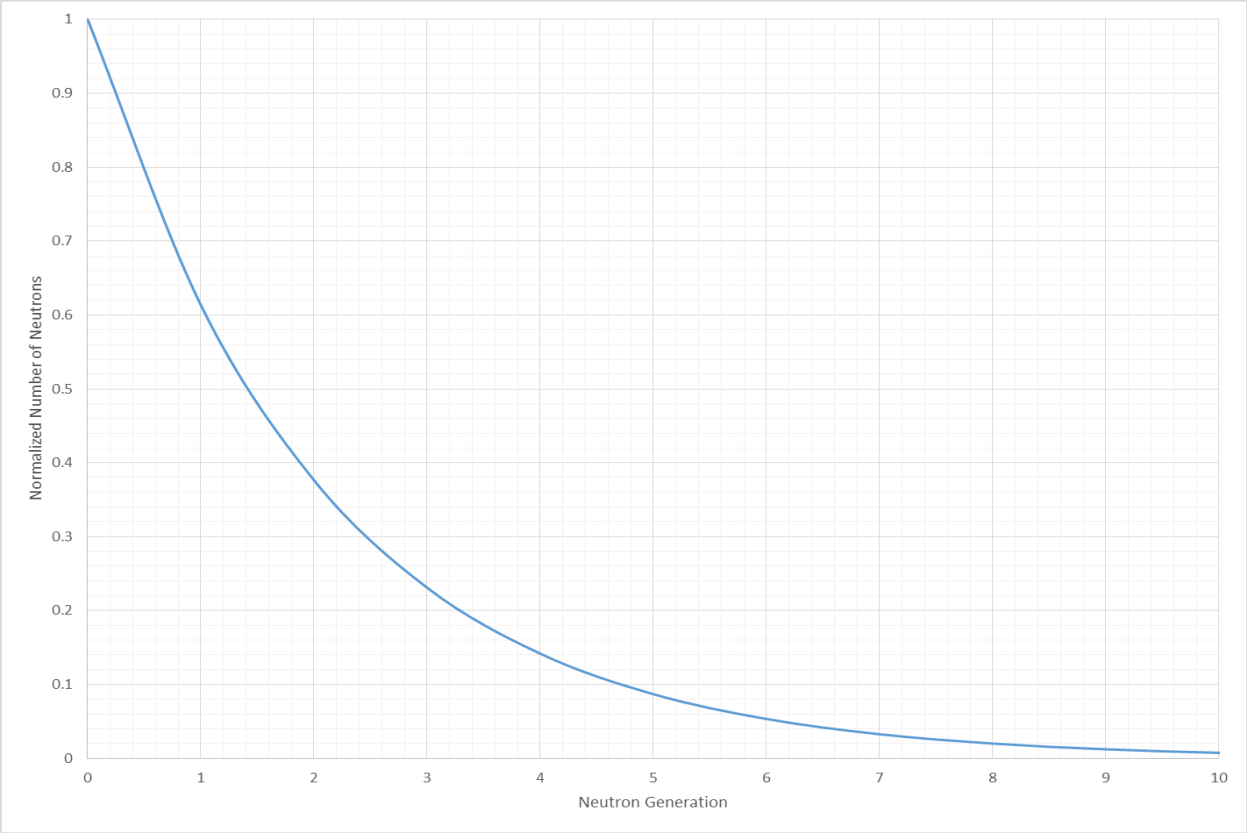

Figure 8-1 Number of neutrons produced from fission as a function of neutron generation.

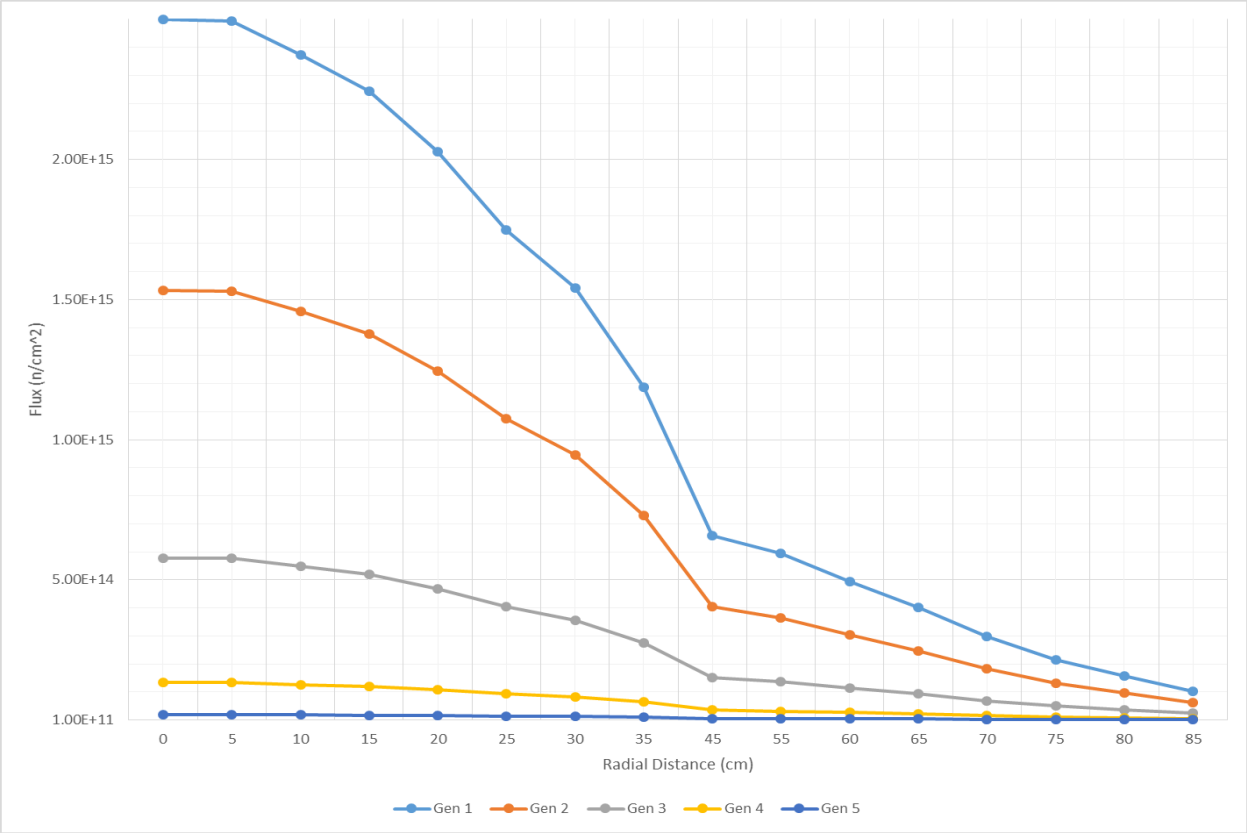

Figure 8-2 Radial flux over different neutron generations.

8.2 Fusion Driver

There are many types of fusion devices that can drive the subcritical reactors investigated in this thesis. The focus has been to utilize inertial electrostatic confinement fusion devices due to their compact and simple designs. One method to drive the subcritical reactors, is to surround the core with several cylindrical IEC devices. This can take the form of something similar to the C-device that is being researched by Dr. Miley and his colleagues at the University of Illinois. The system is composed of an outer vacuum chamber. A cylindrical stainless-steel cathode tube and two circular concave stainless-steel anode reflectors are located inside the glass chamber. The cathode tube is located in the center of the chamber and the anode reflectors are located at the ends. When the system operates the ions are accelerated toward the cathode tube and then pass through and are decelerated before reaching the anodes. Then the ions are accelerated back toward the cathode, resulting in an oscillating motion along the electric field lines many times. Because the cylindrical cathode is effectively transparent to the ions, there is a high ion recirculation in the system. The device is capable of producing a neutron rate of 10^{12} DT n/s [75]. However, to fulfill the requirements of the 318 MW_{th} reactor proposed, neutron rates will need to be several orders of magnitude higher.

Alternatively, one could investigate fusion devices that utilize plasma confinement by magnetic cusp fields such as has been advocated by Robert Bussarard. However, Bussard's polyhedral device geometry is not ideal for the proposed reactors. Several other magnetic cusp arrangements, though, might work better for the cylindrical geometry such as a linear arrangement of ring cusps or a cusp-ended solenoid. Magnetic cusp confinement methods have proven to be capable of producing 10^{6}-10^{12} n/s. With further research and development, it is possible to scale these devices to the source strengths required.

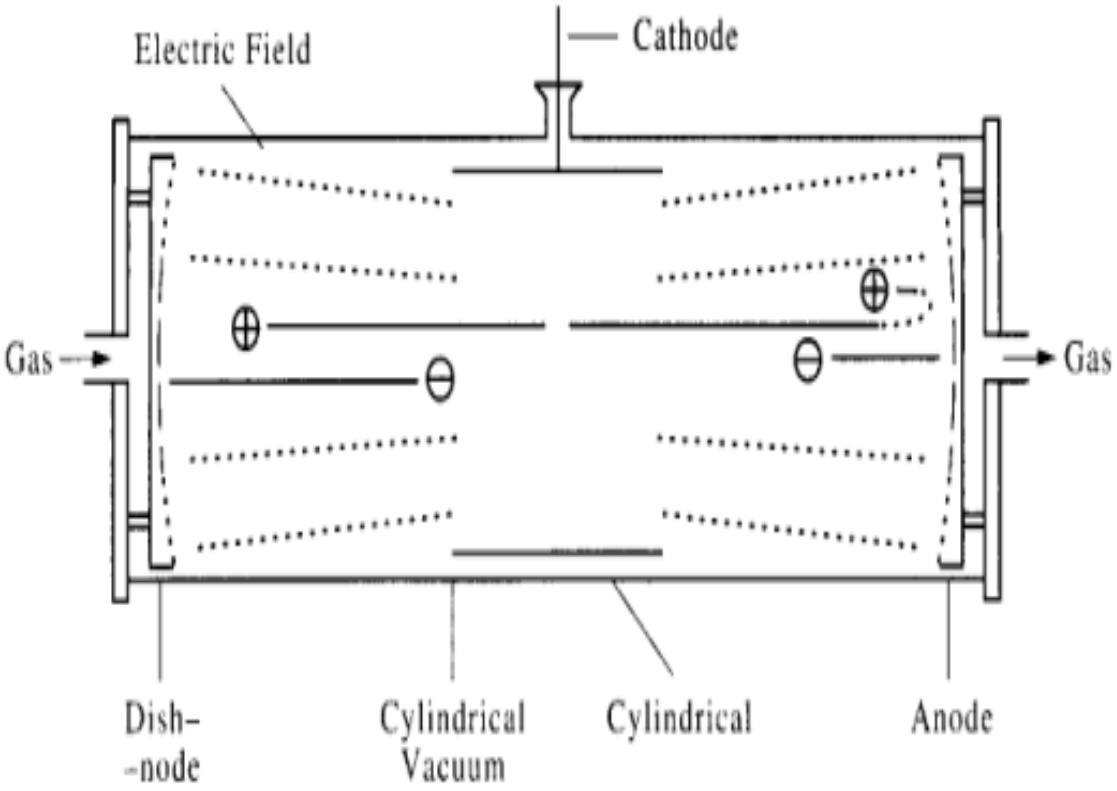

Figure 8-3 C-device schematic [74].

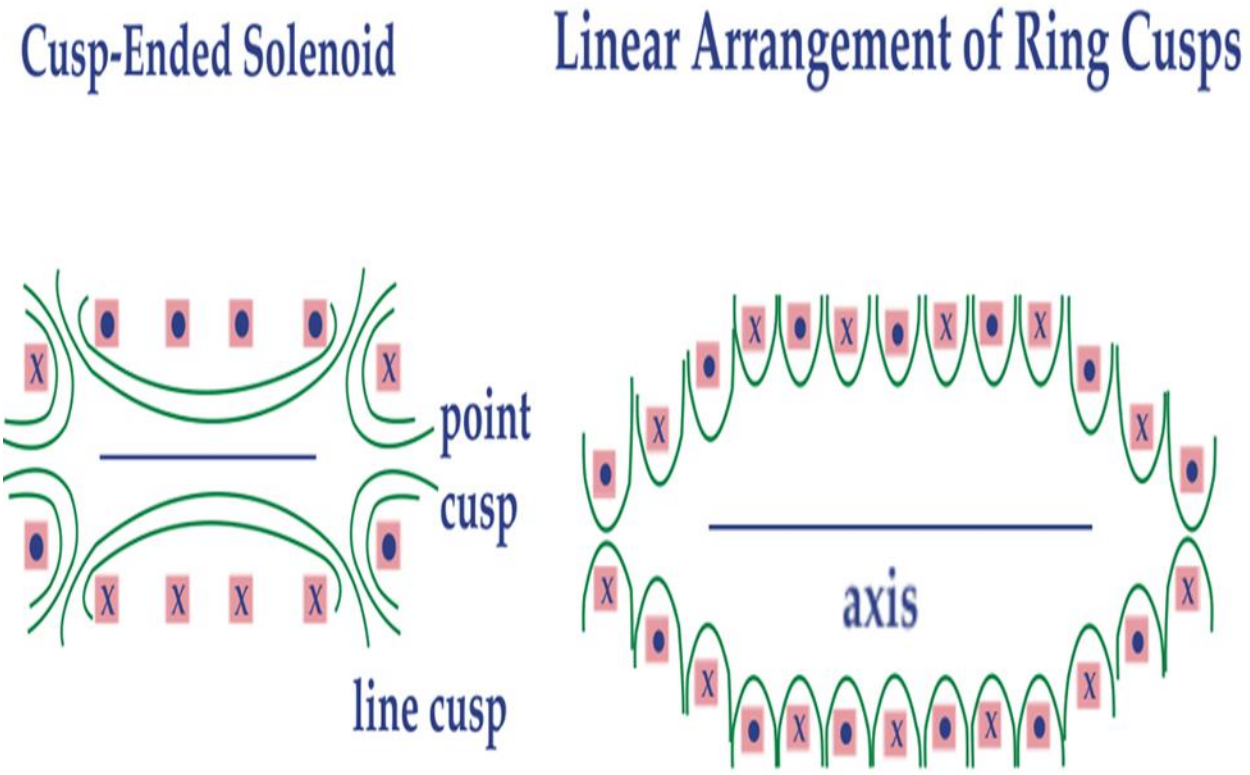

Figure 8-4 Magnetic cusp configurations [75].

CHAPTER 9

DISCUSSION AND CONCLUSIONS

9.1 Discussion of Results

Presented in this work is a design study of a fail-safe nuclear reactor driven by a fissile or fusion-fission neutron source. An analytical and numerical analysis of a unity infinite medium multiplication factor core with an external neutron source was performed and followed by a detailed continuous energy Monte Carlo neutronics analysis using the MCNP5 computer code. Three neutron sources were selected for the study, a fission neutron source, a DD and DT fusion neutron source.

The fissile neutron source driven system was modeled by a spherical molten salt reactor utilizing a ^{232}Th and ^{233}U FLiBe salt. The reactor is made critical with the addition of thin region of salt surrounding the core with a higher fissile material concentration. With a core k_∞ and a system k_{eff} of unity, the flux in the core becomes flat, resulting in uniform fuel burnup. Additionally, fusion neutron sources were studied as possible neutron sources. These systems were modeled by a cylindrical core surrounded by several cylindrical electrodynamic inertial fusion generators. The fission core of these reactors was designed with a $k_\infty = 1$, while the overall system was subcritical with $k_{eff} \leq 0.9$.

From the results obtained, a DD fusion could be the most advantageous neutron source for source driven systems. In terms of blanket multiplication, the energy deposited in the blanket divided by the source neutron energy, both the DD systems had above a hundred fold increase in energy. However, this understates the challenges of the DD system compared to a DT system. To drive a nuclear reactor at the same power level requirements, the DD system would need to have twice the fusion rate, as neutrons are only produced once every two fusion events. Furthermore, the energy confinement time at a given pressure must be thirty times longer than a DT system. This means that DD fusion is harder to achieve and any likely fusion system running on it would have a lower fusion power gain (Q_p). However, as investigated, the DD system does have the advantage of not requiring tritium production, and thus can utilize sodium salts with comparable

results to lithium based systems. Compared to the fission source driven systems, the fusion driven systems alleviate the need utilizing a ^{235}U-^{239}Pu fuel cycle in the source region due to their ability to breed. This provides for lower waste production over the lifetime of the reactor.

The discussed subcritical systems provide improved safety and reactivity management options compared to traditional systems. However, the k_{eff} is lower with the fast fusion neutrons. The implications of this is that the k_{eff} will actually increase when the fusion neutrons are removed. However, k_{eff} will not be able to go above 1, as the system criticality was designed with a $k_{eff} \leq 0.9$. The cause of this decrease in reactivity may be attributed to the presence of fluorine and beryllium in the molten salt, whose absorption cross sections are higher in the 1-20 MeV range. Beryllium, on the other hand, is a desirable neutron multiplier that can contribute to the process of breeding. A fast or intermediate neutron energy neutron spectrum was attempted in this design, and thus graphite moderation was purposely avoided. Graphite lifetimes can be greatly diminished in fast neutron fluxes as well. Another option is to utilize salts without beryllium or fluoride. However, this will be left for further investigation. It is also worth further investigation as the lower k_{eff} essentially means that the fusion neutrons are being less efficiently used in the system.

The results of the investigation suggest that source-driven systems associated with a molten-salt can be contemplated with substantial fail-safe benefits. Running a subcritical reactor eliminates the need for excessive reactivity control systems and provides safety in a loss of power transient situation. Furthermore, utilizing a fissile neutron source yields beneficial power and flux profiles. Lastly, such systems can breed fissile material and support a future alternative Th-U^{233} thorium fuel cycle.

9.2 Recommendations for Future Work

The results from the MCNP5 code in this work are for a static, steady-state system. However, to get a better picture of the proposed reactor system, it would be beneficial to utilize the ORIGEN 2.2 fuel depletion code and Monteburns to couple the two programs. ORIGEN 2.2 is a time dependent isotope generation and fuel depletion code. The Monteburns program can facilitate communication of MCNP and ORIGEN2.2 during a simulation.

MCNP5 sends one group cross section and flux parameters to ORGIEN2.2, which then send back updated material compositions to MCNP to account for nuclide transmutation. In this

way, a more accurate picture of fusile and fissile breeding can be obtained. Additionally the buildup of ^{232}U for in the system for proliferation analysis can also be obtained.

While accelerator-driven systems using spallation sources were briefly discussed in the thesis, they were not simulated as a possible neutron sources. However, these systems are worth investigating as they may hold additional advantages to fusion source driven systems. This can more accurately be done by utilizing the MCNPX (Monte Carlo N-Particle eXtended) code which can simulate proton interactions with a spallation target to get a neutron spectrum for the system.

REFERENCES

1. "U.S. Energy Information Administration - EIA - Independent Statistics and Analysis." EIA. U.S. Energy Information Administration, Sept. 2011. Web. 17 Apr. 2012. <http://www.eia.gov/forecasts/ieo/>.
2. International Atomic Energy Agency, IAEA, "Power Reactor Information System, PRIS," 2012.
3. World Nuclear Association. Another drop in nuclear generation World Nuclear News, 05 May 2010.
4. Shultis, J. Kenneth., and Richard E. Faw. Fundamentals of Nuclear Science and Engineering. 2nd ed. New York: Marcel Dekker, 2002. Print.
5. "Small Nuclear Power Reactors." World Nuclear Association, July 2012. Web. 25 July 2012. <http://www.world-nuclear.org/info/inf33.html>.
6. "Thorium Fuel Cycle - Potential Benefits and Challenges." IAEA, May 2005. Web. 1 June 2012.
7. "Thorium." World Nuclear Association, 11 Nov. 2011. Web. 1 June 2012. <http://world-nuclear.org/info/inf62.html>.
8. Proceedings of the "2nd Thorium Enegy Alliance Conference, The Future Thorium Energy Economy," Google Campus, Mountain View, California, USA, March 29-30, 2010.
9. R.B. Grover, Subhash Chandra, Scenario for growth of electricity in India, Energy Policy, Volume 34, Issue 17, November 2006, Pages 2834-2847, ISSN 0301-4215, 10.1016/j.enpol.2005.04.021. (http://www.sciencedirect.com/science/article/pii/S030142150500131X)
10. "Nuclear Power in India." World Nuclear Association, 21 June 2012. Web. 15 July 2012. <http://www.world-nuclear.org/info/inf53.html>.
11. "China's Nuclear Fuel Cycle." World Nuclear Association, Apr. 2012. Web. 15 July 2012. <http://www.world-nuclear.org/info/default.aspx?id=26187>.
12. Brumfiel, Geoffrey. "Ray of Hope in ITER Cable Crisis." Nature News Blog. Nature Publishing Group, 01 Mar. 2012. Web. 15 July 2012. <http://blogs.nature.com/news/2012/03/ray-of-hope-in-iter-cable-crisis.html>.
13. "Nuclear Fusion Power." World Nuclear Association, Apr. 2012. Web. 22 Aug. 2012. <http://world-nuclear.org/info/inf66.html>.
14. Lidsky, L. M. "Fission-fusion Systems: Hybrid, Symbiotic and Augean." Nuclear Fusion 15 (1975): 151-73. IOP Science. Web. 18 Apr. 2012.
15. Duderstadt, James J., and Louis J. Hamilton. Nuclear Reactor Analysis. New York: Wiley, 1976. Print.
16. Ragheb, Magdi, and Lefteri Tsoukalas. "Global and USA Thorium and Rare Earth Elements Resources." Thorium Energy Alliance. Proc. of 2nd Throium Energy Alliance Conference, The Future Thorium Energy Economy, Google Campus, Mountain View. Mar. 2010. Web. July 2012.
17. Uranium 2007: Resources, Production and Demand, Nuclear Energy Agency (June 2008), NEA#6345 (ISBN 9789264047662).

18. M. Benedict, T H Pigford and H W Levi, Nuclear Chemical Engineering (2nd Ed.), Chapter 6: Thorium, , p.283-317, 1981, McGraw-Hill(ISBN: 0070045313)
19. IAEA. Thorium Fuel Cycle - Potetial Benefits and Challenges. Web. July 2012.
20. Kang, Jungmin, and Frank N. Von Hippel. "U-232 and the Proliferation-resistance of U-233 in Spent Fuel." Science & Global Security 9.1 (2001): 1-32. Print.
21. Moir, R. W. "Fission-suppressed Fusion Breeder on the Thorium Cycle and Nonproliferation." Fusion for Neutrons and Subcritical Nuclear Fission. Proc. of Fusion for Neutrons and Subcritical Nuclear Fusion, Varenna. Vol. 1442. Varenna: AIP, 2011. 346-55. AIP Conference Proceedings. American Institute of Physics, 15 Sept. 2011. Web. July 2012.
22. International Atomic Energy Agency, "The Physical Protection of Nuclear Material and Nuclear Facilities," INFCIRC/225/Rev.4 (http://www.iaea.org/worldatom/program/protection/index.html).
23. Irving Langmuir and Katharine B. Blodgett, "Currents Limited by Space Charge Between Concentric Spheres," Physics Review, 23, pp. 49-59, 1924.
24. Farnsworth, Philo T. "Electric discharge device for producing interactions between nuclei." U.S. Patent No. 3,258,402. 28 Jun. 1966.
25. Farnsworth, Philo T. "Method and Apparatus for Producing Nuclear-Fusion Reactions." U.S. Patent No. 3386,883, June 4, 1968.
26. Hirsch, Robert L. "Inertial-Electrostatic Confinement of Ionized Fusion Gases." Journal of Applied Physics 38.11 (1967): 4522.
27. Hirsch, Robert L. "Experimental Studies of a Deep, Negative, Electrostatic Potential Well in Spherical Geometry." Physics of Fluids, 11:2486-2490, November 1968.
28. WC Elmore et al, "On the Inertial-Electrostatic Confinement of a Plasma" Physics of Fluids 2, 239 (1959); doi:10.1063/1.1705917
29. Miley, G. H., Javedani, J., Nebel, R., Nadler, J., Gu, Y., Satsangi, A. and Heck, P. (1994) An IEC neutron/Proton source. In Third lnt. Conf. on Dense Z-pinches, AIP Conf. Proceedings #299, ed. M. Haines and A. Knight, pp. 675-688. AIP Press, New York.
30. George H. Miley, John Sved, The IEC—A plasma-target-based neutron source, Applied Radiation and Isotopes, Volume 48, Issues 10–12, October–December 1997, Pages 1557-1561, ISSN 0969-8043, 10.1016/S0969-8043(97)00257-1.
31. Miley, G.H.; Yibin Gu; DeMora, J.M.; Stubbers, R.A.; Hochberg, T.A.; Nadler, J.H.; Anderl, R.A.; , "Discharge characteristics of the spherical inertial electrostatic confinement (IEC) device," Plasma Science, IEEE Transactions on , vol.25, no.4, pp.733-739, Aug 1997.
32. Miley, G. H., Y. Shaban, and Y. Yang. "RF Ion Gun Injector in Support of Fusion Ship II Research and Development." AIP Conference Proceedings. Vol. 699. 2004.
33. Miley, G. H., Y. Yang, J. Webber, Y. Shaban, and H. Momota. "RF Ion Source-Driven IEC Design and Operation." Proc. of ANS 16th Topical Meeting on the Technology of Fusion Energy, Wisconsin, Madison. 2004.
34. Barnes, D. C., R. A. Nebel, and Leaf Turner. "Production and Application of Dense Penning Trap Plasmas." Physics of Fluids B: Plasma Physics 5.10 (1993): 3651.
35. Robert W. Bussard; "Some Physics Considerations of Magnetic Inertial Electrostatic Confinement: a New Concept for Spherical Converging-Flow Fusion," 1991, Fusion Technology 19, 273-293

36. Robert W. Bussard, “The Advent of Clean Nuclear Fusion: Superperformance Space Power and Propulsion,” 57th International Astronautically Congress, Valencia, Spain, October 2-6, 2006.
37. Ligon, Tom. "The World's Simplest Fusion Reactor, And How to Make It Work." Analog Science Fiction and Fact 118 (1998): 40-54.
38. Stacey, W. M. "Georgia Tech Studies of Sub-Critical Advanced Burner Reactors with a D-T Fusion Tokamak Neutron Source for the Transmutation of Spent Nuclear Fuel." Journal of Fusion Energy 28.3 (2009): 328-33.
39. Stacey, W. M., et al. "A TRU-Zr Metal-Fuel Sodium-Cooled Fast Subcritical Advanced Burner Reactor." Nuclear Technology 162.1 (2008): 53-79. SCOPUS.
40. Kotschenreuther, M., P. Valanju, S. Mahajan, and E. Schneider. "Fusion–Fission Transmutation Scheme—Efficient Destruction of Nuclear Waste." Fusion Engineering and Design 84.1 (2009): 83-88.
41. Kramer, K. J. “Neutron Transport and Nuclear Burnup Analysis for the Laser Inertial Confinement Fusion-Fission Energy (LIFE) Engine”. Fusion Science and Technology 56: 625-31. (2009).
42. Kramer, K. J., et al. "Parameter Study of the LIFE Engine Nuclear Design." Energy Conversion and Management 51.9 (2010): 1744-50. SCOPUS.
43. Lee, J. D., and R. W. Moir. "Fission-suppressed blankets for fissile fuel breeding fusion reactors." Journal of Fusion Energy 1.3 (1981): 299-303.
44. M.M.H. Ragheb, R. R. Santoro, J. M. Barnes and M. J. Saltmarsh, “Nuclear Performance of Molten Salt Fusion-Fission Symbiotic Systems for Catalyzed Deuterium-Deuterium and Deuterium-Tritium Reactors,” Nuclear Technology, Vol. 4, pp. 216-232, May 1980.
45. Ragheb, Magdi, and Ayman Nour ElDin. "The Fusion-Fission Thorium Hybrid." 1st Thorium Energy Alliance Conference, The Future Thorium Energy Economy," Kellog Conference Center, Gallaudet University, Washington D. C. Vol. 3695. 2002.
46. W.B. Lewis, Report AECL-968, 1952.
47. AEC Research and Development Report, Facilities for Electro-nuclear (MTA) Program. Report LWS-24736, 1953; Status of the MTA Process, Livermore Research Laboratory Report LRL-102, 1954.
48. W.A. Gibson et al., Low-energy neutron production by high energy bombardment of thick targets, in ORNL-3940, p110-111, Electro-nuclear Division, Annual Progress Report, 1965.
49. G.A. Bartholomew, P.R. Tunnicliffe (Eds.), The AECL Study for an Intense Neutron-Generator (ING) (Technical Details), Atomic Energy of Canada Limited Report AECL 2600, 1966.
50. C.M. Van Atta, J.D. Lee, W. Heckrotte, The electronuclear conversion of fertile to fissile material, Lawrence Livermore Laboratory Report UCRL-52144, 1976.
51. ABACS Study Group, Accelerator breeder and converter reactor symbiosis preliminary report on the promise of accelerator breeding and converter reactor symbiosis (ABACS) as an alternative energy system, Oak Ridge National Laboratory, Report ORNL=TM-5750, 1977.
52. G.A. Bartholomew, J.S. Fraser, P.M. Garvey, Accelerator Breeder Concept, Atomic Energy of Canada Limited Report AECL-6363, 1978.
53. T.J. Burns, D.E. Bartine, J.P. Renier, Concept evaluation of a nuclear design for electro-nuclear fuel production: evaluation of ORNLs proposed TME-ENFP (Tennary Metal

Fueled Electro-nuclear Fuel Producer), Oak Ridge National Laboratory Report ORNL=TM-6828, 1979.
54. J.S. Fraser, C.R. Hoffmann, S.O. Schriber, P.M. Garvey, B.M. Townes, Report AECL-7260, Chalk River Nuclear Laboratories, 1981.
55. J.S. Fraser, G.J. Russell, H. Robinson, R.E. Prael, Nucl. Sci. Eng. 99 (1988) 41.
56. F. Carminati et al., Report CERN-AT-93-47(ET), 1993.
57. Rubbia, C. et al.: Fast Neutron Incineration in the Energy Amplifier as Alternative to Geologic Storage: the Case of Spain, CERN/LHC/97-01, 1997.
58. Rubbia, C. et al.: CERN-Group Conceptual Design of a Fast Neutron Operated High Power Energy Amplifier, in: Accelerator driven systems: Energy generation and transmutation of nuclear waste. Status report, IAEA-TECDOC-985, November 1997.
59. Rubbia, Carlo. "Sub-critical Thorium Reactors." Proc. of Energy 2050. Royal Swedish Academy of Sciences, Oct. 2009. Web.
60. C.D. Bowman et al., Nucl. Instr. and Meth. A 320 (1992) 336; F. Venneri et al., Los Alamos Report LA-UR-93-752, 1993.
61. C.D. Bowman et al., "Nuclear energy generation and waste transmutation using accelerator driven intense thermal neutron source", LA-UR-91-2601.
62. Kazuo FURUKAWA, Alfred LECOCQ, Yoshio KATO & Kohshi MITACHI, (1990) Thorium Molten-Salt Nuclear Energy Synergetics. Journal of Nuclear Science and Technology 27:12, pages 1157-1178.
63. K. Furukawa et al., The combined system of accelerator molten salt breeder (AMSB) and molten salt converter reactor (MSCR), Japan–US Seminar on Thorium Fuel Reactors, Naora, Japan, October 1982.
64. Kazuo Furukawa, et al., A road map for the realization of global-scale thorium breeding fuel cycle by single molten-fluoride flow, Energy Conversion and Management, Volume 49, Issue 7, July 2008, Pages 1832-1848, ISSN 0196-8904, 10.1016/j.enconman.2007.09.027. (http://www.sciencedirect.com/science/article/pii/S019689040700427X)
65. Hamid Aït Abderrahim, Peter Baeten, Didier De Bruyn, Rafael Fernandez, MYRRHA – A multi-purpose fast spectrum research reactor, Energy Conversion and Management, Volume 63, November 2012, Pages 4-10, ISSN 0196-8904, 10.1016/j.enconman.2012.02.025. (http://www.sciencedirect.com/science/article/pii/S0196890412000982)
66. Pyeon, Cheol Ho, Tsuyoshi Misawa, Jae-Yong Lim, Hironobu Unesaki, Yoshihiro Ishi, Yasutoshi Kuriyama, Tomonori Uesugi, Yoshiharu Mori, Makoto Inoue, Ken Nakajima, Kaichiro Mishima, and Seiji Shiroya. "First Injection of Spallation Neutrons Generated by High-Energy Protons into the Kyoto University Critical Assembly." Journal of Nuclear Science and Technology 46.12 (2009): 1091-093. Print.
67. Cheol Ho Pyeon, Jae-Yong Lim, Yuki Takemoto, Takahiro Yagi, Tetsushi Azuma, Haksung Kim, Yoshiyuki Takahashi, Tsuyoshi Misawa, Seiji Shiroya, Preliminary study on the thorium-loaded accelerator-driven system with 100 MeV protons at the Kyoto University Critical Assembly, Annals of Nuclear Energy, Volume 38, Issue 10, October 2011, Pages 2298-2302, ISSN 0306-4549, 10.1016/j.anucene.2011.06.024. (http://www.sciencedirect.com/science/article/pii/S0306454911002350)
68. Accelerator-driven Systems (ADS) and Fast Reactors (FR) in Advanced Nuclear Fuel Cycles – A Comparative Study, OECD Nuclear Energy Agency (2002), available on the

NEA webpage on Accelerator-driven Systems (ADS) and Fast Reactors (FR) in Advanced Nuclear Fuel Cycles (http://www.nea.fr/html/ndd/reports/2002/nea3109.html
69. Furukawa, Kazuo, Alfred Lecocq, Yoshio Kato, and Kohshi Mitachi. "Thorium Molten-salt Nuclear Energy Synergetics." Journal of Nuclear Science and Technology 27.12 (1990): 1157-178.
70. Kazimi, M. S., Czerwinski, K. R., Driscoll, M. J., Hejzlar, P., & Meyer, J. E. (1999). On the use of thorium in Light Water Reactors. Dept. of Nuclear Engineering, MIT, MIT-NFCTR-016.
71. X-5 Monte Carlo Team, MCNP-*A General Monte Carlo N-Particle Transport Code*, Version 5, Vol. 1: Overview and Theory, Los Alamos National Laboratory, LA-UR-03-1987, February 2008.
72. LeBlanc, David. "Molten Salt Reactors: A New Vision for a Generation IV Concept."
73. Furukawa, K., K. Arakawa, L. Erbay, Y. Ito, Y. Kato, H. Kiyavitskaya, A. Lecocq, K. Mitachi, R. Moir, and H. Numata. "A Road Map for the Realization of Global-scale Thorium Breeding Fuel Cycle by Single Molten-Fluoride Flow." Energy Conversion and Management 49.7 (2008): 1832-848.
74. Miley, G., and John Sved. "The IEC- A Plasma-target-based Neutron Source." Applied Radiation and Isotopes 48.10-12 (1997): 1557-561.
75. Dolan, T. J. "Magnetic electrostatic plasma confinement." Plasma physics and controlled fusion 36.10 (1994): 1539.
76. "Table of Nuclides." Table of Nuclides. Korea Atomic Energy Research Institute, <http://atom.kaeri.re.kr/>.
77. Ragheb, Magdi, and Monish Singh. "Electrodynamic Inertial Fusion Generators and Fission Satellites." Thorium Energy Alliance, 1 June 2012. Web. <http://www.thoriumenergyalliance.com/>.

APPENDIX A: ONE-GROUP FINITE-DIFFERENCE CRITICALITY MODEL

A.1 Data for One-Group Finite-Difference Code

Table A-1: Fission averaged microscopic cross sections from the JENDL3.2 data files

Isotope	**σ_a (b)**	**σ_s (b)**	**σ_f (b)**	**ν***
U^{233}	2.02	5.645	1.946	2.48
Th^{232}	0.179	7.454	NA	NA
F^{19}	0.0208	3.589	NA	NA
B^{9}	0.0944	2.673	NA	NA
Li^{7}	0.02	1.8447	NA	NA
Graphite	0.002	2.363	NA	NA

*Kazimi, et al.

Table A-2: Core composition and data for fuel salt which yields $k_\infty = 1.00$

	ρ (g/cm^2)	**Σ_a (cm^{-1})**	**Σ_s (cm^{-1})**	**Σ_f (cm^{-1})**	**$\nu * \Sigma_f$ (n/cm)**	**D (cm)**
16%BeF_2 – 69%LiF – 12%ThF_4 – 3%$^{233}UF_4$	4.0345	0.004879	0.288918	0.001968	0.004880	1.1834408

Table A-3: Data for reflector region

	ρ (g/cm^2)	**Σ_a (cm^{-1})**	**Σ_s (cm^{-1})**	**D (cm)**
Graphite	2.267	0.000227531	0.268828152	1.311712192

A.2 One-Group Diffusion Criticality Code

```
!!!!!!!!!!!!!!!!!!!!!!!!!!!!!!!!!!!!!!!!!!!!!!!!!!!!!!!!!!!!!!!!!!!!!!!!!!!!!!!!!!!!!!!!
!		Multiregion One-dimensional One-group Diffusion Theory Criticality Code
!		Evaluation of Effective Multiplication Factor or Eigenvalue and Normalized Neutron Flux
!		Enhanced version of the ODOG procedure using the Power Iteration Method
!  ANSI Fortran-90 or 95 procedure.
!!!!!!!!!!!!!!!!!!!!!!!!!!!!!!!!!!!!!!!!!!!!!!!!!!!!!!!!!!!!!!!!!!!!!!!!!!!!!!!!!!!!!!!!!
!		Dr. M. Ragheb
!		Department of Nuclear, Plasma and Radiological Engineering
!		University of Illinois at Urbana-Champaign
!		103 S. Goodwin Ave., Urbana, Illinois 61801, USA.
!!!!!!!!!!!!!!!!!!!!!!!!!!!!!!!!!!!!!!!!!!!!!!!!!!!!!!!!!!!!!!!!!!!!!!!!!!!!!!!!!!!!!!!!!
		program criticality
!
!		Version 3.5, November 10, 2007
!!!!!!!!!!!!!!!!!!!!!!!!!!!!!!!!!!!!!!!!!!!!!!!!!!!!!!!!!!!!!!!!!!!!!!!!!!!!!!!!!!!!!!!!!
		real lamda1,lamda2
!		lamda1	=		first eigenvalue iteration
!		lamda2	=		second eigenvalue iteration
!		Maximum number of regions in dimension statement = 5
		dimension rr(5),delx(5),n(5),r(100),rp12(100),rm12(100),delr(100)
!		rr			=		distances delimiting regions, measured from plane of symmetry [cm]
!		delx	=		size of interval in each region, chosen as equal to or less than the neutron
!							mean free path in the region [cm]
!		n			=		number of intervals in each region
!		r			=		r(j) = distance of each point from the origin
!		rp12	=		r(j + 1/2)
!		rm12	=		r(j - 1/2)
!		delr	=		r(j+1)-r(j)
		dimension d(5),dp12(100),dm12(100),sigma(5),sigp(100),sigm(100)
!		d			=		diffusion coefficient in each region [cm]
!		dp12	=		d(j + 1/2)
!		dm12	=		d(j - 1/2)
!		sigma	=		macroscopic absorption cross section in each region [cm-1]
!		sigp	=		sigma(j+)
!		sigm	=		sigma(j-)
		dimension ms(5),f(5),fp(100),fm(100),a(100),b(100),c(100),w(100),biga(100,100)
!		ms			=		number of intervals up to and including each region
!		f			=		nu*sigmaf, product of average number of neutrons per fission event and
!							macroscopic fission cross section [neutrons*cm-1]
!		fp			=		f(j+)
!		fm			=		f(j-)
!		a			=		matrix super diagonal
!		b			=		matrix diagonal
!		c			=		matrix sub-diagonal
!		w			=		source term of the diffusion equation in matrix form
!		biga	=		diffusion operator matrix
		dimension phi1(100),phi2(100),s1(100),s2(100),psi(100)
!		phi1	=		first flux iteration
!		phi2	=		second flux iteration
!		s1			=		first source term iteration
!		s2			=		second source term iteration
!		psi			=		source term
		character*1 tab
		tab=char(9)
!		Open the input and output files
!		Input file is:		incrit
!		Output file is:		outcrit
!		Plotting file is plot
		open(unit=10,file='incrit1R.txt',status='old')
		open(unit=11,file='outcrit')
		open(unit=12,file='plot')
!  Write program information
		write (11,23)
		write (*,23)
23		format('Multiregion One-dimensional One-group Diffusion Theory Criticality',/,&
```

```
     &'Effective Multiplication factor or Eigenvalue and neutron flux evaluated',/,&
     &'Enhanced version of the ODOG procedure using the Power Iteration Method',/,&
     &'Fortran-90 or 95 procedure',/,&
     &'Unix or Windows operating system',/&
  &'Dr. Magdi Ragheb',/,&
     &'University of Illinois at Urbana-Champaign',/,&
     &'103 S. Goodwin Ave., Urbana, Illinois 61801, USA.',/)
!    Read problem data from file incrit
!    Write problem output on file outcrit
!    Write plot file on file plot for input to plotting routine, e. g. Microsoft Excel
     read(10,1)m,nn,eps
1    format(2I2,e8.1)
!    m              =    number of regions
!    nn             =    geometry index,    nn=0 cartesian geometry
!                                                nn=1 cylindrical geometry
!                                                nn=2 spherical geometry
!    eps            =    convergence parameter for the eigenvalue iteration
     write (11,91)
     write (*,91)
91   format('Number of regions',2x,'Geometry Index: 0=cartesian 1=cylindrical 2=spherical',&
  &2x,'Convergence parameter')
     write (11,1) m,nn,eps
     write (*,1) m,nn,eps
     read(10,2)(rr(i),i=1,m)
2    format(8f10.3)
     write(11,3)
     write(*,3)
3    format('Regions boundaries')
     write(11,2)(rr(i),i=1,m)
     write(*,2)(rr(i),i=1,m)
     read(10,2)(d(i),i=1,m)
     write(11,4)
     write(*,4)
4    format('Regions diffusion coefficients')
     write(11,2)(d(i),i=1,m)
     write(*,2)(d(i),i=1,m)
     read(10,2)(sigma(i),i=1,m)
     write(11,5)
     write(*,5)
5    format('Regions macroscopic absorption cross section')
     write(11,2)(sigma(i),i=1,m)
     write(*,2)(sigma(i),i=1,m)
     read(10,2)(f(i),i=1,m)
     write(11,6)
     write(*,6)
6    format('Regions nu*macroscopic fission cross section product')
     write(11,2)(f(i),i=1,m)
     write(*,2)(f(i),i=1,m)
     read(10,93)bcz,bpy,bpz
93   format(3f10.3)
     write(11,92)
     write(*,92)
92   format('Buckling corrections')
     write(11,93) bcz,bpy,bpz
     write(*,*) bcz,bpy,bpz
!    Buckling corrections allow for three dimensional effects.
!    The buckling corrections can be assigned zero values.
!    bcz            =    cylindrical geometry buckling axial correction
!    bpy            =    cartesian geometry buckling correction in y direction
!    bpz            =    cartesian geometry buckling correction in z direction
!
     if(nn.eq.2)write(11,7)
     if(nn.eq.2)write(*,7)
7    format('Spherical Geometry')
     if(nn.eq.1)write(11,8)
     if(nn.eq.1)write(*,8)
8    format('Cylindrical Geometry')
     if(nn.eq.0)write(11,9)
     if(nn.eq.0)write(*,9)
9    format('Cartesian Geometry')
```

```
      if(nn.eq.2) go to 222
      if(nn.eq.0) go to 111
!     Buckling correction in the axial direction for a finite height cylinder
      do i=1,m
            sigma(i)=sigma(i)+d(i)*bcz
      end do
      go to 222
!     Buckling correction in the y and z dimensions in cartesian geometry
111   do i=1,m
            sigma(i)=sigma(i)+d(i)*(bpy+bpz)
      end do
!     Computation of the number of intervals in each region
222   n(1)=rr(1)*sigma(1)+1
      n1=n(1)
      if(n1.le.10) n(1)=20
      if(m.gt.1) go to 333
      m=2
      rr(2)=rr(1)
      rr(1)=rr(1)/2.0
      n(1)=rr(1)*sigma(1)+1
      d(2)=d(1)
      f(2)=f(1)
      sigma(2)=sigma(1)
333   do i=2,m
            n(i)=(rr(i)-rr(i-1))*sigma(i)
            ni=n(i)
            if(ni.le.10) n(i)=20
      end do
      write (11,12)
      write(*,12)
12    format('Number of intervals in each region')
      write(11,13)(n(i),i=1,m)
      write(*,13) (n(i),i=1,m)
13    format(5i10)
!     Computation of the size of intervals in each region
      delx(1)=rr(1)/(n(1)-0.5)
      do i=2,m
            delx(i)=(rr(i)-rr(i-1))/n(i)
      end do
      write(11,14)
      write(*,14)
14    format('Interval sizes in each region')
      write(11,2)(delx(i),i=1,m)
      write(*,2)(delx(i),i=1,m)
!     Initialization of first mesh point variables
      r(1)=delx(1)/2.0
      rp12(1)=r(1)+delx(1)/2.0
      rm12(1)=0.0
      delr(1)=delx(1)
      delrm=delx(1)/2.0
      dp12(1)=d(1)
      dm12(1)=d(1)
      sigp(1)=sigma(1)
      sigm(1)=sigma(1)
      fp(1)=+f(1)
      fm(1)=+f(1)
      a(1)=(rp12(1)**nn)*dp12(1)/delr(1)
      c(1)=0.0
      b(1)=a(1)+c(1)+r(1)**nn*(sigp(1)*delr(1)+sigm(1)*delrm)
      w(1)=r(1)**nn*(delr(1)*fp(1)+delrm*fm(1))
      ms(1)=n(1)
      do i=2,m
            ms(i)=ms(i-1)+n(i)
      end do
      nt=ms(m)
!     Computation of mesh parameters in first region
      n1=n(1)
      do 555 i=2,n1
            r(i)=r(1)+(i-1)*delx(1)
            if(i.eq.n1) go to 444
```

```
                rp12(i)=r(i)+delx(1)/2.0
                rm12(i)=r(i)-delx(1)/2.0
                fp(i)=f(1)
                fm(i)=f(1)
                sigp(i)=sigma(1)
                sigm(i)=sigma(1)
                dp12(i)=d(1)
                dm12(i)=d(1)
                go to 555
444             rp12(i)=r(i)+delx(2)/2.0
                rm12(i)=r(i)-delx(1)/2.0
                fp(i)=f(2)
                fm(i)=f(1)
                sigp(i)=sigma(2)
                sigm(i)=sigma(1)
                dp12(i)=d(2)
                dm12(i)=d(1)
555     continue
!       Computation of mesh parameters in other regions
        delx(m+1)=0.0
        f(m+1)=0.0
        sigma(m+1)=0.0
        d(m+1)=0.0
        do 666 i=2,m
                msi=ms(i)
                msm=ms(i-1)
        do 666 k=msm,msi
                r(k)=r(msm)+(k-msm)*delx(i)
                if(k.eq.msm) go to 777
                if(k.eq.msi) go to 888
                rp12(k)=r(k)+delx(i)/2.0
                rm12(k)=r(k)-delx(i)/2.0
                fp(k)=f(i)
                fm(k)=f(i)
                sigp(k)=sigma(i)
                sigm(k)=sigma(i)
                dp12(k)=d(i)
                dm12(k)=d(i)
                go to 666
777             rp12(k)=r(k)+delx(i)/2.0
                rm12(k)=r(k)-delx(i)/2.0
                fp(k)=f(i)
                fm(k)=f(i-1)
                sigp(k)=sigma(i)
                sigm(k)=sigma(i-1)
                dp12(k)=d(i)
                dm12(k)=d(i-1)
                go to 666
888             rp12(k)=r(k)+delx(i+1)/2.0
                rm12(k)=r(k)-delx(i)/2.0
                fp(k)=f(i+1)
                fm(k)=f(i)
                sigp(k)=sigma(i+1)
                sigm(k)=sigma(i)
                dp12(k)=d(i+1)
                dm12(k)=d(i)
666     continue
!       Computation of sub-diagonal, diagonal, super-diagonal, and source terms
        l=nt-1
        do i=2,l
                delr(i)=r(i+1)-r(i)
                a(i)=rp12(i)**nn*dp12(i)/delr(i)
                c(i)=rm12(i)**nn*dm12(i)/delr(i-1)
                b(i)=a(i)+c(i)+r(i)**nn*(sigp(i)*delr(i)+sigm(i)*delr(i-1))/2.0
                w(i)=r(i)**nn*(fp(i)*delr(i)+fm(i)*delr(i-1))/2.0
        end do
        write(11,15)
        write(*,15)
15      format(10x,'Sub-diagonal',10x,'Diagonal',10x,'Super-Diagonal',5x,'Source Term')
        do i=1,l
```

```
                    a(i)=-a(i)
                    c(i)=-c(i)
                    write(11,16)c(i),b(i),a(i),w(i)
                    write(*,16)c(i),b(i),a(i),w(i)
          end do
16        format(4(10x,E10.3))
!         Formation of matrix of coefficients A
          do  i=1,l
                    do j=1,l
                              if(i.eq.j) go to 116
                              if(i.eq.j+1) go to 117
                              if(i.eq.j-1) go to 118
                              biga(i,j)=0.0
                              go to 119
116       biga(i,j)=b(i)
                              go to 119
117                           biga(i,j)=c(i)
                              go to 119
118       biga(i,j)=a(i)
119                 continue
     end do
          end do
!         Coefficients matrix is written as needed by uncommenting the following statements
!         write(*,*) biga
!         do i=1,l
!                   write(11,17)(biga(i,j),j=1,l)
!                   write(*,17)(biga(i,j),j=1,l)
!17                format(5E12.4)
!         end do
121       iff=1
          c(1)=0.0
          a(l)=0.0
          lamda1=1.0
          do i=1,l
                    phi1(i)=1.0
          end do
          kk=1
123       continue
          do i=1,l
                    s1(i)=w(i)*phi1(i)
                    psi(i)=s1(i)/lamda1
          end do
!         Solve tridiagonal linear system of equations
          call tridag(iff,l,c,b,a,psi,phi2)
          phim=0.0
          do i=1,l
                    if(phim.lt.phi2(i)) phim=phi2(i)
          end do
          do i=1,l
                    phi1(i)=phi2(i)/phim
          end do
          do i=1,l
                    s2(i)=w(i)*phi2(i)
          end do
          sumt=0.0
          sumb=0.0
          do i=1,l
                    sumt=sumt+s2(i)*s2(i)
                    sumb=sumb+s2(i)*psi(i)
          end do
          lamda2=sumt/sumb
!         Calculate relative error for use as convergence parameter
          rat=abs((lamda1-lamda2)/lamda1)
          if(rat.lt.eps) go to 122
          lamda1=lamda2
          kk=kk+1
          go to 123
122       continue
          write(11,18)kk
          write(*,18)kk
```

```
18          format('The number of outer iterations is:',I5)
            write(11,19)
            write(*,19)
19          format(3x,'Distance',1x,'Normalized Flux')
            do i=1,l
                        write(11,20)r(i),tab,phi1(i)
                        write(*,20)r(i),tab,phi1(i)
            end do
            do i=1,l
                        write(12,20) r(i),TAB,phi1(i)
            end do
20          format(f10.3,a1,f10.3)
            write(11,21)
            write(*,21)
21          format('Eigenvalue, Effective multiplication factor, k(eff).')
            write(11,22)lamda2
            write(*,22)lamda2
22          format(f12.4)
            end
!
            subroutine tridag(ifirst,ilast,a,b,c,d,v)
!           This procedure solves a system of simultaneous linear equations with a tridiagonal
!  coefficient matrix.
!           a           = array of sub-diagonal coefficients
!           b           = array of diagonal coefficients
!           c           = array of super-diagonal coefficients
!           d           = source vector
!           v(if) ... v(l)= final solution vector
!           ifirst  = first equation number
!           ilast       = last equation number
!           beta, gamma = intermediate arrays
            dimension a(100),b(100),c(100),d(100),v(100),beta(201),gamma(201)
!           Generate intermediate arrays beta an gamma
            beta(ifirst)=b(ifirst)
            gamma(ifirst)=d(ifirst)/beta(ifirst)
            ifirstp1=ifirst+1
            do i=ifirstp1,ilast
                        beta(i)=b(i)-(a(i)*(c(i-1)/beta(i-1)))
                        gamma(i)=(d(i)-a(i)*gamma(i-1))/beta(i)
            end do
!           Computation of final solution vector
            v(ilast)=gamma(ilast)
            last=ilast-ifirst
            do k=1,last
                        i=ilast-k
                        v(i)=gamma(i)-(c(i)*(v(i+1)/beta(i)))
            end do
            return
            end
```

A.3 Sample Input

```
!3 Region problem with geometry index=2 (spherical) and convergence factor
 3 2+0.1e-05
!Thickness of region
   100.000  109.480   149.480
!Diffusion Coefficient
    1.177     1.116     1.312
!Macroscopic absorption cross section
    0.005     0.015     0.000
!Product of the number of neutrons per fission and macroscopic fission cross section
    0.003     0.030     0.000
!Geometric buckling correction factor
    0.000     0.000     0.000
```

APPENDIX B: MCNP5 INPUT FILES

B.1 k_∞ Input

```
k∞ Calculation
c
c         Cell Cards
   1  1  -3.8715  -1  imp:n=1
   2  0              1  imp:n=0

c         Surface cards
c    Fuel Region
*1  so 50                          $All neutrons are reflected back into fuel

c         Geometry Cards
mode  n
m1       4009.66c      0.062758683     $Fuel material
         3007.50       0.27856383
         90232.66c     0.047069013
         92233.66c     0.003850245
         9019.66c      0.607758228
c
c         Source Cards
kcode 1000 1.0 30 130
ksrc 0 0 0
print
```

B.2 Fissile Source Region Design

```
Fissile Source Region Design
c         Cell cards
  1  1  -3.8715  -1  imp:n=1
  2  2  -8.6900   1 -2  imp:n=1
  3  3  -2.5330   2 -3  imp:n=1
  4  2  -8.6900   3 -4  imp:n=1
  5  4  -1.7000   4 -5  imp:n=1
  6  0              5    imp:n=0

c         Surface cards
c    Fuel Region
   1       so 40.00
c    Hastelloy Region
   2       so 41.70
c    Source Region
   3       so 51.70
c    Hastelloy Region
   4       so 52.55
c    Reflector Region
   5       so 92.55

c         Material cards
mode  n p
m1    4009.66c      0.062758683       $Fuel region material
      3007.66c      0.278563830
      90232.66c     0.047069013
      92233.66c     0.003850245
      9019.66c      0.607758228
m2    28000.    -.7760                $Hastelloy N
      42000.    -.1200
      24000.    -.0700
      22000.    -.0236
      41093.66c    -.0100
      25055.66c    -.0002
      26056.66c     -.0001
      14028.    -.0001
m3    4009.66c      0.132309006       $ Fissile source region material
      3007.66c      0.289799402
      92233.66c     0.004694836
      9019.66c      0.573196756
m4    6000.70c      -1                $Graphite reflector
c         Flux at a point
F5:n 0 0 0 1.5
```

```
F15:n 5 0 0 1.5
F25:n 10 0 0 1.5
F35:n 15 0 0 1.5
F45:n 20 0 0 1.35
F55:n 25 0 0 1.5
F65:n 30 0 0 1.5
F75:n 35 0 0 1.5
F85:n 45 0 0 1.5
F95:n 55 0 0 1.3
F105:n 60 0 0 1.3
F115:n 65 0 0 1.3
F125:n 70 0 0 1.15
F135:n 75 0 0 1.3
F145:n 80 0 0 1.3
F155:n 85 0 0 1.3
c         Flux averaged over cell 1
F14:n 1
FM14 (-1 1 102)       $(n,γ) reaction rate
         (-1 1 -4)        $Energy deposition (everything but gamma-ray heating)
         (-1 1 -6 -8)     $Fission energy deposition
         (-1 1 -6)        $Fission rate
F24:n 3
FM24 (-1 3 -4)        $Energy deposition (everything but gamma-ray heating)
         (-1 3 -6 -8)     $Fission energy deposition
         (-1 3 -6)        $Fission rate
c
F6:n,p 1 3            $Total energy deposition in cell 1 and cell 3
c
e4:n 1.00E-09 1.58E-09 2.51E-09 3.98E-09 6.31E-09       $Energy Bins for F4 Tally
   1.00E-08 1.58E-08 2.51E-08 3.98E-08 6.31E-08
   1.00E-07 1.58E-07 2.51E-07 3.98E-07 6.31E-07
   1.00E-06 1.58E-06 2.51E-06 3.98E-06 6.31E-06
   1.00E-05 1.58E-05 2.51E-05 3.98E-05 6.31E-05
   1.00E-04 1.58E-04 2.51E-04 3.98E-04 6.31E-04
   1.00E-03 1.58E-03 2.51E-03 3.98E-03 6.31E-03
   1.00E-02 1.58E-02 2.51E-02 3.98E-02 6.31E-02
   1.00E-01 1.58E-01 2.51E-01 3.98E-01 6.31E-01
   1.00E+00 1.58E+00 2.51E+00 3.98E+00 6.31E+00
   1.00E+01 1.58E+01 2.51E+01
C         Source cards
kcode 100000 1.0 30 200
ksrc 0 0 0
print
```

B.3 Fusion Source Design

```
Fusion Source
c         Cell cards
   1  1  -3.8924  -1 -6 8  imp:n=1
   2  2  -8.6900   1 -2 -6 8  imp:n=1
   3  0             2 -3 -6 8  imp:n=1
   4  2  -8.6900   3 -4 -6 8  imp:n=1
   5  3  -1.7000   4 -5 -6 8  imp:n=1
   6  3  -1.7000   6 -7 -5 imp:n=1
   7  3  -1.7000  -8 9 -5  imp:n=1
   8  0            -9  imp:n=0
   9  0             7  imp:n=0
   10 0             5 -7 9  imp:n=0

c         Surface cards
c    Core Region
     1       cz 75
c    Hastelloy Region
     2       cz 75.85
c    Source Region
     3       cz 85.85
c    Hastelloy Region
     4       cz 86.70
c    Reflector Region
     5       cz 126.70
c    Axial Reflector (Top)
     6       pz 75
     7       pz 115
c    Axial Reflector (Bottom)
     8       pz -75
     9       pz -115

c         Material cards
mode  n p
m1       4009.66c        0.062664003   $Fuel region material
         3007.50         0.276807778
         90232.66c       0.046998003
         92233.66c       0.004347315
         9019.66c        0.608349978
         3006.50          0.000832922
m2       28000.    -.7760              $Hastelloy N
         42000.    -.1200
         24000.    -.0700
         22000.    -.0236
```

```
          41093.66c    -.0100
          25055.66c    -.0002
          26056.66c    -.0001
          14028.    -.0001
m3        6000.70c       -1                  $Graphite reflector
c
c         Source specification
SDEF erg=d1 par=1 cel=3 ext=d2 pos=0 0 0 rad=d3
sp1   -4 -0.01 -1
si2   L   -75  75
sp2   -21 0
si3   H   75.85  85.85
sp3   -21 1
c
c         Flux at a point
F5:n 0 0 0 1.5
F15:n 5 0 0 1.5
F25:n 10 0 0 1.5
F35:n 20 0 0 1.5
F45:n 30 0 0 1.35
F55:n 40 0 0 1.5
F65:n 50 0 0 1.5
F75:n 60 0 0 1.5
F85:n 65 0 0 1.5
F95:n 70 0 0 1.5
F105:n 0 0 5 1.5
F115:n 0 0 10 1.5
F125:n 0 0 20 1.5
F135:n 0 0 30 1.5
F145:n 0 0 40 1.5
F155:n 0 0 50 1.5
F165:n 0 0 60 1.5
F175:n 0 0 65 1.5
F185:n 0 0 70 1.5
c         Flux averaged over cell 1
F14:n 1
FM14 (-1 1 102)        $(n,γ) reaction rate
          (-1 1 -4)        $Energy deposition (everything but gamma-ray heating)
          (-1 1 -6 -8)     $Fission energy deposition
          (-1 1 -6)        $Fission rate
c
F6:n,p 1                   $Total energy deposition in cell 1 and cell 3
c
e4:n 1.00E-09 1.58E-09 2.51E-09 3.98E-09 6.31E-09        $Energy bins for F4 tally
    1.00E-08 1.58E-08 2.51E-08 3.98E-08 6.31E-08
    1.00E-07 1.58E-07 2.51E-07 3.98E-07 6.31E-07
```

```
     1.00E-06 1.58E-06 2.51E-06 3.98E-06 6.31E-06
     1.00E-05 1.58E-05 2.51E-05 3.98E-05 6.31E-05
     1.00E-04 1.58E-04 2.51E-04 3.98E-04 6.31E-04
     1.00E-03 1.58E-03 2.51E-03 3.98E-03 6.31E-03
     1.00E-02 1.58E-02 2.51E-02 3.98E-02 6.31E-02
     1.00E-01 1.58E-01 2.51E-01 3.98E-01 6.31E-01
     1.00E+00 1.58E+00 2.51E+00 3.98E+00 6.31E+00
     1.00E+01 1.58E+01 2.51E+01
NPS 5000
C         Source cards
kcode 2000 1.0 30 200
c
print
```

APPENDIX C: TABULATED RESULTS

Table C-1: Fissile fail-safe reactor MCNP results

	Composition	Mass (kg)	Volume (L)	Density (g/cm^3)	Heat Rate (MeV/fns)	Fission Rate (#/fns)	Fissile Production Rate (#/fns)
Core Region	16% BeF_2 – 71.02% LiF – 12% ThF_4 – 0.98% UF_4	1037.9	268.1	3.872	25.4	0.134	0.197
Fissile Source Region	31% BeF_2 – 67.9% LiF – 1.1% UF_4	671.8	265.2	2.533	47.8	0.272	NA

Table C-2: DT driven reactor MCNP results for different ^6Li concentrations

	Composition	Mass (metric tonne)	Volume (L)	Density (g/cm^3)	Heat Rate (MeV/fns)	Fission Rate (#/fns)	Fissile Production Rate (#/fns)	Tritium Production (#/fns)
0% Li-6	16% BeF_2 – 71.02% LiF – 12% ThF_4 – 0.98% UF_4	10.3	2650.7	3.872	294.28	1.57	2.01	0.36
0.5% Li-6	16% BeF_2 – 70.85% LiF – 12% ThF_4 – 1.15% UF_4	10.3	2650.7	3.890	246.69	1.31	1.58	0.53
2.25% Li-6	16% BeF_2 – 70.38% LiF – 12% ThF_4 – 1.62% UF_4	10.4	2650.7	3.925	231.47	1.28	1.28	0.89
2.5% Li-6	16% BeF_2 – 70.32% LiF – 12% ThF_4 – 1.68% UF_4	10.4	2650.7	3.934	244.32	1.29	1.26	0.93
3% Li-6	16% BeF_2 – 70.2% LiF – 12% ThF_4 – 1.8% UF_4	10.4	2650.7	3.940	245.59	1.30	1.22	1.00
NA Li-6	16% BeF_2 – 69.35% LiF – 12% ThF_4 – 2.65% UF_4	10.6	2650.7	4.0095	267.68	1.42	1.00	1.47

Table C-3: DD driven reactor MCNP results for different types of salts

	Composition	Mass (tonnes)	Volume (L)	Density (g/cm^3)	Heat Rate (MeV/fns)	Fission Rate (#/fns)	Fissile Production Rate (#/fns)
Li Salt	16% BeF_2 – 71.02% LiF – 12% ThF_4 – 0.98% UF_4	10.3	2650.7	3.872	292.67	1.57	2.00
Na Salt	16% BeF_2 – 70.94% NaF– 12% ThF_4 – 1.06% UF_4	9.45	2650.7	3.565	251.28	1.35	1.70

Table C-4: Computed results of fusion driven systems

System	Composition	M_{net}	k_{eff}	k_{eff}^{FS}	Source Strength [n/s]	Source Power [MW_{th}]	Net Fissile Production Rate [kg/yr]	Doubling Time [yr]	Fusion Neutron Wall Load (MW/m^2]	BEMR
DT Li	16% BeF_2 – 70.38% LiF – 12% ThF_4 – 1.62% UF_4	3.0888 (+/-) 0.0080	0.88332 (+/-) 0.00281	0.776	7.92E18	22.3	0	NA	3.15	16.5
DD Li	6% BeF_2 – 71.02% LiF – 12% ThF_4 – 0.98% UF_4	3.3706 (+/-) 0.0091	0.90225 (+/-) 0.00034	0.798	6.72E18	7.9	35.2	10.2	1.12	119.5
DD Na	16% BeF_2 – 70.94% NaF– 12% ThF_4 – 1.06% UF_4	3.0642 (+/-) 0.0036	0.88526 (+/-) 0.0017	0.775	7.70E18	9.0	32.9	9.2	1.27	102.6